THEORETICAL ANALYSIS AND EXPERIMENTAL DESIGN OF DUAL-BEAM OPTICAL TRAP FOR LARGE PARTICLES

by

Demi Rose St. John

A thesis submitted in partial fulfillment
of the requirements for the degree

of

Master of Science

in

Optics and Photonics

MONTANA STATE UNIVERSITY
Bozeman, Montana

November 2018

ACKNOWLEDGEMENTS

First and foremost, I am thankful to Jordan Love for his encouragement and love throughout this entire experience. Without his unwavering support I would have never accomplished the work presented in this thesis. Additionally, I am incredibly thankful to my family and friends outside of Bozeman for their never-ending support.

To Randy Babbitt, thank you for believing in me from the start. I am so grateful for the potential you saw in me and your willingness to always teach me something new. Thanks to my committee members, Charles Thiel and Brian D'Urso for their patience and guidance throughout this project. To all others that helped support and steer me back on track - thank you: Margaret Jarrett, Diane Harn, Hannah Gilroy, Sarah Barutha, Tino Woodburn, Lou Oberto, Travis Robson, Ryan Galloway, and Aislinn Daniels.

The support by the Montana Board of Research and Commercialization Technology (MBRCT) and the Office of Naval Research (ONR) is gratefully acknowledged.

TABLE OF CONTENTS

1. INTRODUCTION 1

Optical Levitation 1
Motivation 2
Overview of Thesis 4

2. BACKGROUND 5

Gaussian Beams 5
Theory of Optical Trapping 6
 Geometric Optics Regime 7
 Rayleigh Regime 11
 Mie Regime 12
Theory of Laser Cooling 12
 Bulk Cooling Theory 12
  Bulk Cooling Demonstration of Yb:YAG 14
 Fabrication of Doped Particles 15
 Thermometry 17

3. THEORY OF DUAL-BEAM TRAPPING AND TOLERANCING 20

Rayleigh Regime 20
 Background 20
 Modifications and Additions to Inherited Code 20
 New Rayleigh Regime Code 21
Optical Tweezers in Geometrical Optics (OTGO) 24
 Background 24
 Work-space Modifications to OTGO 28
 Dual-beam Addition to OTGO 33
  Silica Particle Example 33
  Longitudinal Separation of Laser Beams 37
  Transverse Separation of Laser Beams 41
  Potential Wells 44
  Particle Dynamics 46

4. OPTICAL TRAPPING EXPERIMENT 49

Lasers 49
Vertical Trap 49
Launching Particles 52
 Old Method: Microscope Slide Cantilever 52

TABLE OF CONTENTS – CONTINUED

Assembly and Operation 52
Downfalls 53
New Method 1: Aluminum Cantilever with Drop Hole 54
New Method 2: Aluminum Cantilever with Trenched Channel 55
Assembly and Operation 56
Fundamental Physics of the Designs 58
Bar Vibrational Modes 58
Michelson Interferometer 59
Horizontal Dual-beam Trap 60
Laser Diode Tuning 60
Optical Setup Designs 61
Setup 1: Single Laser Diode 62
Setup 2: Two Laser Diodes 66
Setup 3: Fiber System 67
Imaging 70
Time-lapse Imaging 72

5. SYSTEM ANALYSIS 76

Silica Particles 76
Previous Discussion 76
X-Tolerance 76
Z-tolerance 81
YAG Particles 85
Practical Lab Conditions 85
Large YAG Particles 87

6. CONCLUSIONS 90

Recommendations for Current Experimental Setup 90
Future Work 91
Launching Improvements 91
Imaging Improvements 92
Code 93
Cooling and Loss Pressure 93

REFERENCES CITED 95

TABLE OF CONTENTS – CONTINUED

APPENDICES 98

APPENDIX A : Rayleigh Dual-beam Theory 99
APPENDIX B : OTGO Dual-beam Theory 107
APPENDIX C : Automatic Loading and Image Detection........................... 121
APPENDIX D : Particle Loading Dynamics... 131

LIST OF TABLES

Table Page

3.1 Plot legend descriptions 22

4.1 Loader Frequency 59

LIST OF FIGURES

Figure Page

1.1 The average chamber pressure when 3 micron spherical particles are lost as a function of laser intensity. Each point represents the average loss pressure for 5 trapped particles at a given intensity. [7, 10] 3

2.1 Gaussian beam parameters: w_0 - beam waist, $w(z)$ - beam width at a point z along the beam, z_R - a distance away from the beam waist where $w(z) = \sqrt{2}$ known as the Rayleigh range. 5

2.2 The ray tracing and momentum changes due to propagation of a laser beam with a strong intensity gradient of radius smaller than the particle diameter. The figure is similar to that of Ashkin's original paper [2]. The combination of the change in momentum per photon and the transverse gradient of the laser beam results in two net forces: a gradient force towards the beam axis (F_G) and a scattering force in the direction of the laser beams propagation (F_S). 7

2.3 Left: A particle is displaced axially along the propagation of the laser. Middle: A particle is trapped at the focus of the laser. Right: A particle is displaced radially above the focus of the laser. Restoring forces are shown inside the dotted-green circles. 9

2.4 Two counter-propagating focused laser beams for an optical trap. 10

2.5 Basic concept of solid-state (anti-Stokes) laser cooling. The absorbed light from a thermally excited ground state level to the lowest excited state level and subsequent emission from a thermally excited state level to a lower ground state level results in a net loss in energy from the material. 13

LIST OF FIGURES – CONTINUED

Figure Page

2.6 Imaging of Yb^{3+}-doped YAG crystals under laser excitation traveling down the center of the rod. a) Yb^{3+}:YAG single crystal rod (1 mm diameter) under laser excitation by 200 mW of non-resonant laser light at 1040 nm as seen through a 950nm filter. Minimal fluorescence is observed. b) Observation of 950 nm anti-Stokes fluorescence from Yb^{3+} ions as laser is tuned near resonance at 1030 nm. c) Strong anti-Stokes emission observed when laser is tuned to peak of resonance at 1030 nm. d) Thermal image of crystal with 200 mW of on-resonance 1030 nm laser light, demonstrating no significant heating of crystal relative to ambient temperature (74°F) even when laser light is strongly absorbed. These measurements were done by Tino Woodburn and Jason Carr in Dr. Charles Thiel's lab. 15

2.7 Yb:YAG particles fabricated in Dr. Charles Thiel's lab. Top Left: 3240x Magnification Yb:YAG, Scale $10\mu m$. Top Right: 18560x Magnification Yb:YAG, Scale $2\mu m$. Bottom Left: 21560x Magnification Yb:YAG, Scale $1\mu m$. Bottom Right: 49310x Magnification Yb:YAG, Scale 200nm. 16

2.8 Examples of spherical particles of birefringent vaterite crystals ($CaCO_3$) fabricated and characterized at MSU by Tino Woodburn and Dr. Charles Thiel. Left: Typical particles produced with sizes in the 1 to 10 micron size range. Middle: Example of larger 30 micron diameter vaterite particle produced by increasing growth time. Right: Example fluorescence image of rare-earth-doped vaterite particles produced with Eu^{3+} ions used as the fluorescence marker, demonstrating the ability to dope the vaterite particles with rare-earth ions. 16

2.9 Optical thermometry setup for a bulk Yb:YAG crystal Setup by Jason Carr, Tino Woodburn, and Dr. Charles Thiel for calibration of fluorescence ratios as a function of temperature. 18

LIST OF FIGURES – CONTINUED

Figure Page

2.10 Results from fluorescence thermometry experiment carried out by Tino Woodburn, Jason Carr, and Dr. Charles Thiel showing a linear relationship of the fluorescence ratio above room temperature. 19

3.1 Forces in the axial (left) and transverse (right) directions from the inherited MATLAB code. Position in meters is along the horizontal axis with force in Newtons along the vertical axis. 21

3.2 Trapping forces in the z and x-directions for a horizontal dual-beam trap with no z-separation in the Rayleigh regime for a new MATLAB program following [15] directly. The bottom plot is a zoomed in view of the top plot for a $2\mu m$ silica particle focused by a 2.2W 1064nm laser. 23

3.3 The new Rayleigh code with z-separation defined as $10\mu m$. A $2\mu m$ silica particle trapped by 2.2W of 1064nm laser light is shown in both plots. The right plot is a zoomed in view of the left plot. Note the scale differences for force in each plot. 24

3.4 Trapping efficiencies in the longitudinal direction of the original OTGO *efficiencies_beam.m* example file. The scattering trapping efficiency (Q_s, solid pink line) and gradient trapping efficiency (Q_g, solid blue line) are shown along with the total trapping efficiency (Q, solid black line). All efficiencies are directed along the z-axis. 26

3.5 Trapping efficiencies in the transverse direction of the original OTGO *efficiencies_beam.m* example file. The scattering trapping efficiency (Q_s, solid pink line) and gradient trapping efficiency (Q_g, solid blue line) are shown along with the total trapping efficiency (Q, solid black line). The gradient trapping efficiency and total trapping efficiency are directed along the x-axis while the scattering trapping efficiency is directed along the z-axis. 27

LIST OF FIGURES – CONTINUED

Figure Page

3.6 Trapping forces in the longitudinal direction of the original OTGO *efficiencies_beam.m* example file. The scattering force (F_s, solid pink line) and gradient force (F_g, solid blue line) are shown along with the total force, including the force of gravity (F, solid black line). The force of gravity (F_G, solid green line) has been added. 30

3.7 Trapping forces in the transverse direction of the original OTGO *efficiencies_beam.m* example file. The scattering force (F_s, solid pink line) and the gradient force (F_g, solid blue line) are shown along with the total trapping force (F, solid black line), including the force of gravity. The force of gravity (F_G, solid green line) has been added. 31

3.8 Individual rays modeled after parameter definitions defined in OTGO code. 32

3.9 Longitudinal forces along the z-axis for an ideal horizontal dual-beam trap. An 8μm diameter silica particle is trapped by two 1030nm lasers where each is focused by an 8mm lens. Powers of the beams are balanced with 0.03W in each beam. 34

3.10 Transverse forces along the x-axis at z=0 for an ideal horizontal dual-beam trap. An 8μm diameter silica particle is trapped by two 1030nm lasers where each is focused by an 8mm lens. Powers of the beams are balanced with 0.03W in each beam. 36

3.11 Longitudinal forces along the z-axis for an ideal horizontal dual-beam trap with unbalanced powers between the beams. An 8μm diameter silica particle is trapped by two 1030nm lasers each focused by an 8mm lens. Powers of the beams are 0.04W in Laser 1 and 0.03W in Laser 2. 37

3.12 Transverse forces along the x-axis at z=0 for an ideal horizontal dual-beam trap with unbalanced powers between the beams. An 8μm diameter silica particle is trapped by two 1030nm lasers each focused by an 8mm lens. Powers of the beams are 0.04W in Laser 1 and 0.03W in Laser 2. 38

LIST OF FIGURES – CONTINUED

Figure Page

3.13 Longitudinal forces along the z-axis for a horizontal dual-beam trap with unbalanced powers between the two beams. A z-separation of 50μm is present between the foci. An 8μm diameter silica particle is trapped by two 1030nm lasers each focused by an 8mm lens. Powers of the beams are 0.04W in Laser 1 and 0.03W in Laser 2. 40

3.14 Transverse forces along the x-axis at z = 0 for a horizontal dual-beam trap with unbalanced powers between the two beams. A z-separation of 50μm is present between the foci. An 8μm diameter silica particle is trapped by two 1030nm lasers each focused by an 8mm lens. Powers of the beams are 0.04W in Laser 1 and 0.03W in Laser 2. 40

3.15 Longitudinal forces along the z-axis for a horizontal dual-beam trap with an x-separation of 10μm between the foci with $z_{sep} = 0$. An 8μm diameter silica particle is trapped by two 1030nm lasers each focused by an 8mm lens. Powers of the beams are balanced with 0.03W in each beam. 42

3.16 Transverse forces along the x-axis for a horizontal dual-beam trap with an x-separation of 10μm between the foci with $z_{sep} = 0$. An 8μm diameter silica particle is trapped by two 1030nm lasers each focused by an 8mm lens. Powers of the beams are balanced with 0.03W in each beam. 42

3.17 Longitudinal forces along the z-axis for a horizontal dual-beam trap with an x-separation of 10μm and z-separation of 50μm between the foci. An 8μm diameter silica particle is trapped by two 1030nm lasers each focused by an 8mm lens. Powers of the beams are balanced with 0.03W in each beam. 43

3.18 Transverse forces along the x-axis for a horizontal dual-beam trap with an x-separation of 10μm and z-separation of 50μm between the foci. An 8μm diameter silica particle is trapped by two 1030nm lasers each focused by an 8mm lens. Powers of the beams are balanced with 0.03W in each beam. 43

LIST OF FIGURES – CONTINUED

Figure Page

3.19 Potential well in the longitudinal direction for an ideal horizontal dual-beam trap. Powers are balanced with 0.03W in each beam. 45

3.20 Potential well in the transverse direction for an ideal horizontal dual-beam trap. Powers are balanced with 0.03W in each beam. 46

3.21 An 8μm diameter silica particle dropped into an ideal horizontal dual-beam trap. Each line represents a different initial position with the same initial velocity, v_{term} 47

3.22 An 8μm diameter silica particle dropped into an ideal horizontal dual-beam trap. Each line represents a different initial position with initial longitudinal velocity set to zero. 48

4.1 A 532 nm wavelength laser beam is directed vertically into the vacuum chamber after passing through a telescope to create the vertical optical trap. 50

4.2 A schematic of the vertical optical trap for trapping particles in air. An expanded 532nm laser beam enters the bottom of the vacuum chamber passing through a 50mm focusing lens to create the optical trap. 50

4.3 Trapped soda lime glass particle (5-50 micron in diameter) in the vertical optical trap. A microscope slide sits on top of the focusing lens to collect particles that do not get trapped. 51

4.4 A photo of the microscope slide cantilever launcher on a tip/tilt stage. 53

4.5 Left: Launcher with reservoir and small drop hole. Right: Launcher with reservoir loosely placed in vacuum chamber for the horizontal dual-beam configuration. 54

4.6 The aluminum cantilever with milled reservoir and trenched channel. A small piezoelectric transducer is shown sandwiched between a ball-tip screw and the launching arm. 56

LIST OF FIGURES – CONTINUED

Figure Page

4.7 The final iteration of our aluminum cantilever launcher with control over movements in the horizontal plane for alignment above the trap focus. 57

4.8 Fundamental vibrational mode of a thin clamped bar. 58

4.9 Michelson interferometer constructed to test frequency of aluminum cantilever launcher. 59

4.10 Current tuning curve for 1030 nm laser diode (QLD-1030-250S, QPhotonics, LLC) at 25°C with current in mA along the horizontal axis and wavelength in nm along the vertical axis. 61

4.11 A schematic of our first horizontal dual-beam optical trap for trapping particles in air. A single 1030nm laser beam is split into two counter-propagating beams (B1 and B2) with a polarizing beam splitter (PBS) and balanced in power with a Babinet-compensator (BC). The beams enter the vacuum chamber and each pass through an 8mm aspheric lens. 63

4.12 A 5μm pinhole in an aluminum mount which is attached to an XYZ-translation stage that sits atop the vacuum chamber for dual-beam alignment. 65

4.13 Trapped soda lime glass particle (5-25 micron diameter) in horizontal dual-beam optical trap. 65

4.14 A schematic of our second horizontal dual-beam optical trap for trapping particles in air. Two 1030 nm laser beams (Laser 1 and Laser 2) enter the vacuum chamber and each pass through an 8 mm aspheric lens to create the trap. Laser 2 passes through a Babinet-compensator to change the polarization of the beam. 66

LIST OF FIGURES – CONTINUED

Figure Page

4.15 A schematic of our third horizontal dual-beam optical trap for trapping particles in air. Two 1030 nm laser beams (Laser 1 and Laser 2) pass through anamorphic prism pairs and polarization maintaing fibers. Beams then enter the vacuum chamber and pass through an 8 mm aspheric lens to create the trap. Laser 2 passes through a Babinet-compensator to change the polarization of the beam. A single plano-convex lens on an XYZ-stage serves as our fine control over separation of the two focal points inside the chamber. 68

4.16 A look inside the vacuum chamber with the aluminum cantilever launcher and two 8 mm aspheric lenses in place. Left: Top view. Right: Side view. 70

4.17 Example Image Report created from our 'Main Detection' MATLAB code. This example report was created with the spot of a HeNe laser beam focused by a 125mm lens. Every report includes a photo of the trapped particle (top left), horizontal (top right) and vertical (bottom left) intensity profiles of the trapped particle and text information about the time it took for a particle to become trapped, the horizontal and vertical radius as determined from the image and the image energy.......... 71

4.18 Time-lapse images of silica particles falling into the trap region. Z-separation is set to $-75\mu m$ during this capture. Each row is one second in time and each frame is $\frac{1}{6}s$. When particles interact with the laser beam they become bright white in the image.......... 73

4.19 Time-lapse images of silica particles falling into the trap region. Z-separation is set to $-50\mu m$ during this capture. Each row is one second in time and each frame is $\frac{1}{6}s$. When particles interact with the laser beam they become bright white in the image.......... 73

LIST OF FIGURES – CONTINUED

Figure Page

4.20 Image of loader inside vacuum chamber along the longitudinal axis of laser beams to use as a calibration measurement of μm/pixel with MATLAB tools. This calibration indicated $\sim 19\mu m$/pixel wide. 74

4.21 Four individual frames from Figure 4.18 of a silica particle remaining in the same position over time in images from top to bottom. The camera was shut off before more frames were captured. Z-separation is $\sim 75\mu m$. 75

4.22 Four individual frames from Figure 4.19 of a silica particle traveling through the trap in roughly the same position and then being lost over time in images from top to bottom. Z-separation is $\sim 50\mu m$. 75

5.1 An $8\mu m$ diameter silica particle is analyzed in 3 plots for no z-separation and no x-separation. Transverse forces, transverse potential well, and particle dynamics as the particle is dropped above the trap region with terminal velocity are shown. 78

5.2 An $8\mu m$ diameter silica particle is analyzed in 3 plots for no z-separation and $2.5\mu m$ x-separation. Transverse forces, transverse potential well, and particle dynamics as the particle is dropped above the trap region with terminal velocity are shown. 78

5.3 An $8\mu m$ diameter silica particle is analyzed in 3 plots for no z-separation and $5\mu m$ x-separation. Transverse forces, transverse potential well, and particle dynamics as the particle is dropped above the trap region with terminal velocity are shown. 79

5.4 An $8\mu m$ diameter silica particle is analyzed in 3 plots for no z-separation and $7.5\mu m$ x-separation. Transverse forces, transverse potential well, and particle dynamics as the particle is dropped above the trap region with terminal velocity are shown. 79

LIST OF FIGURES – CONTINUED

Figure Page

5.5 An 8μm diameter silica particle is analyzed in 3 plots for no z-separation and 10μm x-separation. Transverse forces, transverse potential well, and particle dynamics as the particle is dropped above the trap region with terminal velocity are shown. ... 80

5.6 An 8μm diameter silica particle is analyzed in 3 plots for 30μm z-separation and no x-separation. Transverse forces, transverse potential well, and particle dynamics as the particle is dropped above the trap region with terminal velocity are shown. ... 82

5.7 An 8μm diameter silica particle is analyzed in 3 plots for 30μm z-separation and 1μm x-separation. Longitudinal forces, longitudinal potential well, and particle dynamics as the particle is dropped above the trap region with 0 initial velocity are shown. ... 83

5.8 An 8μm diameter silica particle is analyzed in 3 plots for 30μm z-separation and 2μm x-separation. Longitudinal forces, longitudinal potential well, and particle dynamics as the particle is dropped above the trap region with 0 initial velocity are shown. ... 83

5.9 An 8μm diameter silica particle is analyzed in 3 plots for 30μm z-separation and 3μm x-separation. Longitudinal forces, longitudinal potential well, and particle dynamics as the particle is dropped above the trap region with 0 initial velocity are shown. ... 84

5.10 An 8μm diameter silica particle is analyzed in 3 plots for 30μm z-separation and 4μm x-separation. Longitudinal forces, longitudinal potential well, and particle dynamics as the particle is dropped above the trap region with 0 initial velocity are shown. ... 84

LIST OF FIGURES – CONTINUED

Figure Page

5.11 An $8\mu m$ diameter YAG particle is analyzed in 3 plots for 30 z-separation and no x-separation. Transverse forces, transverse potential well, and particle dynamics as the particle is dropped above the trap region with terminal velocity are shown. 86

5.12 An $8\mu m$ diameter YAG particle is analyzed in 3 plots for 30 z-separation and no x-separation. Longitudinal forces, longitudinal potential well, and particle dynamics as the particle is dropped above the trap region with 0 initial velocity are shown. 86

5.13 A $20\mu m$ diameter YAG particle is analyzed in 3 plots for $30\mu m$ z-separation and no x-separation. Transverse forces, transverse potential well, and particle dynamics as the particle is dropped above the trap region with terminal velocity are shown. 88

5.14 An $20\mu m$ diameter YAG particle is analyzed in 3 plots for $30\mu m$ z-separation and no x-separation. Transverse forces, transverse potential well, and particle dynamics as the particle is dropped above the trap region with 0 initial velocity are shown. 89

5.15 An $20\mu m$ diameter YAG particle is analyzed in 3 plots for $30\mu m$ z-separation and no x-separation. Longitudinal forces, longitudinal potential well, and particle dynamics as the particle is dropped above the trap region with 0 initial velocity are shown. 89

6.1 Left: Quadrant photodetector design. Right: Printed circuit boards for quadrant photodetector. 92

ABSTRACT

Ultra-high sensitivity acceleration and gryometric sensors have been proposed as optically levitated particles in ultra-high vacuum (UHV). Larger particles (10-30 microns in diameter) provide higher sensitivity, but they are difficult to trap in UHV without particle loss. To overcome the radiometric forces that lead to particle loss, rare earth (RE) ion dopants can be incorporated into the particles to enable solid-state laser cooling of the particles internal temperature. This thesis theoretically and experimentally explores development of optical traps designed for trapping and internally laser cooling large particles. The analysis focuses on dual-beam horizontal traps and the development of code to analyze dual-beam trap potentials and particle loading dynamics. Tolerance analysis, improved particle loader designs, and monitoring and automation of the loading process are investigated. The thesis provides a road map for achieving efficient optical trapping, cooling, and control of large particles.

INTRODUCTION

Optical Levitation

Optical levitation has been used since 1970 when Arthur Ashkin trapped the first particles at Bell Laboratories using a focused continuous wave laser beam [1–3]. Ashkin's groundbreaking work made it possible to use a 3-dimensional optical beam that would trap particles with only radiation forces. Now commonly known as optical tweezers, these traps are used to study atoms, molecules, variously sized dielectric particles, and even biological cells. Levitated particles in vacuum could also serve as ultra-high sensitivity sensors, with industry applications such as inertial navigation systems (accelerometers and gyroscopes) and time-keeping technology. The 3-dimensional ability to study forces with an optical trap is an improvement over current accelerometer technology. This technique would work well for space applications where there is no gravity. Particles in optical traps are also capable of precise gravity measurements [4, 5].

There are two popular types of optical tweezer traps for precision measurements: single and dual-beam. A single beam optical trap is usually a vertical trap that requires the force of gravity to create a stable trap. Dual-beam traps are typically horizontal in nature with counter-propagating laser beams that create the stable trap. Both trap types have been researched and will be discussed in this thesis.

Motivation

To achieve high levels of sensitivity for an accelerometer or gyroscope, large particles ($>> 1\mu m$) levitated in ultra-high vacuum work best. The current technique for levitating particles (particles $< 1\mu m$) in vacuum is to first trap them at atmospheric pressures and then pump down the pressure to high vacuum. Large levitated particles become unstable during the pump down to vacuum due the absorption of the trap laser causing internal heating of the particles and producing strong radiometric forces that kick the particles out of the trap. Therefore, finding a way to counteract this heating is essential to maintaining a stable trap during pump down to high vacuum.

Here the heating process is discussed in more detail. A trapped particle will always have a finite optical absorption. As such, the strong trapping laser intensity inside the particle will induce heating of the particle. Temperature rises can be so high as to melt down the particle [6]. At atmospheric pressures, the air or buffer gas surrounding the optically trapped particle conducts the heat away and the particle's temperature is on the order of the surrounding gas temperature. As the pressure is lowered, the conductive cooling of the gases decreases and the temperature of the particle increases. Gas molecules colliding with the particle carry away more kinetic energy than they had before the collision. Radiometric forces arise from temperature gradients on the surface of the sphere. Differential surface temperatures result in differential forces acting on the particle, which create instabilities that can result in the particle being kicked out of the trap. At ultra-high vacuum these forces diminish, but to get from trapping at atmosphere to ultra-high vacuum, the particle must go through the transition of strong radiometric forces [7–9].

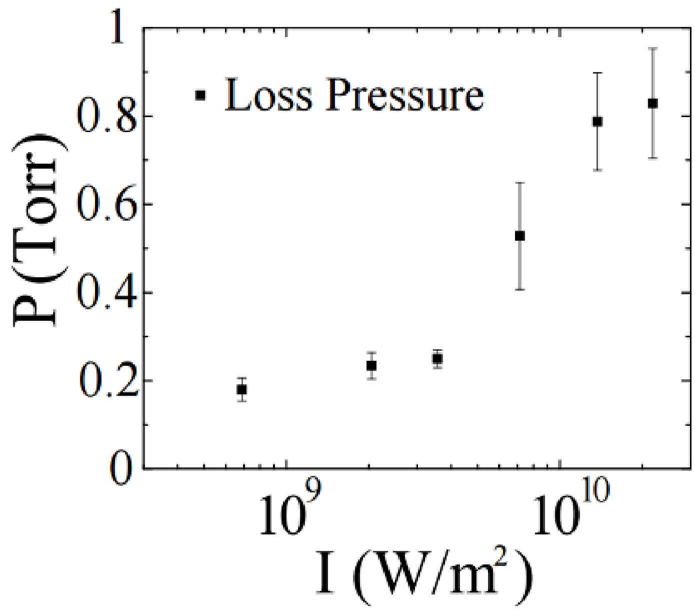

Figure 1.1: The average chamber pressure when 3 micron spherical particles are lost as a function of laser intensity. Each point represents the average loss pressure for 5 trapped particles at a given intensity. [7, 10]

The main result is losing the particle from the trap at a certain gas pressure while evacuating the trapping chamber. This is called the loss pressure. The loss pressure depends on the particle's size, shape, composition, and the laser intensity, as well as the other trapping parameters. Figure 1.1 shows the dependencies on laser intensity for a 3μm particle. The loss pressure increases rapidly with increasing laser intensities [7, 10].

To combat these instabilities, common solutions include reducing the trap intensity and trapping small particles. Our interest is in increased sensitivity of precision sensors for accelerometry or gyroscopes, which improves with large particles. Our solution to combat radiometric forces and the issues of loss pressure is to introduce rare-earth dopants into the fabrication of our particles and implement solid-state laser cooling.

Solid-state laser cooling is well known and will be discussed in detail in chapter 2. The first demonstration of cooling of trapped particles by solid-state laser cooling was from Barkers group with Yb^{3+}:YLF nanocrystals [11]. By keeping the particles relatively cool as the particle is transitioned from atmosphere to high-vacuum, the radiometric forces will be greatly reduced, hopefully to a level that particle loss on vacuum pump down will not be an issue.

Overview of Thesis

Chapter 2: *Background* will introduce optical trapping theory with an emphasis on the ray optics regime since we are concerned with large particles. It will also provide the basic theory of solid state laser cooling, and the rare-earth doped particles chosen for our analysis, experiments, and our trap wavelength. Chapter 3: *Theory of Dual-Beam Trapping and Tolerancing* goes through the steps of our theoretical analysis with an emphasis on the ray optics regime. Chapter 4: *Experiment* covers the details of the optical trapping experiment design and implementation, including the laser, particle launching methods, optical traps (vertical and horizontal dual-beam), our imaging methods, and automation techniques. Results from the theoretical analysis of chapter 3 are presented in chapter 5: *System Analysis*. Recommendations and future work are detailed in chapter 6: *Conclusions*.

BACKGROUND

Gaussian Beams

Most of the analysis provided in this thesis can be understood with fundamental optics. A Gaussian beam of monochromatic light with the fundamental transverse mode (TEM_{00}) serves as the preferred mode of the laser beams being described. Here we will conceptually define the common components of a Gaussian beam. Mathematical descriptions will be detailed in later sections and chapters.

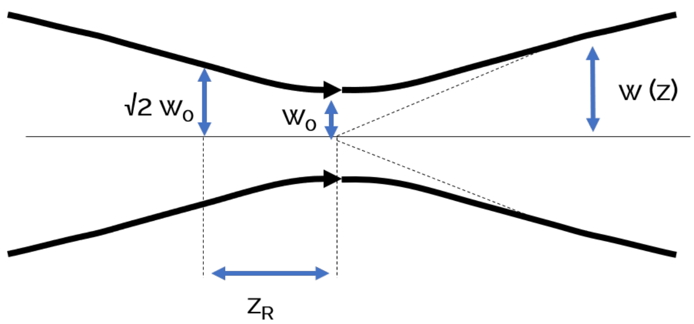

Figure 2.1: Gaussian beam parameters: w_0 - beam waist, $w(z)$ - beam width at a point z along the beam, z_R - a distance away from the beam waist where $w(z) = \sqrt{2}$ known as the Rayleigh range.

The beam waist (w_0) defines the shape of a Gaussian beam and is measured at the point of the beam's focus ($z = 0$). The waist is also the $\frac{1}{e^2}$ radius when looking at a cross-sectional image of the beam at $z = 0$. The radius of the beam at any given z-value along the beam is defined as $w(z)$ and changes with different wavelengths of light. At a point z_R away from the beam's waist, the radius of the beam is $\sqrt{2}w_0$. This distance (z_R) is known as the Rayleigh range. One final value that is not shown in the figure is the numerical aperture (NA). The NA is a unit-less number that defines the range of angles over which a system can accept or emit light.

Theory of Optical Trapping

Radiation pressure is simply the pressure exerted upon any surface due to the exchange of momentum between the object and the electromagnetic field. The best way to visualize this is to consider light hitting a mirror. When a flat laser beam strikes a mirror normal to its surface, the momentum of each incident photon is $\frac{h\nu}{c}$, where c is the speed of light in vacuum, h is Planck's constant, and ν is the frequency of the light reversed. Consider, a flux of photons, $\frac{P}{\hbar\nu}$ (photons per second) on the mirror surface, where P is the incident power. Due to reflection from the mirror, the photon flux creates a total change in momentum per unit time $\frac{2P}{c}$. By conservation of momentum, this produces a force of $\frac{2P}{c}$ on the mirror in the direction away from the incident beam.

In Ashkin's seminal paper on this subject, [1–3] he describes the radiation pressure on a particle due to a focused light beam. Ashkin showed that in addition to the longitudinal radiation forces exerted on a particle in the direction of the laser beam (either by absorption or reflection) there was an additional transverse radiation force on the particle towards the axis of the focused laser beam. These transverse restoring forces produce a two dimensional potential well about the center of the laser beam. By using two counter propagating focused laser beams, Ashkin showed that the longitudinal forces could roughly cancel and produce a potential well in the longitudinal direction and thus produce a three dimensional well for trapping particles.

This phenomenon is most easily described in the geometric optics regime, that holds when the radius of the particle is much larger than the wavelength of the pump laser (R $>>$ λ), which is the regime of interest when trapping large particles. For particles with radii less than or on the order of the wavelength of the trapping beam, optical trapping is also possible, though better described using Rayleigh (R << λ) and Mie (R $\sim$ λ) scattering theories because the ray optics description breaks down.

Geometric Optics Regime

In the geometric optics regime, where the particle radius, R, is much larger than the wavelength of light, λ, we can utilize ray optics to help in our descriptions of the radiation pressure force. We consider a sphere that is entirely refractive, ignoring reflective properties at this time [12, 13]. Figure 2.2 shows the sphere in the presence of a laser beam with two individual rays striking the sphere, a and b, equally displaced from the equator of the sphere.

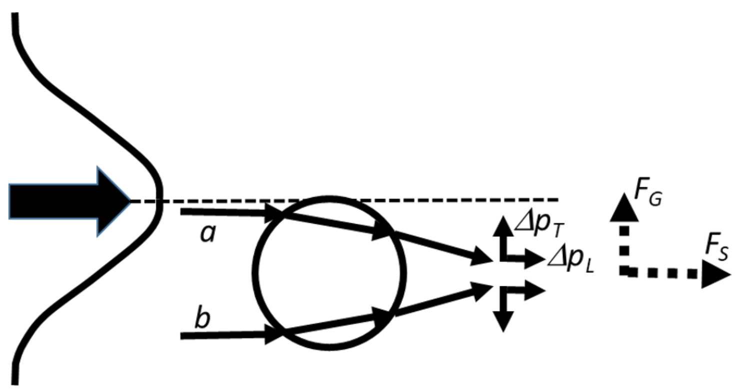

Figure 2.2: The ray tracing and momentum changes due to propagation of a laser beam with a strong intensity gradient of radius smaller than the particle diameter. The figure is similar to that of Ashkin's original paper [2]. The combination of the change in momentum per photon and the transverse gradient of the laser beam results in two net forces: a gradient force towards the beam axis (F_G) and a scattering force in the direction of the laser beams propagation (F_S).

The rays can be thought of as momentum vectors. If we track the photon's momentum along these two paths, we see that on the output, the a photon is deflected down, and the b photon is deflected up. To get the change in momentum imparted on the sphere by each photon, we subtract the output momentum vector of the photon from the input momentum vector. The two photons impart a change in momentum,

Δp_L, onto the sphere in the positive longitudinal direction. The momentum imparted per photon in the transverse direction, Δp_T, are equal and opposite.

However, if we consider the intensity of the laser beam, the photons per second with ray a, which is closer to the center of the beam, are much higher than the photons per second with ray b. Thus, net transverse force, F_G, due to the transverse gradient of the laser beam is towards the axis of the laser beam. The net force on a particle can be calculated by considering the force per photon for all possible rays and their respective photon fluxes due to the intensity gradient of the beam. This is done in a computer code, Optical Tweezers in Geometrical Optics (OTGO) developed by Agnese Callegari, et. al. [14]. The OTGO code takes reflections into account. The following section will provide details on OTGO and a theoretical analysis of our experimental setup.

Only when the sphere is centered on the laser beam's axis are the net transverse gradient forces zero. In all positions there is still a net longitudinal scattering force, F_S, in the direction of the laser beam. Thus, for a single laser beam passing through a particle, these combined forces will push the particle not only in the direction of the laser beam, but also towards the axis of the laser beam. This transverse gradient force acts as a restoring force to trap the particle along the axis of the laser beam.

Another representation using ray optics from Ashkin is pictured in Figure 2.3. A laser beam is propagating left to right and is focused at the center of the dotted red circle. The particle is acting as a lens and will be trapped when it is at the focus, as shown by the middle image, where forces (momentum changes) are balanced, while ignoring gravity. When the particle moves axially along the beam (left image in Figure 2.3), it focuses the light causing the momentum in the direction of propagation of the outgoing photons to be greater than the incoming photons. The resulting force brings the particle back to the focal point. When the particle moves radially to the beam, momentum of the outgoing photons will increase in the direction of motion from the beam's axis and create a restoring force pushing the particle back to the focus. This example is possible when scattering forces along the propagation direction are negligible. A 3D optical trap is possible due to the focused laser beam [12, 13], but this picture does not include surface reflections.

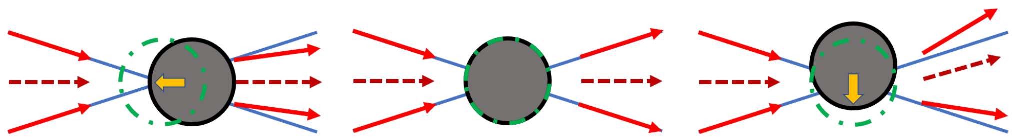

Figure 2.3: Left: A particle is displaced axially along the propagation of the laser. Middle: A particle is trapped at the focus of the laser. Right: A particle is displaced radially above the focus of the laser. Restoring forces are shown inside the dotted-green circles.

If a focused laser beam was pointed upward in a gravitational field (pointing downward), and the optical power level and focused beam waist are appropriately chosen, a stable point can be found above the focal point of the beam where the gravitational force and the scattering force balance. Above and below this point, either the gravitational force or the scattering force dominates, resulting in a restoring force back to the balance point. Thus, a three dimensional gravitational vertical optical trap can be achieved. This type of trap is also known as an optical levitation trap.

If two counter-propagating focused beams are used, the longitudinal forces of the two beams are in opposite directions. If the two beams have the same foci, the scattering forces would cancel at all positions in an ideal scenario, where there is perfect alignment (no separation of beams), and the gradient forces described above would form a longitudinal trap. This ideal scenario would be hard to achieve in the lab because it would require identical laser beams with identical powers and identical lenses. For example, it is possible to order two 'identical' laser diodes, from the same place, at the same time, but when comparing the two specification sheets it is evident the manufacturing produced slightly different outputs with slightly different operating powers or currents. A non-ideal scenario would have the scattering forces dominate and a trap would no longer be possible. However, if a separation is introduced between the foci, as shown in Figure 2.4, the scattering forces don't need to cancel, but instead help to form a longitudinal trap. For either beam, the scattering forces are strongest at the beam's focus. At the right propagating beam's focus (grey), the scattering force of the right propagating beam is greater than the opposite scattering forces of the left propagating beam (black) at this same point, since it is away from its focus. The result is that a particle at the focus of the right propagating beam's focus would have a net force to the right. Likewise, particles at the focus of the left propagating beam would have a net force to the left. At the center point between the two foci, the forces cancel. This results in a stable longitudinal trap of the particle. If there is an imbalance in power or waist of the two beams, the balance point will shift, but a stable trap can still form.

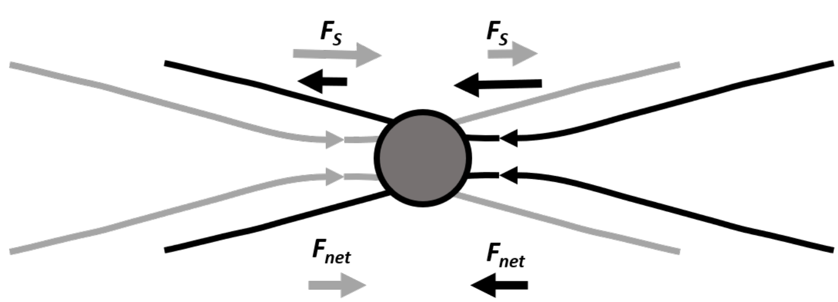

Figure 2.4: Two counter-propagating focused laser beams for an optical trap.

Rayleigh Regime

For the Rayleigh regime (R << λ) we can no longer use geometric optics in our descriptions. The particle itself can be thought of as a dipole and the dipole forces that result in trapping can be calculated analytically [15]. Following the formulas from [15], the optical forces are shown below.

A particle with radius R is illuminated by a linearly polarized Gaussian laser beam along the z-axis with a minimum waist, w_0 at $z = 0$. The beam radius goes as

$$w(z) = w_0[1 + (\frac{\lambda z}{\pi w_0^2})^2]^{\frac{1}{2}}, \tag{2.1}$$

where λ is the wavelength of light. The Rayleigh range (z_R) is given by

$$z_R = \frac{\pi w_0^2}{\lambda_{md}} \tag{2.2}$$

and is defined as the distance over which the radius increases by a factor of $\sqrt{2}$. The intensity of the Gaussian beam is

$$I(x, y, z) = I_0 e^{-2(x^2+y^2)/w(z)^2} = \frac{2P}{\pi w(z)^2} e^{-2(x^2+y^2)/w(z)^2}, \tag{2.3}$$

where P is the power of the laser beam.

As with geometrical optics, the total force can be split into two components: the scattering force, $\overrightarrow{F}_{scat}$, and the gradient force, $\overrightarrow{F}_{grad}$. The scattering force is in the direction of the laser beam while the gradient force is proportional to the gradient of the intensity of the laser beam. Both forces, $\overrightarrow{F}_{scat}$ and $\overrightarrow{F}_{grad}$, are shown here:

$$\overrightarrow{F}_{scat} = \frac{128\pi^5 r^6}{3c\lambda^4}(\frac{m^2-1}{m^2+2})^2 I\hat{z} \tag{2.4}$$

$$\overrightarrow{F}_{grad} = \frac{2\pi n_{md} r^3}{c}(\frac{m^2-1}{m^2+2})^2 \nabla I \tag{2.5}$$

When the gradient force is greater than the scattering force, a stable optical trap is formed. Chapter 3 goes into detail regarding MATLAB code we developed for an optical trap in the Rayleigh regime.

Mie Regime

In the Mie regime, Lorentz-Mie theory is used. The necessary mathematical calculations can be quite complex. MATLAB code was inherited from colleague, Dr. David Atherton, that was developed to model the Mie regime by following [16] from Christian Mätzler. However, an analysis in the Mie regime is not included in this thesis.

Theory of Laser Cooling

Although this thesis has a primary focus on understanding optical traps, the ultimate goal of the project (beyond this thesis) is to reduce loss pressure during pump down to vacuum by using rare-earth doped particles. Included here is the theory for cooling in bulk materials and the initial experiments carried out in collaboration with members of Dr. Charles Thiel's research group that provides the foundation for future experiments.

Bulk Cooling Theory

Solid-state laser cooling of rare-earth doped host materials (crystals and glasses) has previously been realized by several researchers in bulk host materials [17,18]. The cooling results from pumping the rare-earth doped materials with photons that have less energy than the photons that are emitted by fluorescence. This process is possible due to vibrational modes of the host material, which populate higher energy levels of the ground and excited state manifolds. The net release of energy reduces the internal temperature of the material.

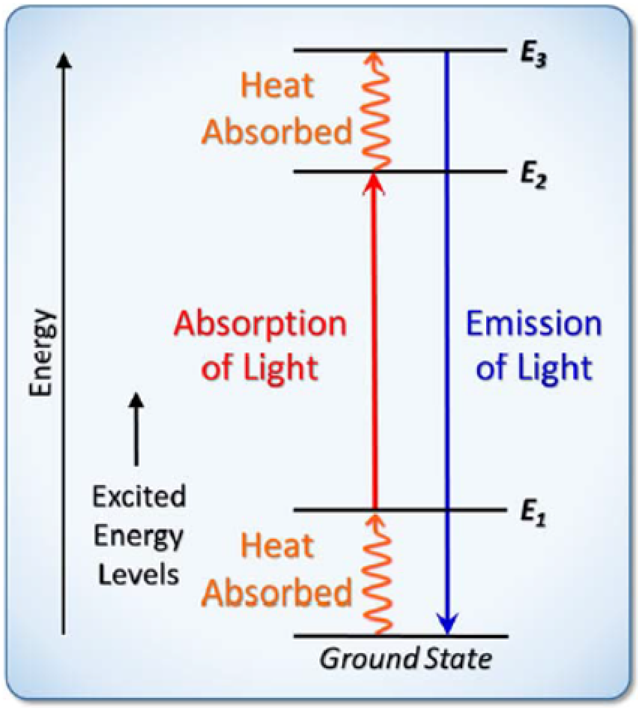

Figure 2.5: Basic concept of solid-state (anti-Stokes) laser cooling. The absorbed light from a thermally excited ground state level to the lowest excited state level and subsequent emission from a thermally excited state level to a lower ground state level results in a net loss in energy from the material.

The appropriate wavelength must be chosen within the absorption bands of the rare-earth dopant. Figure 2.5 shows a simplified model of solid-state laser cooling. A laser is used to excite ions from the thermally excited levels of the ground state to the lowest level of the excited state. With a choice of appropriate material, rapid thermalization of the excited state populates thermally excited upper state levels, which can then decay to the ground state, on average, to levels below the initial level that was excited by the laser. Therefore, the photon emitted contains more energy than the excitation photon, which results in a net removal of energy. Rare-earth ions that are good for laser cooling have an energy gap between the ground state and the first electronic excited state that can absorb the available thermal energy in the material in a given temperature range and have long-lived excited states that decay optically with small quantum defect, such as thulium at $2\mu m$, erbium at $1.5\mu m$, and ytterbium at $1\mu m$ [17, 18].

Bulk Cooling Demonstration of Yb:YAG The following work was part of our project but was carried out by other members of the research project at Montana State University (MSU). It is included here because it lays the foundation for the cooling experiments that will be done with particles in the optical trap. It was decided to focus efforts on ytterbium-doped yttrium aluminum garnet (Yb:YAG) particles. To demonstrate the potential for anti-Stokes cooling in Yb:YAG particles, a bulk 1mm diameter crystal rod was first used. This work was completed by Tino Woodburn and Jason Carr in Dr. Charles Thiel's lab in the MSU Physics Department [19].

A standard silicon CCD camera with interference filters was used to create a two-color hyperspectral imaging system to observe the laser excitation at 1030nm and material fluorescence at 950nm. Figure 2.6 shows these efforts along with a thermal image of the rod when a 200mW laser was tuned to resonantly excited the Yb^{3+} ions. The ambient temperature in the room was 74°F and as shown in the far right panel, no significant observable heating was observed. The observed width of the resonance was 2-3nm [20].

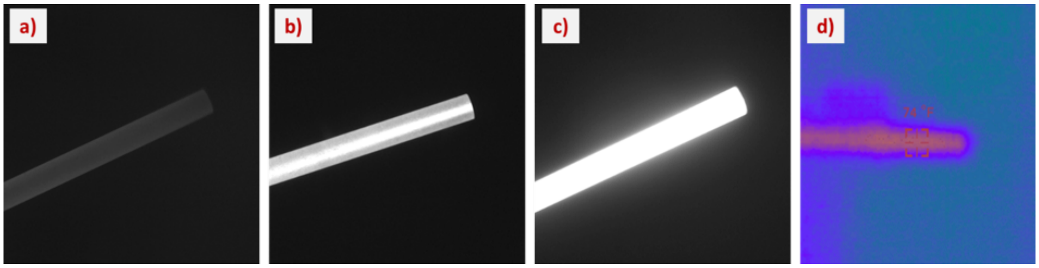

Figure 2.6: Imaging of Yb^{3+}-doped YAG crystals under laser excitation traveling down the center of the rod. a) Yb^{3+}:YAG single crystal rod (1 mm diameter) under laser excitation by 200 mW of non-resonant laser light at 1040 nm as seen through a 950nm filter. Minimal fluorescence is observed. b) Observation of 950 nm anti-Stokes fluorescence from Yb^{3+} ions as laser is tuned near resonance at 1030 nm. c) Strong anti-Stokes emission observed when laser is tuned to peak of resonance at 1030 nm. d) Thermal image of crystal with 200 mW of on-resonance 1030 nm laser light, demonstrating no significant heating of crystal relative to ambient temperature (74°F) even when laser light is strongly absorbed. These measurements were done by Tino Woodburn and Jason Carr in Dr. Charles Thiel's lab.

Fabrication of Doped Particles

Fabrication methods have been developed and carried out by Dr. Charles Thiel and Tino Woodburn to produce Yb:YAG particles that are large in size (5-30 microns) [19]. Figure 2.7 shows SEM images of Yb:YAG particles that have been fabricated. In addition, fabrication methods for other materials that could be utilized for optical traps are being explored. Figure 2.8 shows birefringent vaterite crystals ($CaCO_3$) with sizes ranging from 1-30 microns. These particles have been successfully doped with the rare-earth ion Eu^{3+}. The right panel in the figure shows the visible fluorescence marker.

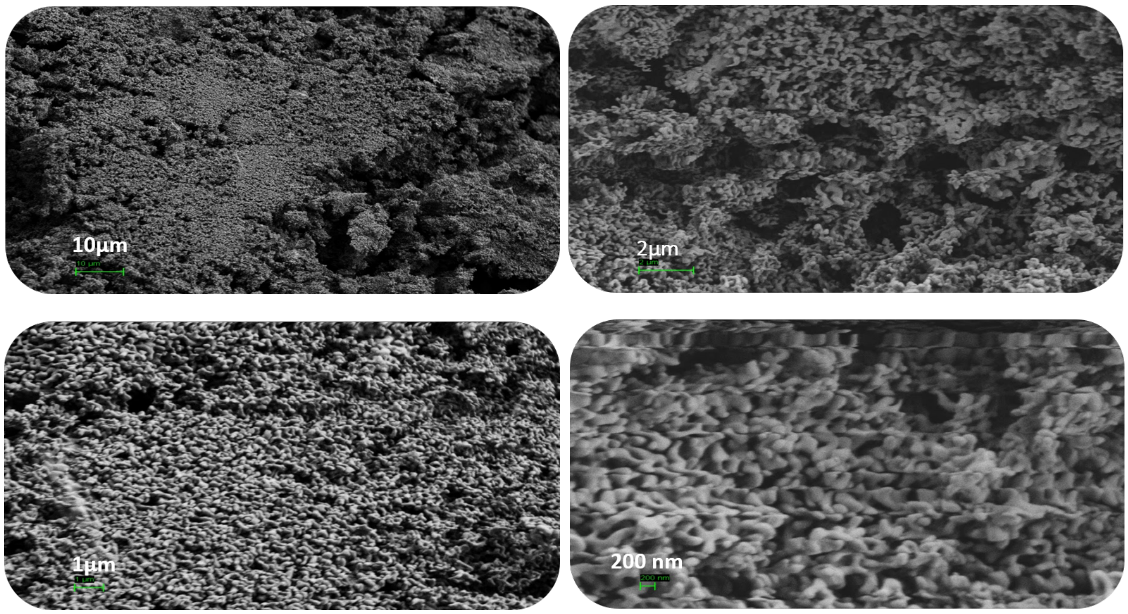

Figure 2.7: Yb:YAG particles fabricated in Dr. Charles Thiel's lab. Top Left: 3240x Magnification Yb:YAG, Scale $10\mu m$. Top Right: 18560x Magnification Yb:YAG, Scale $2\mu m$. Bottom Left: 21560x Magnification Yb:YAG, Scale $1\mu m$. Bottom Right: 49310x Magnification Yb:YAG, Scale 200nm.

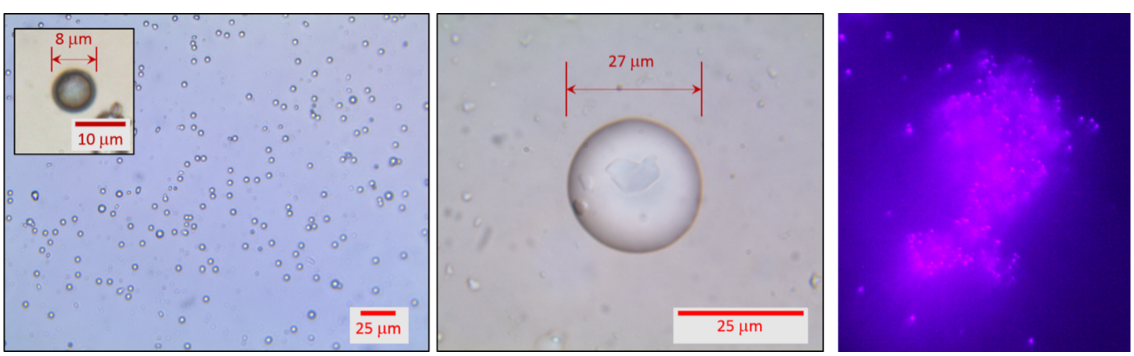

Figure 2.8: Examples of spherical particles of birefringent vaterite crystals ($CaCO_3$) fabricated and characterized at MSU by Tino Woodburn and Dr. Charles Thiel. Left: Typical particles produced with sizes in the 1 to 10 micron size range. Middle: Example of larger 30 micron diameter vaterite particle produced by increasing growth time. Right: Example fluorescence image of rare-earth-doped vaterite particles produced with Eu^{3+} ions used as the fluorescence marker, demonstrating the ability to dope the vaterite particles with rare-earth ions.

Thermometry

As a precursor to the method we would eventually use to observe the anti-Stokes cooling in trapped particles, a simple setup was created by Tino Woodburn, Jason Carr, and Dr. Charles Thiel to test the ability to measure the temperature of a bulk crystal (Yb:YAG) through fluorescence thermometry. The fluorescence of each transition depends on relative level populations determined by the Boltzmann distribution.

The ratio of Yb^{3+} fluorescence for two different transitions was measured while pumping at the 1030nm cooling transition. Two 10nm band-pass filters centered at 940nm and 970nm were used. Figure 2.9 shows the experimental setup with results in Figure 2.10. With a simple setup and calibration in the bulk materials, the temperature of trapped particles can be measured using this technique to within a few degrees. Chapter 6 will comment on the future work of the cooling experiments.

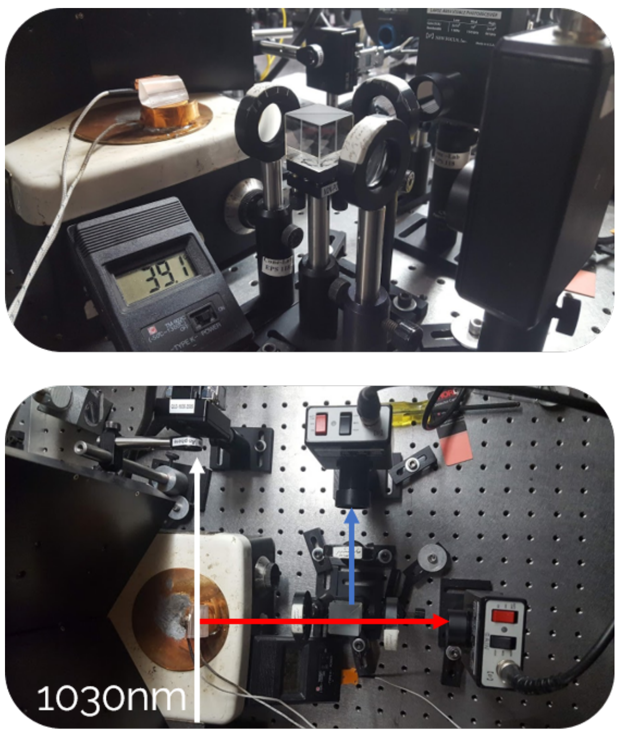

Figure 2.9: Optical thermometry setup for a bulk Yb:YAG crystal Setup by Jason Carr, Tino Woodburn, and Dr. Charles Thiel for calibration of fluorescence ratios as a function of temperature.

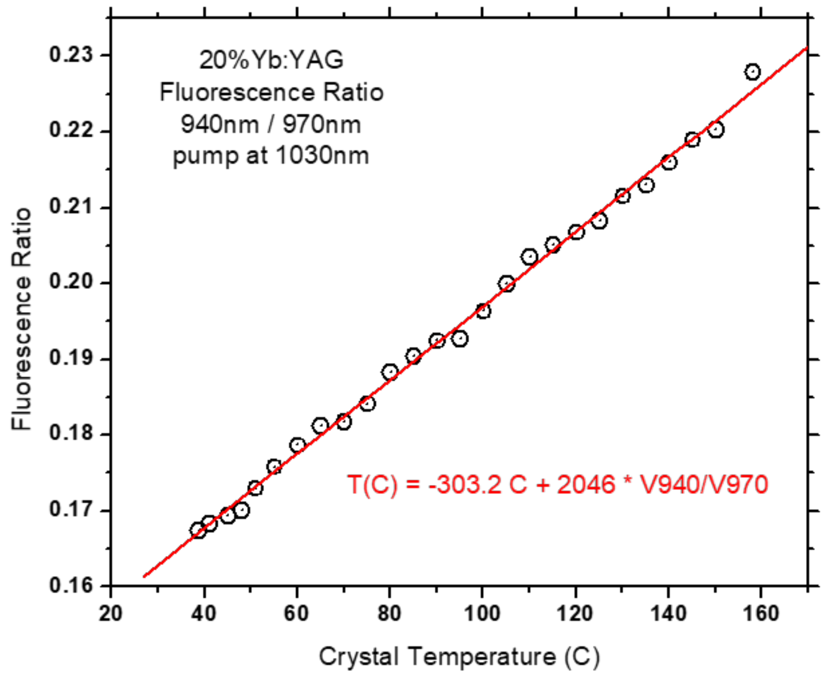

Figure 2.10: Results from fluorescence thermometry experiment carried out by Tino Woodburn, Jason Carr, and Dr. Charles Thiel showing a linear relationship of the fluorescence ratio above room temperature.

THEORY OF DUAL-BEAM TRAPPING AND TOLERANCING

Rayleigh Regime

Background

Colleague Dr. David Atherton studied optical traps in the Rayleigh and Mie regimes under Dr. Andrew Geraci at the University of Nevada, Reno. In an effort to understand the theory behind optical traps we began by using MATLAB code that was inherited from Atherton and used for his dissertation [10]. The goal for using this code was to be able to recreate plots that Atherton produced and gain a detailed understanding of how the overall system works together. In his dissertation, Atherton focused on a single beam analysis in the axial direction by varying the numerical aperture (NA) values and a dual-beam analysis for axial separation with varying waist sizes in the Rayleigh regime. The inherited code was only for a single beam in the Rayleigh regime and did not include a dependence on the force of gravity. From this code, it was unclear how his dual-beam scenarios were created for his dissertation. This is where our theoretical analysis begins.

Modifications and Additions to Inherited Code

Figure 3.1 shows the axial and transverse plots from the inherited MATLAB code for a 150nm glass particle with a 3mW 780nm laser. Only total force in a given direction is plotted, which is what was seen throughout Atherton's dissertation [10].

The main modification to this code was to make a horizontal dual-beam trap with a dependence on the force of gravity in the transverse direction (not originally present). This inherited MATLAB code was a good starting point, but it was incomplete in what it was capable of doing, visually uninformative, and there was limited documentation on how the code was written, which made continued modifications difficult. We decided to no longer use this code and instead wrote a new program.

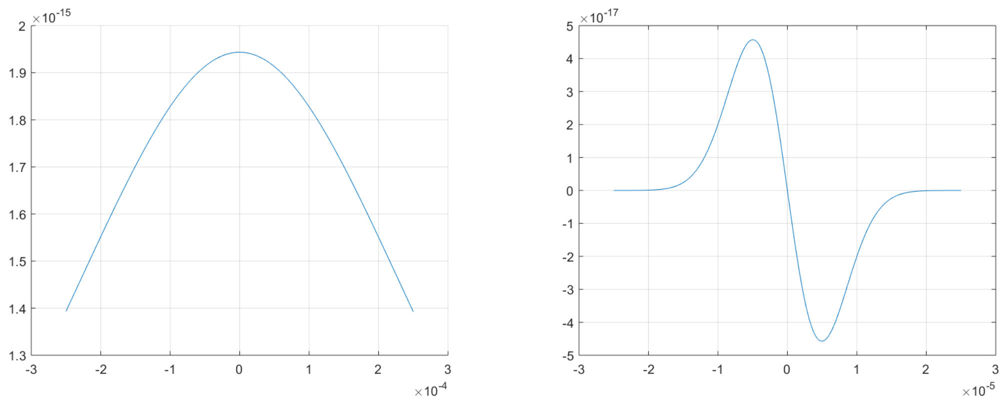

Figure 3.1: Forces in the axial (left) and transverse (right) directions from the inherited MATLAB code. Position in meters is along the horizontal axis with force in Newtons along the vertical axis.

New Rayleigh Regime Code

New code for the Rayleigh regime was written in MATLAB by directly following the equations in [15] to simulate a horizontal dual-beam trap. A single beam is described in the paper [15], and when implemented in MATLAB, the second beam is made to be negative along the z-direction to represent its counter-propagating nature. This new code also included the ability to separate the beams along the axial direction with a *z-separation* (z_{sep}) parameter that moves beam-1 $\frac{-z_{sep}}{2}$ and moves beam-2 $\frac{z_{sep}}{2}$. Atherton's dissertation commented on scenarios with an axial separation which is why we knew this would be an important piece of code to implement.

Figure 3.2 shows both the z and x-directions on a plot for no separation of the 2.2W 1064nm laser beams and a 2μm silica particle. The bottom plot in figure 3.2 is zoomed in to see the remaining forces because the scattering forces dominate under these conditions.

Throughout this chapter the legend on each plot will identify the forces from each laser beam by following the descriptions in table 3.1, unless otherwise noted.

Table 3.1: Plot legend descriptions

Legend Entry	**Description**
F grad z1	Gradient force in z-direction from beam 1
F grad z2	Gradient force in z-direction from beam 2
F scat z1	Scattering force in z-direction from beam 1
F scat z2	Scattering force in z-direction from beam 2
F total z	Sum of scattering forces and gradient forces in z-direction
F grav x	Force of gravity in x-direction
F grad x1	Gradient force in x-direction from beam 1
F grad x2	Gradient force in x-direction from beam 2
F total x	Sum of gradient forces in x-direction and the force of gravity

Figure 3.3 shows two plots with z-separation of $10\mu m$ in the Rayleigh regime. The plot on the right is zoomed in from the plot on the left. In this code, beam 2 is defined to be focused at $z = z_{sep}$ and comes from positive z. For any separation in the z-direction, there will be an effect in the x-direction. This code does not tie the two directions together, therefore a z-separation does not produce an effect in the x-direction.

Balancing beam powers and modes in practice is very difficult. A slight imbalance for $z_{sep} = 0$ will spoil the trap, as the scattering forces will dominate. The introduction of z_{sep} alleviates this problem. The opposite scattering force now forms the trap in the axial direction. The gradient forces are negligible as shown in the zoomed in plot in Figure 3.3.

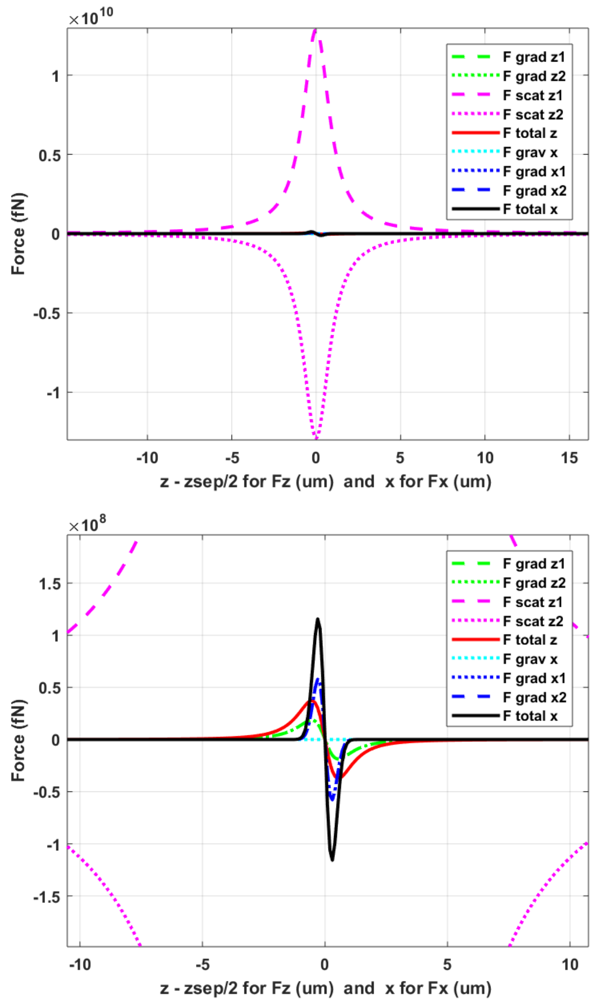

Figure 3.2: Trapping forces in the z and x-directions for a horizontal dual-beam trap with no z-separation in the Rayleigh regime for a new MATLAB program following [15] directly. The bottom plot is a zoomed in view of the top plot for a $2\mu m$ silica particle focused by a 2.2W 1064nm laser.

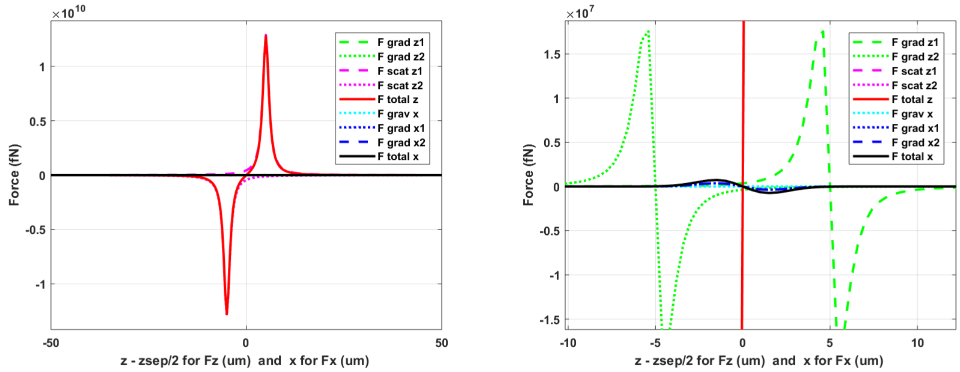

Figure 3.3: The new Rayleigh code with z-separation defined as $10\mu m$. A $2\mu m$ silica particle trapped by 2.2W of 1064nm laser light is shown in both plots. The right plot is a zoomed in view of the left plot. Note the scale differences for force in each plot.

These Rayleigh codes primarily served as a foundation to understanding all the forces involved in an optical trap and what will need to be included in a theoretical analysis. This thesis does not focus on small particles with sizes in the Rayleigh regime, but large particles in the geometric optics regime. The next section will describe how the dual-beam and z_{sep} are implemented in more detail in the geometric optics regime.

Optical Tweezers in Geometrical Optics (OTGO)

Background

Optical Tweezers in Geometrical Optics (OTGO) is a complete MATLAB software package that performs the calculation of optical forces in the geometric optics regime. The entire toolbox is available for download. An updated version of OTGO called Optical Tweezers Software (OTS) is also available for download [21]. OTS uses OTGO as its foundation and includes new example codes. We primarily used the original OTGO for the theoretical analysis in this thesis.

OTGO calculates the total force of a laser beam focused onto a particle by summing all of the rays' contributions. Equation 3.1 shows that the force of an individual ray of unit intensity is the sum of the scattering force component and the gradient force component of that ray.

$$\overrightarrow{F}_{ray} = \overrightarrow{F}_{ray,s} + \overrightarrow{F}_{ray,g} \tag{3.1}$$

The force of a beam in equation 3.2 is when all rays are summed together, weighted by the intensity of the beam.

$$\overrightarrow{F}_{beam} = \sum_{m} \overrightarrow{F}^{(m)}_{ray} I^G(\rho_m) \tag{3.2}$$

OTGO utilizes the intensity profile of a Gaussian laser beam at its waist, which follows equation 3.3,

$$I^G(\rho) = I_0 e^{-\frac{\rho^2}{2w_0^2}} \tag{3.3}$$

where ρ is the radial coordinate, w_o is the beam waist, $I_0 = \frac{1}{2}c\epsilon_0 n_m E_0^2$ is the beam intensity at $\rho = 0$, ϵ_0 is the dielectric permittivity of vacuum, and E_0 is the modulus of the electric field magnitude at $\rho = 0$ [14].

The OTGO software package provides example code and this is where the analysis begins. Included code, *efficiencies_beam.m*, calculates and plots the trapping efficiencies corresponding to the scattering of a focused laser beam on a spherical particle as a function of the position of the particle with respect to the focal point. The trapping efficiency for an entire beam is defined by equation 3.4,

$$Q_{beam} = \frac{c}{n_i P_{beam}} \mid F_{beam} \mid, \tag{3.4}$$

where P_{beam} is the power of the beam, c is the speed of light, and n_i is the index of refraction of the surrounding medium.

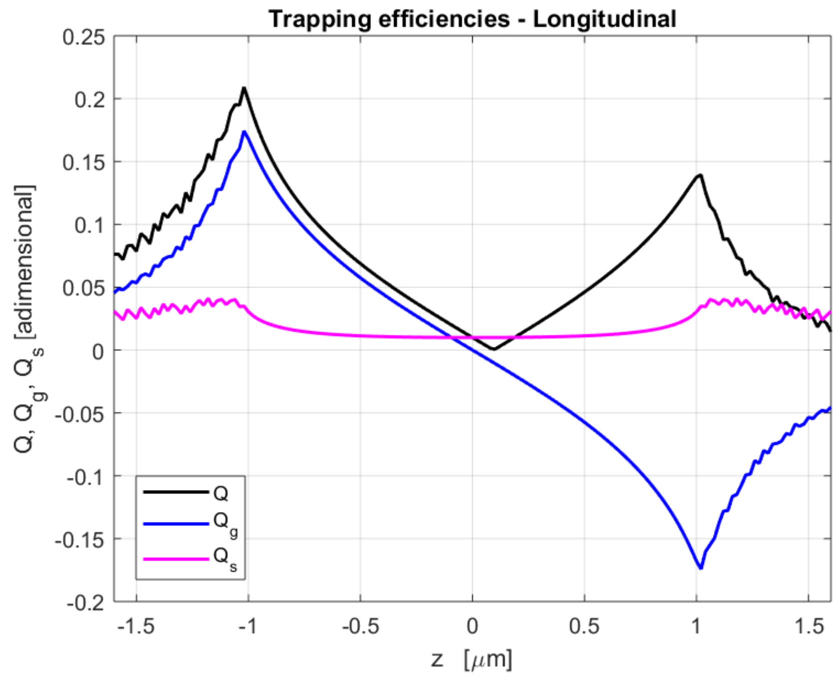

Figure 3.4: Trapping efficiencies in the longitudinal direction of the original OTGO *efficiencies_beam.m* example file. The scattering trapping efficiency (Q_s, solid pink line) and gradient trapping efficiency (Q_g, solid blue line) are shown along with the total trapping efficiency (Q, solid black line). All efficiencies are directed along the z-axis.

Callegari, et. al describe the trapping efficiency as a way to quantify the effectiveness of the transfer of momentum from the beam to the particle. Like forces, trapping efficiencies can also be broken into a scattering component and a gradient component, Q_s and Q_g. Figure 3.4 shows the trapping efficiencies in the longitudinal direction, (Q, Q_s, Q_g) which is along the beam's direction of propagation, the z-axis. Figure 3.5 shows the transverse direction that is defined along the x-axis. It is important to note that in the OTGO plot in Figure 3.5, Q_s is along the longitudinal direction as described by the authors [14]. The trapping efficiencies in the transverse direction dominate the scattering trapping efficiency in the longitudinal direction.

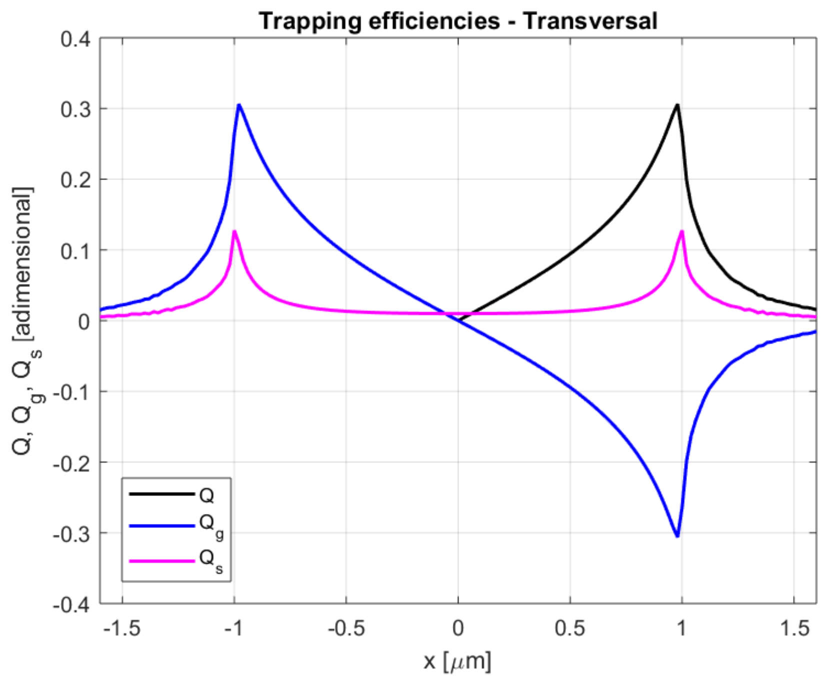

Figure 3.5: Trapping efficiencies in the transverse direction of the original OTGO *efficiencies_beam.m* example file. The scattering trapping efficiency (Q_s, solid pink line) and gradient trapping efficiency (Q_g, solid blue line) are shown along with the total trapping efficiency (Q, solid black line). The gradient trapping efficiency and total trapping efficiency are directed along the x-axis while the scattering trapping efficiency is directed along the z-axis.

Both plots show a single laser beam (no specified wavelength) with a power of 5 mW being focused by a 10 μm focal length lens with NA = 1.3. The 2 μm diameter glass particle (np = 1.5) is in water (nm = 1.33) and gravity dependence is not included in the example code.

efficiencies_beam.m served as the foundation for our theory analysis in the geometric optics regime. Modifying this code was done in stages and reflected the overall progression of the project. First, work-space modifications were made to make the code more user-friendly and informative. Then new additions were made to reflect the trapping scenarios being explored in the lab. Both sets of changes will be described in detail in the following sections.

Work-space Modifications to OTGO

Modifications to *efficiencies_beam.m* began by defining the axes to model a three-dimensional trap. A vertical trap and a horizontal trap will have axes that differ slightly. For a vertical trap, the axes are defined as follows: z is the longitudinal axis along the propagation direction of the laser (vertical and includes gravity), x and y are the horizontal transverse axes parallel to the optical table and orthogonal to each other. For a horizontal dual-beam trap, the axes are defined as follows: z is the longitudinal axis along the propagation direction of the laser (parallel to the optical table), x is the vertical transverse axis (includes gravity), and y is the horizontal transverse axis (parallel to the optical table and orthogonal to the z axis).

The example code calculates and plots trapping efficiencies, but these values are not very intuitive. Therefore the plots were changed to no longer show trapping efficiencies, but instead forces, which could then be used to calculate potential wells and used in dynamic studies of particle motion. Calculating the forces was required in order to find the trapping efficiencies which made the change very straightforward to implement. On the transverse direction plot the scattering force in the z-direction has been removed.

The resolution of the final plots is dictated by each axis definition and the azimuthal (*Nphi*) and radial (*Nr*) divisions. The azimuthal and radial divisions are parameters for the representation of the beam as a set of rays. *Nr* is the number of concentric circles with equal thickness up to size of the iris aperture with *Nphi* regularly spaced points around each circle. Understanding these values was key to obtaining quality plots and working in a timely manner. One of the general work-space modifications was in the definition of each axis.

The z-axis was originally defined as $z =$ *(-1.6:0.02:1.6)*R*, where R is the radius of the particle and 0.02 is the step size. Under these conditions, the program can take minutes to run. New parameters, *z_max_factor*, *Nxz*, and *dz=z_max_factor/Nxz*, were added to make the definition of the axis more general. The new z-axis is defined as *z = (-z_max_factor:dz:z_max_factor)*R*. The x-axis was defined in a similar way. On a daily basis, it is not productive to have the program take minutes to run for each trial. Lowering *Nxz* allows the program to be run in seconds while still providing an accurate plot. Manipulating the *max_factors* is also very important when trying to obtain the best quality of a plot, especially as more complicated scenarios are investigated.

Most values in the provided example code were hard-wired in and key variables were not included, such as the force of gravity on the particle. Therefore, addressing the *Parameter* work-space was key. Since the force of gravity was missing altogether, it was one of the first items added and included in the plots. This addition included the need for a *mass* equation that depended on the density of the particle's material (ρ_p) which follows equation 3.5,

$$mass = \frac{4}{3}\pi R^3 \rho_p, \tag{3.5}$$

where R is the radius of the particle. Additional variables were included for the ability to change between material types, such as silica and different crystals, by setting ρ_p equal to ρ_{Si} or $\rho_{crystal}$. In Chapter 5, an analysis for YAG crystals (ρ_{YAG}) will be discussed. Different materials will affect the ability to create a stable trap, which is why this is so essential to the code.

Figure 3.6 shows the trapping forces along the longitudinal direction with the addition of the force of gravity. Figure 3.7 shows the trapping forces along the transverse direction with the addition of the force of gravity and the removal of the scattering forces along the z-direction. Gravity will only be included in one direction

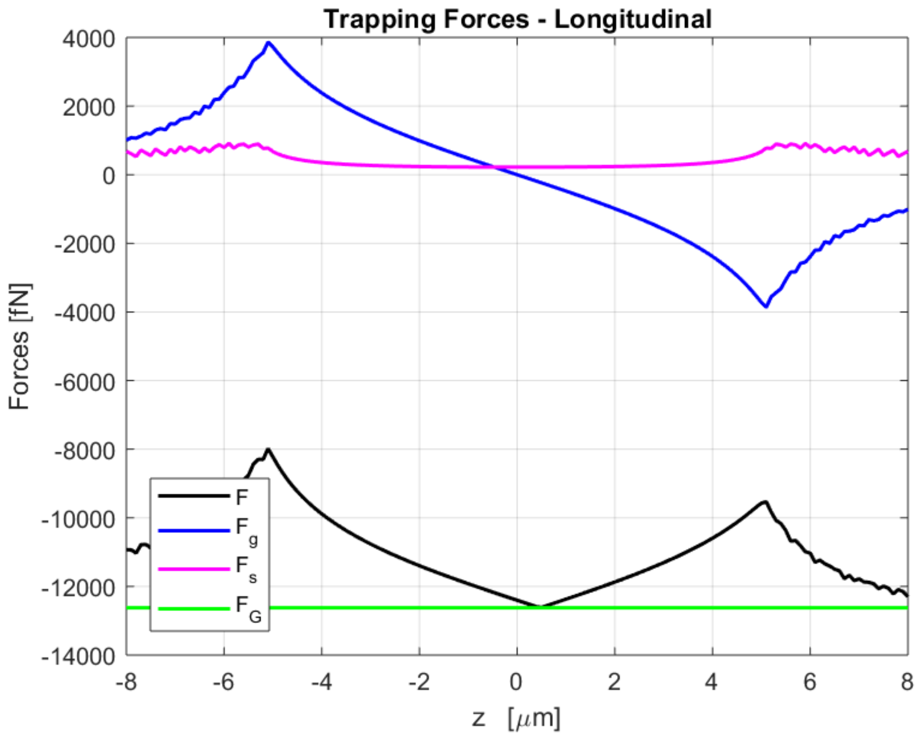

Figure 3.6: Trapping forces in the longitudinal direction of the original OTGO *efficiencies_beam.m* example file. The scattering force (F_s, solid pink line) and gradient force (F_g, solid blue line) are shown along with the total force, including the force of gravity (F, solid black line). The force of gravity (F_G, solid green line) has been added.

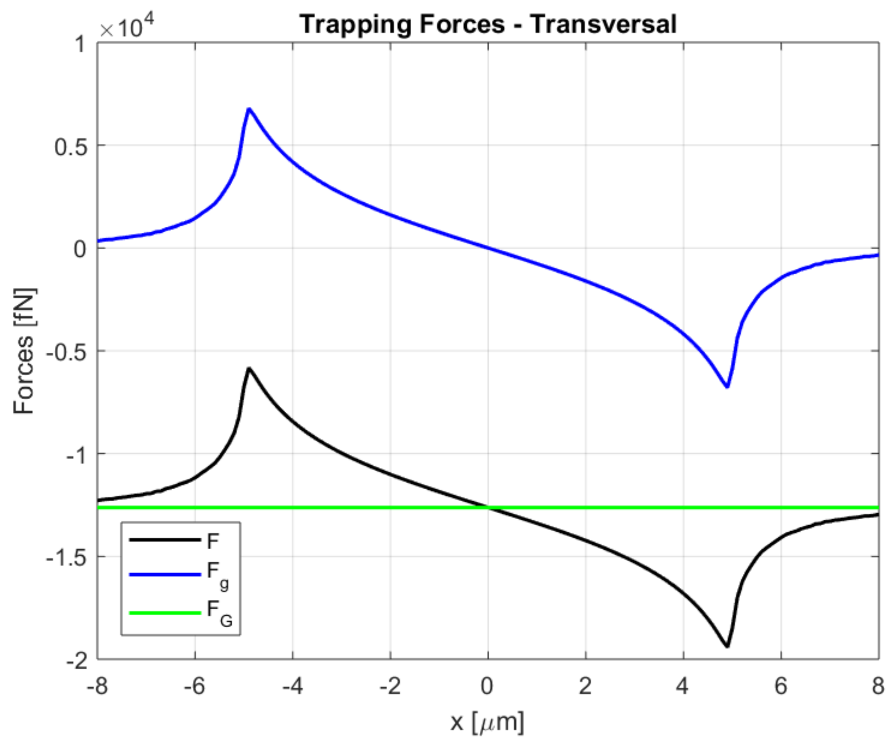

Figure 3.7: Trapping forces in the transverse direction of the original OTGO *efficiencies_beam.m* example file. The scattering force (F_s, solid pink line) and the gradient force (F_g, solid blue line) are shown along with the total trapping force (F, solid black line), including the force of gravity. The force of gravity (F_G, solid green line) has been added.

for any given trapping scenario, but is shown in both directions here to highlight that it does make an impact in each direction and must be included to get a complete picture.

OTGO models the individual rays as if they are part of a Gaussian beam of waist w_L focused to a spot by the lens of focal length *f*, through an aperture of diameter D, to a spot f away. However, the original OTGO code allowed the beam waist at the lens, w_L, and the iris diameter to be set independently. This arbitrary nature of the code could lead to non-physical situations being modeled. In order to have a Gaussian beam shape at the particle ($z = 0$), it is important that the iris aperture not significantly clip the beam at the lens.

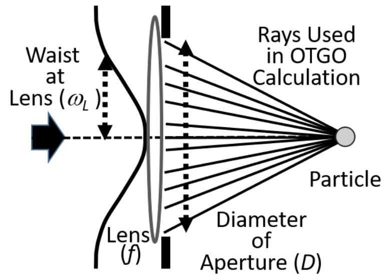

Figure 3.8: Individual rays modeled after parameter definitions defined in OTGO code.

In order to address this beam construction problem, the iris aperture, D, was chosen to be $D = 4w_L$. This creates a waist, w_0, at $z = 0$ of $w_0 = \lambda f / \pi w_L$. The numerical aperture (NA_G) of the Gaussian beam is

$$NA_G = \frac{\lambda}{\pi w_0} = \frac{w_L}{f} = \frac{D}{4f}. \tag{3.6}$$

The numerical aperture of the lens (in vacuum) is given by equation 3.7,

$$NA = \frac{D}{2f} = 2NA_G, \tag{3.7}$$

where D is the beam diameter of the aperture at the lens and f is the focal length of the lens. Although the system could be set up with NA_G of a Gaussian beam = NA of the lens, with acceptable distortion of the spot, we chose the NA of the lens to be twice NA_G of a Gaussian beam. Tighter focuses and higher gradients may be possible with $NA = NA_G$, but we chose to be on the conservative side where a good beam quality at $z = 0$ was still assured.

Cleaning up these fundamental equations was necessary to have a program that was going to most closely match what is occurring in the lab. Fixing these programming items made making larger changes and additions to the code more feasible.

Dual-beam Addition to OTGO

The OTGO software available for download is only written for a single laser beam. However, the primary analysis detailed in this thesis will be for a horizontal dual-beam trap. Reasons for choosing this trap style are discussed in Chapter 4. In order to study a horizontal dual-beam trap, modifications to the code were required. A second beam was created by taking the pre-defined functions for the original beam, duplicating them, and flipping the axis dependence. A shift between the two beams (z_{sep}) is also introduced and discussed in later sections. In the longitudinal direction, the scattering force for the second beam was made negative as it was in a counter-propagating direction from the first beam. Total forces now include all forces from both laser beams in either the longitudinal or transverse directions. The following discussion will show how we are able to use OTGO to analyze the dual-beam horizontal optical trap.

Silica Particle Example Our first example is of silica particles of refractive index 1.5 with a diameter of 8μm, $\lambda = 1030$nm, and each trapping laser focused by an 8mm lens of NA = 0.5. Balanced powers indicates each laser has a power of 0.03W while unbalanced powers indicates Laser 1 has a power of 0.04W and Laser 2 has a power of 0.03W. Laser 1 is the right propagating beam while Laser 2 is the left propagating beam. Figures 3.9 and 3.10 show a spherical particle in an ideal horizontal dual-beam trap along the longitudinal and transverse directions.

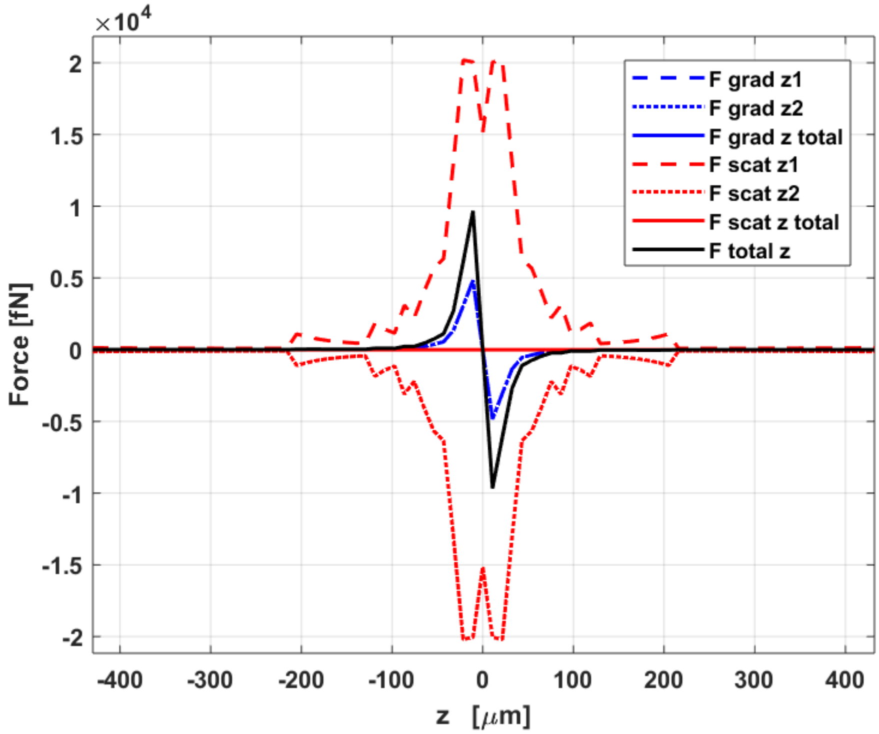

Figure 3.9: Longitudinal forces along the z-axis for an ideal horizontal dual-beam trap. An 8μm diameter silica particle is trapped by two 1030nm lasers where each is focused by an 8mm lens. Powers of the beams are balanced with 0.03W in each beam.

It is seen in the plot shown in Figure 3.9 that the scattering forces (F_{scatz1} and F_{scatz2}) of each trap laser (dashed red lines) are dominating. Since the two lasers are perfectly aligned, with identical foci, and balanced powers, the scattering forces completely cancel (solid red line). Therefore, the optical trap in the longitudinal direction is created with only the gradient forces for each beam (dashed blue lines) summed together (solid black line) along the z-axis. The total longitudinal force is represented by

$$F_{totalz} = F_{scatz1} + F_{scatz2} + F_{gradz1} + F_{gradz2}. \tag{3.8}$$

Figure 3.10 shows the same parameters described above for the transverse direction along the x-axis, where the x-axis is perpendicular to the optical table. Gravity on the silica particle is shown by the straight, solid cyan line. The gradient forces for each beam are shown by the dashed blue lines with total force shown by the solid black line. The total transverse force is represented by

$$F_{totalx} = F_{gradz1} + F_{gradz2} + F_{gravx}. \tag{3.9}$$

In both plots, the total force crosses 0N and is relatively balanced on either side of 0N. This is our first indicator that we can create a stable optical trap. More criteria for a stable trap will be described throughout this section.

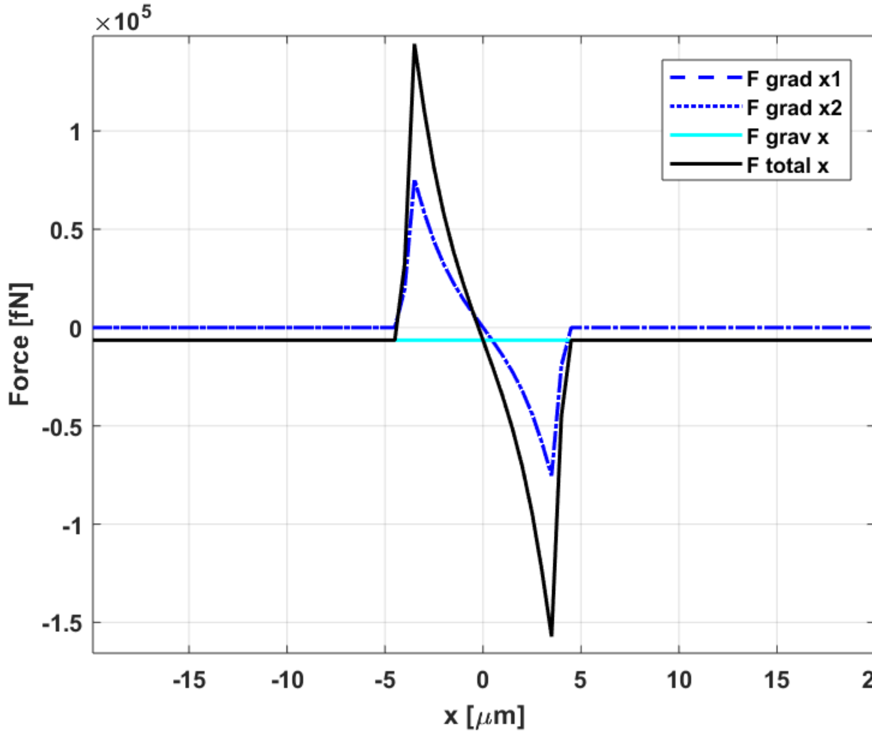

Figure 3.10: Transverse forces along the x-axis at z=0 for an ideal horizontal dual-beam trap. An 8μm diameter silica particle is trapped by two 1030nm lasers where each is focused by an 8mm lens. Powers of the beams are balanced with 0.03W in each beam.

Longitudinal Separation of Laser Beams In the lab, a power imbalance would be likely as each path of the setup may not not transmit the light in an identical way. Figures 3.11 and 3.12 show perfectly aligned beams with a power imbalance, 40mW in Laser 1 and 30mW in Laser 2, for both the longitudinal and transverse directions.

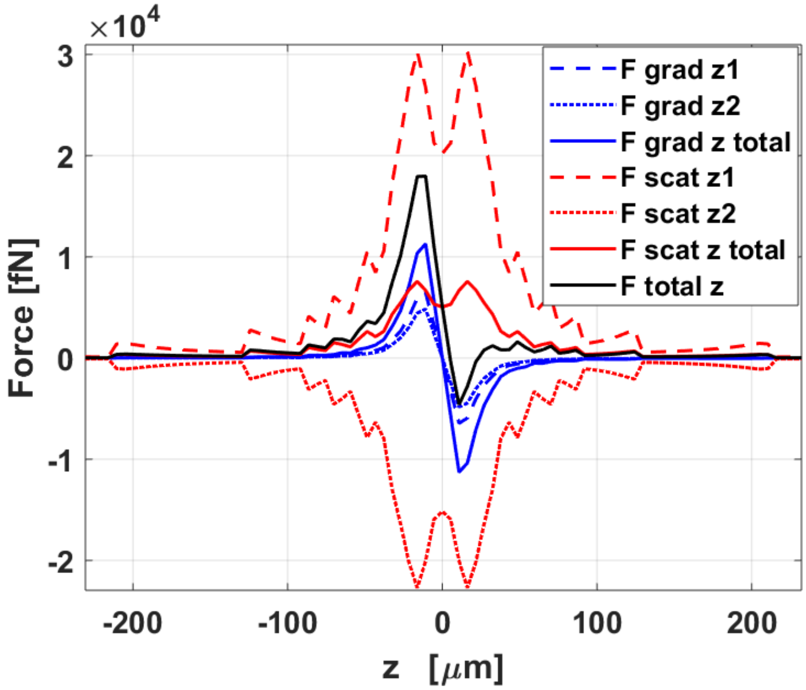

Figure 3.11: Longitudinal forces along the z-axis for an ideal horizontal dual-beam trap with unbalanced powers between the beams. An 8μm diameter silica particle is trapped by two 1030nm lasers each focused by an 8mm lens. Powers of the beams are 0.04W in Laser 1 and 0.03W in Laser 2.

Here, we no longer have our scattering forces cancel with each other in the longitudinal direction and our total force never crosses 0N. Although our transverse plot has not significantly changed compared to Figure 3.10, our longitudinal plot is a good indicator that we would not be able to create a stable optical trap with these parameters due to the fact that the total force never crosses 0N. The imbalance in powers between the two beams create a scattering force that dominates the system and will push the particle away from the trap region.

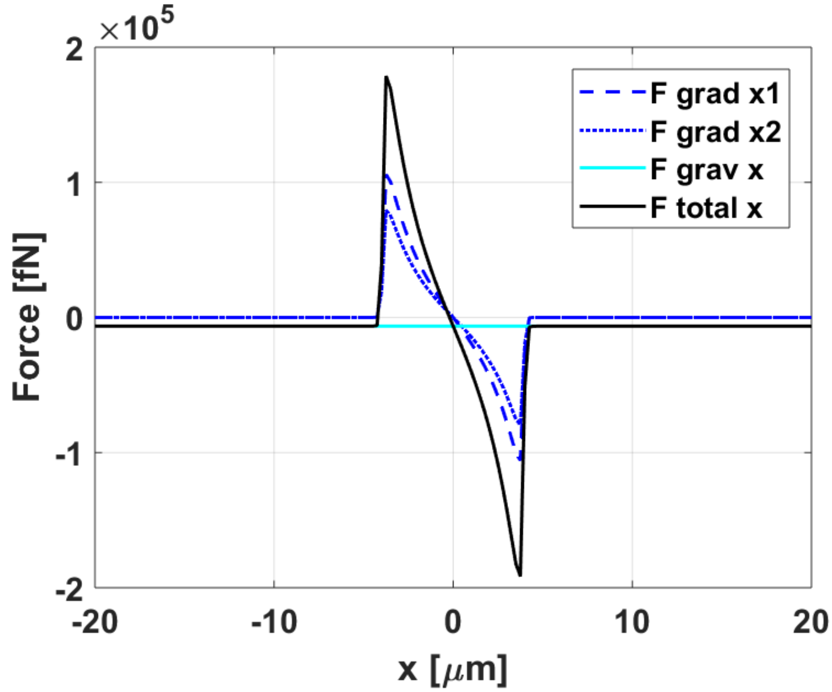

Figure 3.12: Transverse forces along the x-axis at z=0 for an ideal horizontal dual-beam trap with unbalanced powers between the beams. An 8μm diameter silica particle is trapped by two 1030nm lasers each focused by an 8mm lens. Powers of the beams are 0.04W in Laser 1 and 0.03W in Laser 2.

Alignment of the laser beams is critical to creating a stable trap, regardless of their powers. It would be very difficult (and time consuming) to perfectly align two lasers with one another. Thus, a separation along the z-axis between the foci, as described in Chapter 2, is introduced. Introducing this z-separation, z_{sep}, creates a more user-friendly experiment with more possibilities for a stable optical trap with an acceptable tolerance. The process by which the separation is created in the lab will be described in Chapter 4.

Figures 3.13 and 3.14 show the same power imbalance as figures 3.11 and 3.12, but with $z_{sep} = 50\mu$m between the foci. Once again, a stable optical trap is possible in the longitudinal direction just by introducing this new parameter. The transverse plot in figure 3.14 still maintains total force crossing 0N, but the question of “how much z_{sep} is possible for a stable trap to form" is brought to the surface. As z_{sep} gets larger, the total force in the transverse direction no longer cross 0N. This tolerance value will be discussed in Chapter 5. It is important to note that our plots have only been showing the x-axis for the transverse direction that includes gravity. The y-axis is symmetric to the x-axis (minus gravity), and would maintain a stable trap whenever the x-axis is stable. Due to this symmetry, we have omitted the y-axis transverse plots from the discussion.

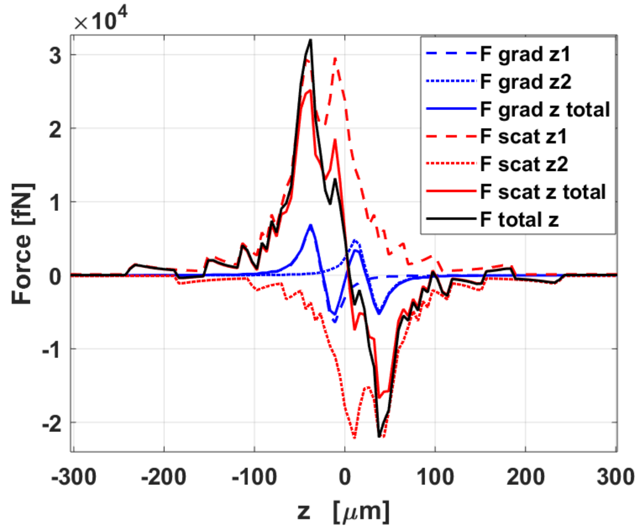

Figure 3.13: Longitudinal forces along the z-axis for a horizontal dual-beam trap with unbalanced powers between the two beams. A z-separation of 50μm is present between the foci. An 8μm diameter silica particle is trapped by two 1030nm lasers each focused by an 8mm lens. Powers of the beams are 0.04W in Laser 1 and 0.03W in Laser 2.

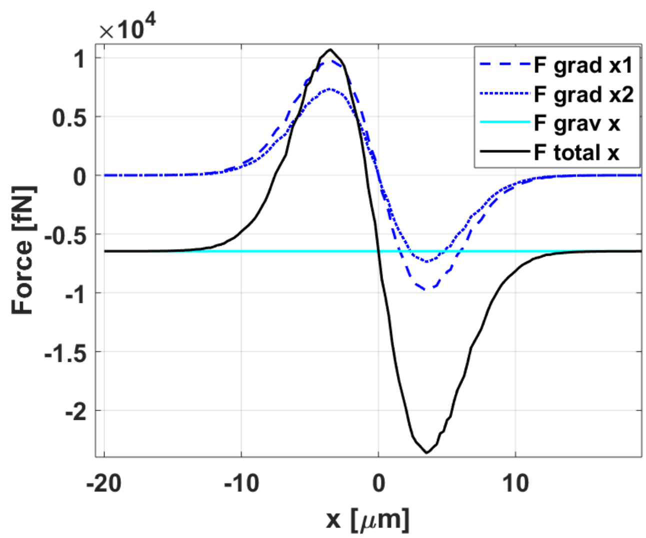

Figure 3.14: Transverse forces along the x-axis at z = 0 for a horizontal dual-beam trap with unbalanced powers between the two beams. A z-separation of 50μm is present between the foci. An 8μm diameter silica particle is trapped by two 1030nm lasers each focused by an 8mm lens. Powers of the beams are 0.04W in Laser 1 and 0.03W in Laser 2.

Transverse Separation of Laser Beams Not only is it possible for the two laser beams to have a separation along the z-axis, it is possible for the lasers to have separation in the transverse direction. Unlike z-separation, which improves the longitudinal trap, x-separation always makes the transverse trap worse. However, due to error in alignment, some x-separation is unavoidable. By studying the effects of x-separation on transverse and longitudinal trapping, we can establish the required tolerances on our alignment of beam overlap.

X-separation is a new addition to the OTGO code, like the addition of z-separation, and is calculated at z=0. Both separations display effects in the opposite direction (i.e z-separation causes changes in the transverse direction). Figures 3.15 and 3.16 show a balanced dual-beam trap for the longitudinal and transverse forces with an x-separation, x_{sep}, set at 10μm. With these plots, it can be seen that there will be a different tolerance in the transverse direction as a 10μm separation in the x-direction creates a different effect than the 50μm separation in the z-direction.

In reality, both the x-separation and z-separation will occur at the same time and will need to be accounted for. Figures 3.17 and 3.18 show this example. These combinations can become complicated very quickly and it becomes harder to "tell" if we are able to create a stable optical trap just from analyzing the forces of our setup. Therefore, we move on to looking at the potential well in each direction of the trap.

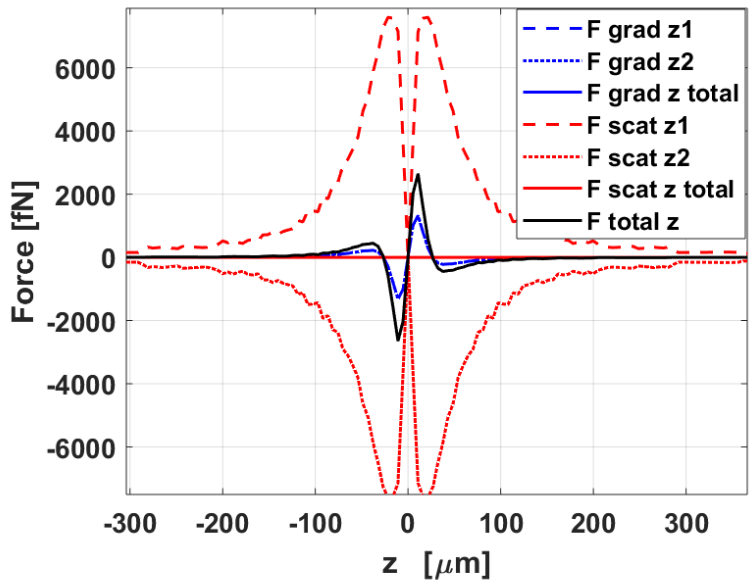

Figure 3.15: Longitudinal forces along the z-axis for a horizontal dual-beam trap with an x-separation of 10μm between the foci with $z_{sep} = 0$. An 8μm diameter silica particle is trapped by two 1030nm lasers each focused by an 8mm lens. Powers of the beams are balanced with 0.03W in each beam.

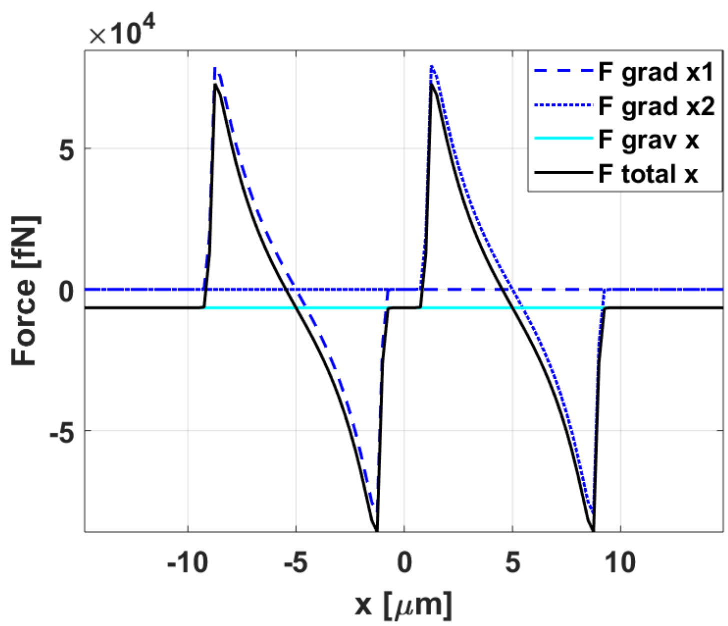

Figure 3.16: Transverse forces along the x-axis for a horizontal dual-beam trap with an x-separation of 10μm between the foci with $z_{sep} = 0$. An 8μm diameter silica particle is trapped by two 1030nm lasers each focused by an 8mm lens. Powers of the beams are balanced with 0.03W in each beam.

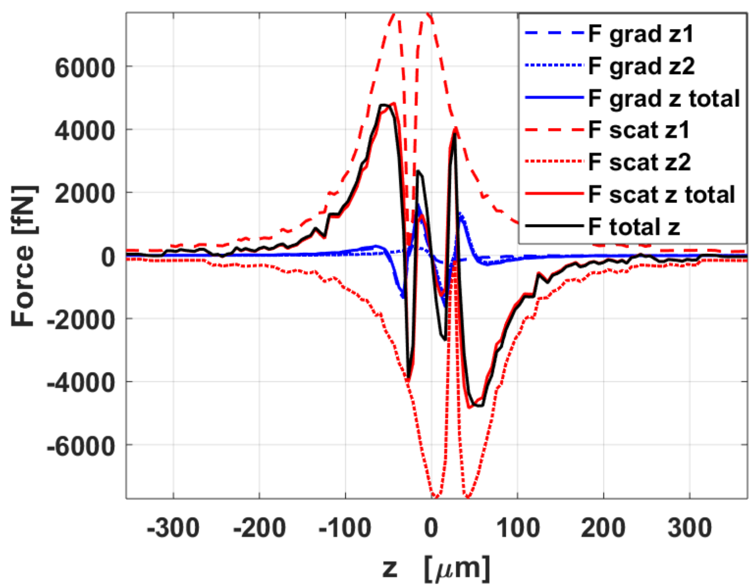

Figure 3.17: Longitudinal forces along the z-axis for a horizontal dual-beam trap with an x-separation of 10μm and z-separation of 50μm between the foci. An 8μm diameter silica particle is trapped by two 1030nm lasers each focused by an 8mm lens. Powers of the beams are balanced with 0.03W in each beam.

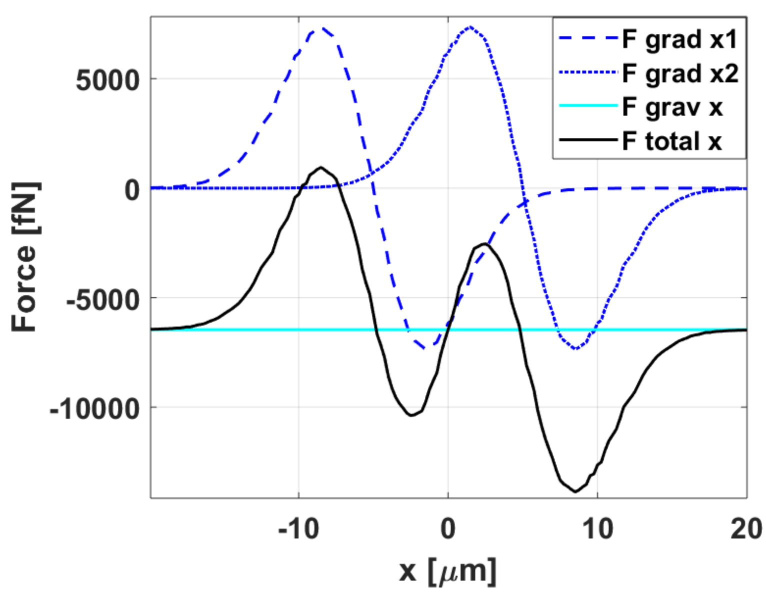

Figure 3.18: Transverse forces along the x-axis for a horizontal dual-beam trap with an x-separation of 10μm and z-separation of 50μm between the foci. An 8μm diameter silica particle is trapped by two 1030nm lasers each focused by an 8mm lens. Powers of the beams are balanced with 0.03W in each beam.

Potential Wells Another extension of the OTGO code we developed is the ability to calculate the potential well for both the longitudinal and transverse directions. The chamber being used for experiments does not begin at vacuum, thus it still contains air inside. When the particle is launched, there will be collisions with the gas particles which will slow the particle down. If the particle is trapped, it will come to thermal equilibrium in the trap and it follows the Maxwell-Boltzmann distribution at thermal equilibrium. Each direction in the optical trap will have an average energy of $\frac{1}{2}k_BT$ where k_B is the Boltzmann constant (k_B =1.380652 x 10^{-23}J/K) and T is the temperature in Kelvin.

All of the trap designs presented would be deep enough to be stable under thermal excitation. In this thesis, the concentration is on the dynamics of loading particles into the optical trap, thus thermal excitation can be ignored. Collisions of the particles with the air are not ignored. These provide the damping force that slow the particle prior to loading and damps out the oscillations in the trap. For a horizontal dual-beam trap, the particles will be dropped from above the trap region in a gravity field and will enter the potential well with terminal velocity. This velocity, along with the physical setup of the trap (power and alignment of beams) will determine if the particle is going to be trapped or not. Without the damping that produces the terminal velocity in freefall, the particles would exit the bottom of the trap on the first pass, without a single oscillation.

Figures 3.19 and 3.20 show the potential wells for the longitudinal and transverse directions of an 8μm diameter silica particle in an ideal horizontal dual-beam trap. The potential follows equation 3.10,

$$V(x) = \int_{-\infty}^{x} F(x)dx \tag{3.10}$$

where *F(x)* is the total force on the particle for either the longitudinal or transverse direction. This extension of OTGO takes the total forces and integrates over the associated axis to create the potential wells. The transverse well shown in Figure 3.20 is at an angle due to the force of gravity. The next step we took sheds light on what is actually happening in these potential wells with a particle dynamics analysis.

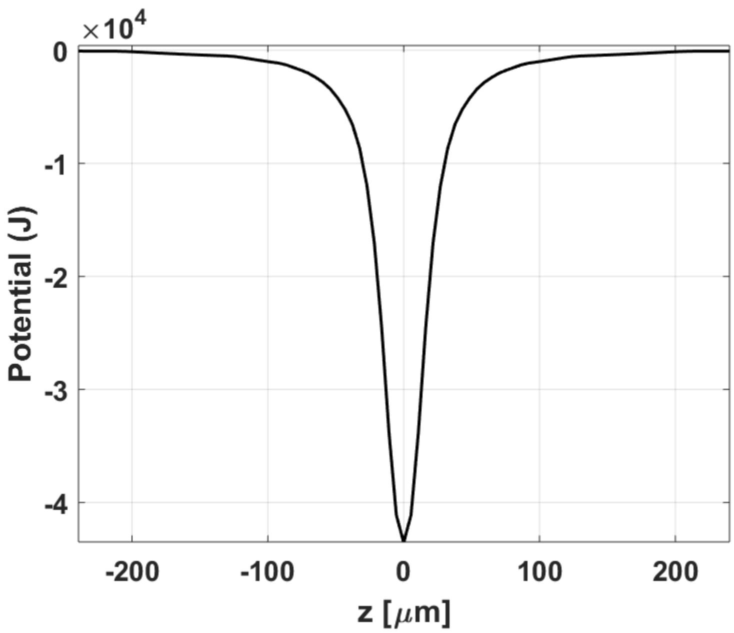

Figure 3.19: Potential well in the longitudinal direction for an ideal horizontal dual-beam trap. Powers are balanced with 0.03W in each beam.

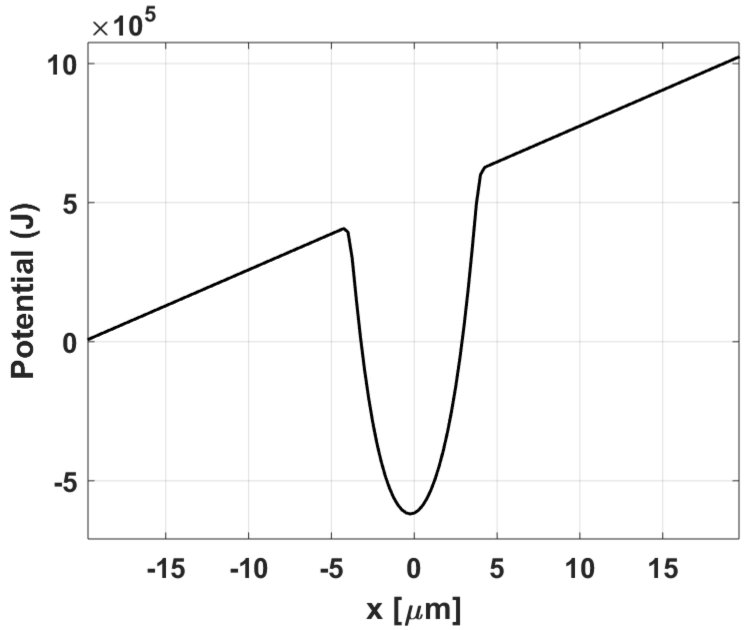

Figure 3.20: Potential well in the transverse direction for an ideal horizontal dual-beam trap. Powers are balanced with 0.03W in each beam.

Particle Dynamics A MATLAB program was written to import force data from OTGO and use it to calculate particle motion during loading to analyze if efficient loading into the trap was possible. The particle's initial position is above the trap and with a terminal velocity as the particle enters the well. The transverse x-axis has positive values 'up'. This program enables us to determine if a given particle will be trapped for any given experimental setup in air. Terminal velocity is calculated with equation 3.11,

$$v_{term} = \frac{2\rho g R^2}{9\mu}, \tag{3.11}$$

where ρ is the density of the particle, g is gravity, R is the particle radius, and μ =18.54 Pa-s is the viscosity of air. For an 8μm diameter silica particle, the terminal velocity (v_{term}) is -0.00462m/s and $\rho_{Si} = 2.46kg/m^3$. Figures 3.21 and 3.22 show the behavior of an 8μm diameter silica particle in the ideal horizontal dual-beam trap with balanced powers in each beam for the transverse direction and longitudinal directions.

Results for non-ideal scenarios are discussed in Chapter 5 for both silica and yttrium aluminum garnet (YAG) particles. Using OTGO was important in determining the necessary steps to take during the experimental phases of this project. We could determine the characteristics that would create a stable trap before making any physical changes in our setup, which saves time. If we were unable to load the trap given the current conditions of the lab, then a conversation would determine what actions needed to take place in order to successfully trap particles.

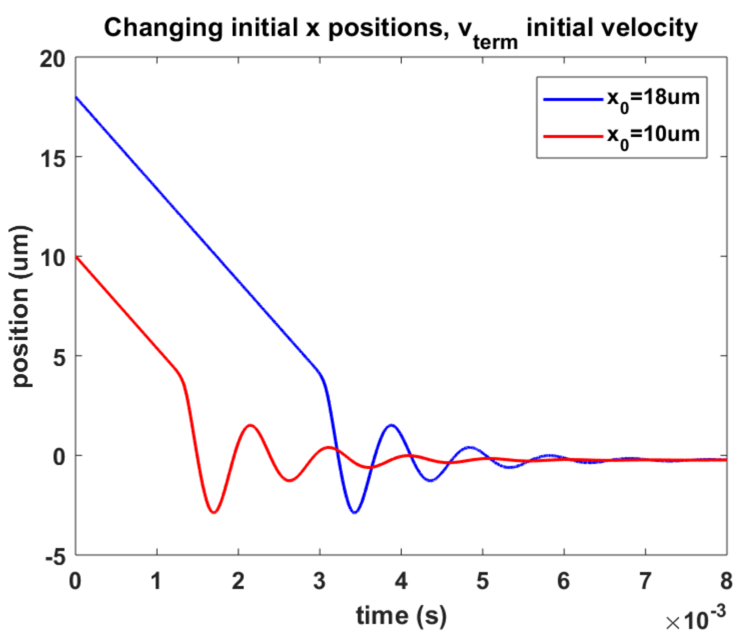

Figure 3.21: An 8μm diameter silica particle dropped into an ideal horizontal dual-beam trap. Each line represents a different initial position with the same initial velocity, v_{term}

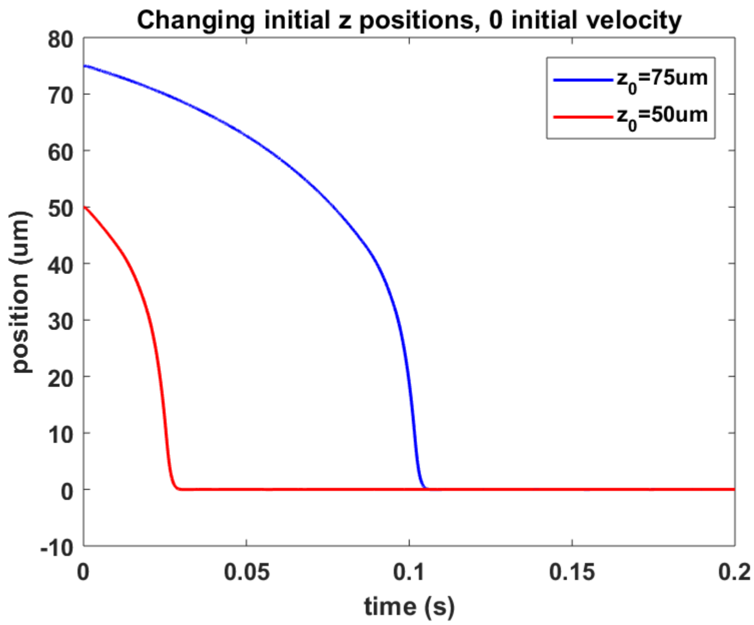

Figure 3.22: An 8μm diameter silica particle dropped into an ideal horizontal dual-beam trap. Each line represents a different initial position with initial longitudinal velocity set to zero.

OPTICAL TRAPPING EXPERIMENT

Optical trapping involves multiple intricate processes that must fit together to conduct a single experiment. This chapter will describe the lasers, launching mechanisms of particles, our optical trap designs and implementations, and the image detection system. Both vertical and horizontal traps will be discussed. Future work will be discussed in Chapter 6.

Lasers

To gain experience in trapping, we initially set up a vertical optical trap. We utilized a 532nm continuous wave laser (Spectra-Physics: Millennia V) with a maximum power of 5W for this setup. For the horizontal dual-beam trap we used 1030nm laser diodes (QLD-1030-250S, QPhotonics, LLC). The wavelength of light for the trap laser in this setup was chosen to be tunable around the absorption bands of the rare-earth dopant, Yb^{3+}, which has a cooling transition at 1030nm.

Vertical Trap

The vertical trap was the first trap implemented. Figure 4.1 shows a photo of the optical table setup with the 532nm laser beam entering the bottom of the vacuum chamber while figure 4.2 shows a schematic of the optical design. The beam leaves the laser and is directed to be lower to the table with two mirrors so it is able to enter the bottom of the vacuum chamber. The beam is expanded through a telescope that consists of a 100mm plano-convex lens and a 300mm plano-convex lens. Mirror 4 (M4) is placed underneath the chamber and directs the light through the bottom window of the chamber and through a 50mm focusing lens inside the chamber. This lens creates a focused beam that forms the optical trap.

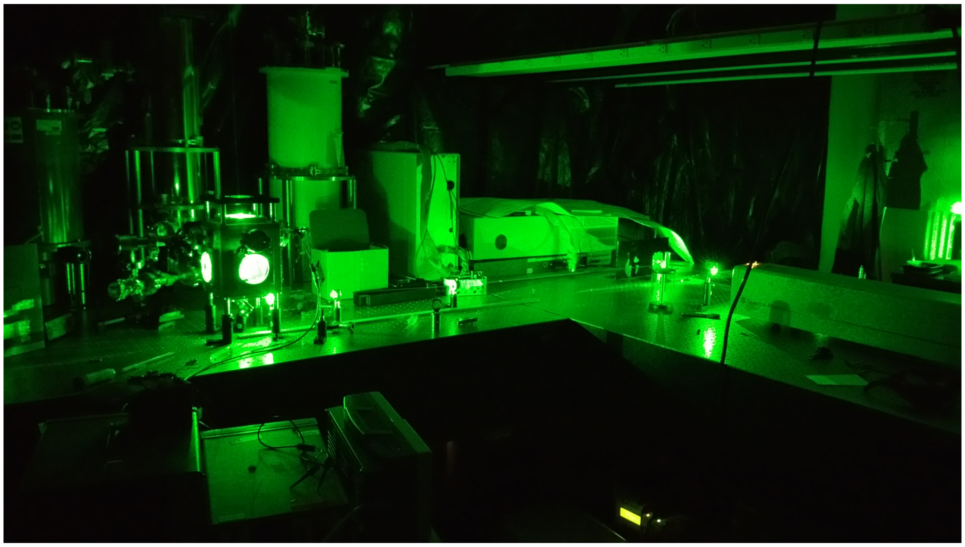

Figure 4.1: A 532 nm wavelength laser beam is directed vertically into the vacuum chamber after passing through a telescope to create the vertical optical trap.

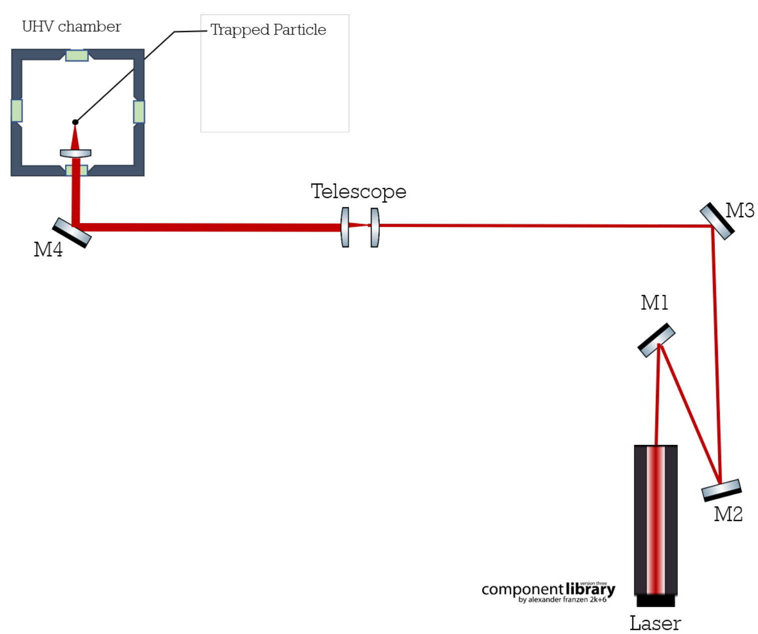

Figure 4.2: A schematic of the vertical optical trap for trapping particles in air. An expanded 532nm laser beam enters the bottom of the vacuum chamber passing through a 50mm focusing lens to create the vertical optical trap.

A microscope slide cantilever launcher is placed above the focal point of the laser beam and secured inside the chamber. Particles are launched into the air and begin to fall to the bottom of the vacuum chamber due to gravity. When the particles are in the path of the laser beam they may become trapped at a stable point above the focal point where the gravitational force and scattering force balance.

Figure 4.3 shows a soda lime glass particle trapped in a vertical trap (at the end of the arrow tip). The Millennia V laser was used as the trapping laser and the particle was 5-50 microns in diameter. This vertical trap is conceptually straightforward and easy to use. Although successful, the launcher used in this vertical trap was inefficient at trapping particles due to the launching mechanism. Particles were free to move

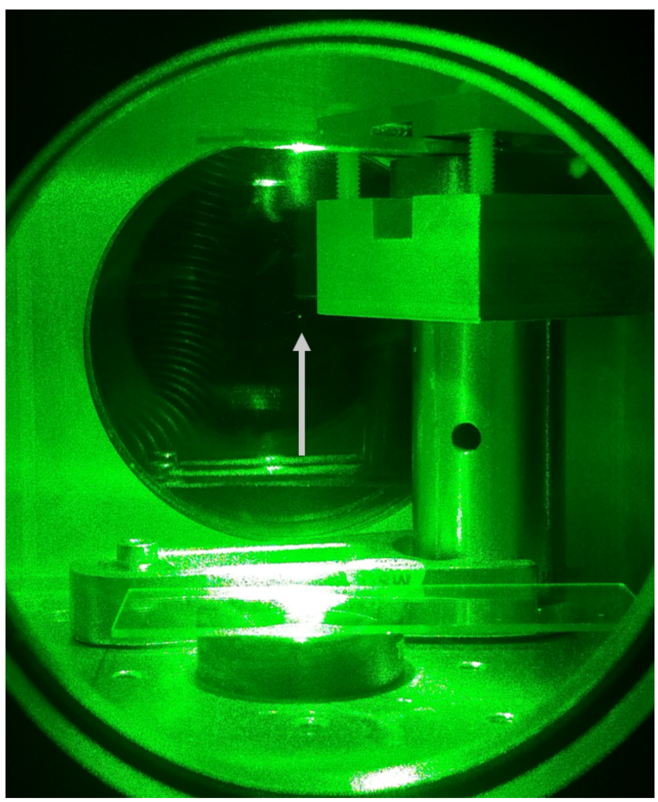

Figure 4.3: Trapped soda lime glass particle (5-50 micron in diameter) in the vertical optical trap. A microscope slide sits on top of the focusing lens to collect particles that do not get trapped.

about the edge of the microscope slide and weren't guaranteed to fall within the path of the laser. Additionally, a dusting of particles over the focusing lens was common. A microscope slide was placed on top of the lens to catch the falling particles, but they were still capable of interfering with the trapping beam and the slide would need to be cleaned off frequently.

Launching Particles

Launching particles is a critical aspect to trapping a particle. The microscope slide cantilever used for the vertical trap served as the foundation for launching methods used with the dual-beam horizontal trap. Two new launching methods were implemented and improved upon during the course of this project. These launching methods are described in detail here, while further improvements for launching particles will be detailed in Chapter 6.

Old Method: Microscope Slide Cantilever

The microscope slide cantilever was used for the vertical optical trap and served as the basis for the improved launching designs detailed in this chapter. A glass microscope slide is positioned on top of a piezoelectric ring and then both items are clamped between an aluminum block base and top plate. Particles were then placed on the glass microscope slide near its edge. Vibrating the piezoelectric ring causes the particles to fall off the slide.

Assembly and Operation The microscope slide cantilever launcher pictured in Figure 4.4 was built in-house. The piezoelectric ring (APC International) is placed between an aluminum block base and top plate that is secured with four plastic 8/32" screws. The piezoelectric ring has an outer diameter of 38mm, an inner diameter of

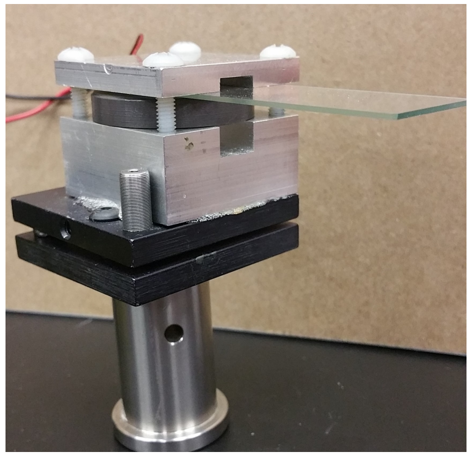

Figure 4.4: A photo of the microscope slide cantilever launcher on a tip/tilt stage.

13mm, and a thickness of 6.35mm. It is then connected to a function generator (Wavetek: Model 187), which produces a sine wave that oscillates at approximately 140kHz corresponding to the resonant mode of the piezo. The aluminum block base is secured to a tip/tilt stage with a 1" base that allowed for adjustment of the angle of the slide.

Downfalls This microscope slide cantilever was inconsistent with the quantity of particles that would be dropped into the trap region at any given time. Additionally, as the particles were placed near the edge of the slide there was nothing keeping them from spreading broadly, over several millimeters. This spread of particles was significantly broader than the trap region, which proved to be wasteful of the supply of particles. For future experiments pertaining to loss pressure, many trap and loss cycles will need to take place. Only having a small fraction of particles potentially fall in the trap region is inefficient with both time and particles. Additionally, we will have a significantly smaller supply of doped particles (such as Yb:YAG) for those experiments due to their fabrication process compared to commercially buying fabricated particles, requiring high efficiency of loading particles into the trap. Thus, two new designs were explored to gain more efficient launching of particles into our trap region.

New Method 1: Aluminum Cantilever with Drop Hole

An aluminum cantilever with a drop hole was used for both the vertical and horizontal optical traps. This first redesign tried to correct the inefficient use of particles by creating a milled reservoir 4mm in diameter with a drop hole (milled using a .040 drill-bit) in the center. This new cantilever arm still sat atop the large piezoelectric ring as described in the previous section. Figure 4.5 shows the milled reservoir in the left image along with it placed in the vacuum chamber in the right image.

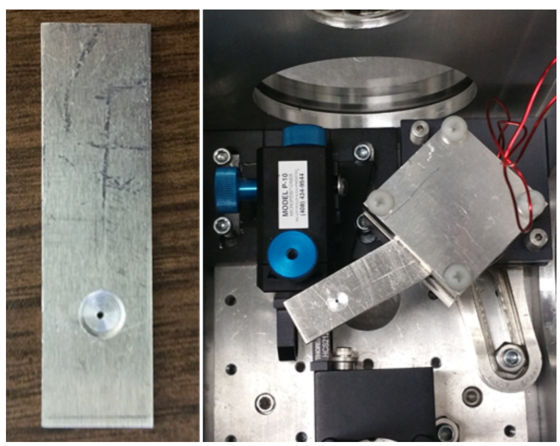

Figure 4.5: Left: Launcher with reservoir and small drop hole. Right: Launcher with reservoir loosely placed in vacuum chamber for the horizontal dual-beam configuration.

As we transitioned to a horizontal dual-beam trap we continued using a large piezoelectric transducer as a base design for vibrating the drop hole launcher. Although this drop hole design worked well for alignment with the vertical trap, imperfections in fabricating this piece were still evident. Particles would congregate to either the outer edges of the reservoir or near the center resulting in poor drop efficiency. It was common for a lot of particles to fall all at once which is also not a suitable condition for trapping, as a trapped particle can become untrapped if another particle enters the beam.

The working distance between the two trap lenses in the horizontal dual-beam trap design was 1 cm. Holding these lenses required more components being placed inside the vacuum chamber, thus limiting the space we could use for launching the particles. Therefore, the scale of all components had to be considerably reduced in size to create the second iteration of the aluminum cantilever. Reducing the size of the piezoelectric transducer was also consistent with launching larger particles. These large particles do not require a large frequency to be ejected from the loader. Thus, the large high resonant frequency piezoelectric transducer that was being used was now overkill in frequency.

New Method 2: Aluminum Cantilever with Trenched Channel

Keeping the milled reservoir, we changed the drop hole to a trenched channel where the particles can flow out of the reservoir as shown in Figure 4.6. The narrow 0.4 mm channel allows for much finer control and efficient launching of the particles into the trap region. A small piezoelectric transducer (5mm x 5mm x 2.4 mm) vibrates the aluminum cantilever arm. An Arduino controlled chirped drive circuit (provided by Prof. Brian D'Urso's group) enabled computer controlled (MATLAB code triggered) pulsing of the particle launching. Tip-tilt control was still in use with the aluminum block mount from previous designs. These additions resulted in a more efficient and consistent launcher.

The new launcher has a narrower spread of particles and required better precision in its position over the trap region. The next iteration of this launcher thus includes control over movements in the horizontal plane for alignment above the trap focus. Tip-tilt control was removed to allow better fit within the vacuum chamber. The disadvantage with removing tip-tilt capabilities is some control over how particles congregate in the reservoir. Figure 4.7 shows a photo of this launcher.

The mini-stages ended up having too much play and did not provide the precision needed for launching. A temporary solution is to use an external precision XYZ-stage with added tip-tilt control. This allows the precision needed, but will not allow the chamber to be evacuated. A new vacuum chamber design is needed to accommodate all the components needed.

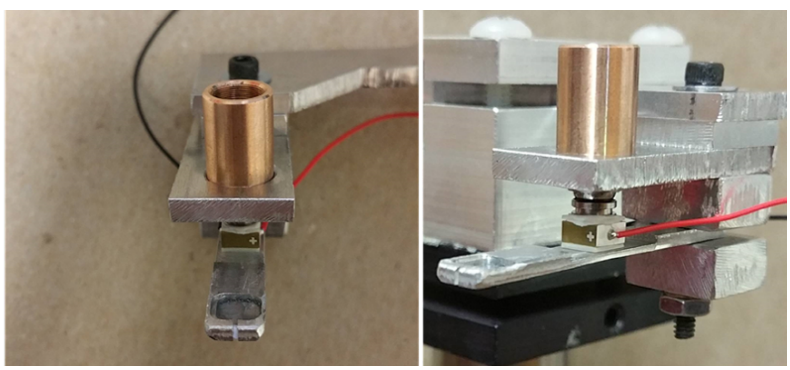

Figure 4.6: The aluminum cantilever with milled reservoir and trenched channel. A small piezoelectric transducer is shown sandwiched between a ball-tip screw and the launching arm.

Assembly and Operation The aluminum cantilever launcher was designed and built in-house. The launching arm (5mm wide) contains a milled reservoir with a 0.4mm trenched channel. A piezoelectric chip (Thorlabs: TA0505D024W) is clamped on top of the launching arm roughly 1 cm back with a 1/4-100" ball-tip hex adjuster, which was adjusted to set the proper loading of the piezoelectric transducer. Two

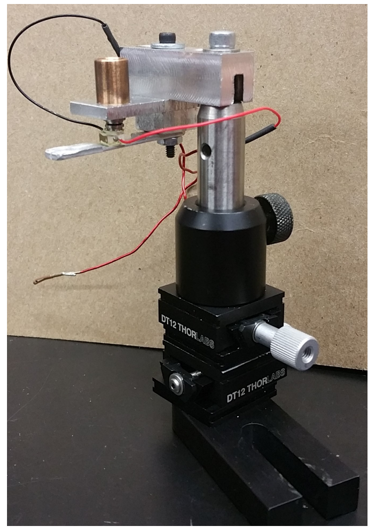

Figure 4.7: The final iteration of our aluminum cantilever launcher with control over movements in the horizontal plane for alignment above the trap focus.

ceramic end plates are attached to the top and bottom of the piezoelectric chip by an ultra high-vacuum compatible epoxy (Torr Seal Epoxy). A 5mm stainless steel conical end cup (Thorlabs) is placed on one of the ceramic end plate surfaces with epoxy and is used to ensure the applied stress is restricted to the axial direction. The piezoelectric chip is placed on the launching arm that is sandwiched between one 5mm aluminum spacer and a 4/40" nut. These components sit below the bushing arm, which contains the 1/4-100" compatible bushing and hex adjuster, which rests in the conical end cup. All components are secured together with a 4/40" screw.

Once inside the vacuum chamber the piezoelectric transducer is connected to the Arduino controlled chirped drive circuit, fabricated based on designs provided by Dr. Brian D'Urso's group. The drive circuit produces a chirped square-wave whose amplitude is adjusted via voltage (0-30V) from a power supply. The Arduino code can be edited to change the sweep range and chirp rate that executes the piezoelectric transducer. MATLAB code for triggering the chirper was written in collaboration with Montana State University undergraduate Alec Dinerstein. The code enabled automated pulsing of the launcher by controlling a National Instruments data acquisition module with analog and digital input/output that provided the pulses to the chirper. The code is included in Appendix C.

Fundamental Physics of the Designs

Bar Vibrational Modes The cantilever launcher can be modeled as a clamped thin bar at one end. The resonances of a clamped bar are well known [22], and can be defined by equation 4.1 for the fundamental mode, as depicted in Figure 4.8,

$$f_1 \approx 0.162 \frac{a}{L^2}\sqrt{\frac{Y}{d}}, \tag{4.1}$$

where a is the thickness of the bar, L is the length of the bar, d is the density of the material, and Y is Young's modulus. The properties for our aluminum cantilever

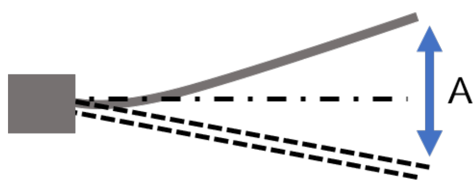

Figure 4.8: Fundamental vibrational mode of a thin clamped bar.

launcher are in Table 4.1 with the calculated frequency from the above equation. The error for the calculated frequency follows equation 4.2.

$$\Delta f(\%) = \sqrt{(\%)_a^2 + 2(\%)_L^2 + \frac{1}{2}(\%)_Y^2 + \frac{1}{2}(\%)_d^2} \tag{4.2}$$

Table 4.1: Loader Frequency

Property	**Value**
Thickness (a)	.9 mm ± 10%
Length (L)	17.9 mm ± 10%
Density (d) of Aluminum	2710 $\frac{kg}{m^3}$ ± 5%
Young's Modulus (Y)	$70 * 10^9 \frac{N}{m^2}$ ± 5%
Calculated Frequency (f)	2313 Hz ± 18%

Michelson Interferometer In order to confirm our launcher operated within the calculated frequency range and to measure its amplitude, a Michelson interferometer was constructed. A HeNe laser, two beam splitters, one mirror, a 100 mm lens and a photodetector were used, along with our launcher, to create the interferometer as shown in Figure 4.6. The mirror is vertically mounted above the launcher. A Wavetek waveform generator produced a sine wave that was sent to the launcher and also triggered an oscilloscope. The signal captured by the photodetector was monitored by the oscilloscope.

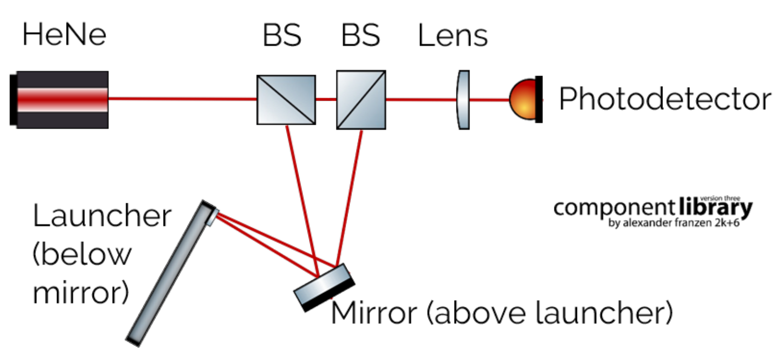

Figure 4.9: Michelson interferometer constructed to test frequency of aluminum cantilever launcher.

Michelson interferometers are commonly used for precise distance measurements and in our test, our launcher acts as the movable mirror that would be seen in a traditional setup. Light passes through the first beam splitter to our mirror and is directed downward to the launcher. A small (∼2mm square) piece of silverd mylar was glued to the end of the launcher arm. The light is then reflected back up to the mirror and directed through the second beam splitter and recombined with the original beam. Then the light is focused onto the photodetector and monitored for interference with the signal monitored on an oscilloscope. We could vary the amplitude of the clamped bar (A in Figure 4.8) by adjusting the hex screw, with the maximum amplitude obtained when the set screw was adjusted to set the optimal load on the piezoelectric transducer. The resonant frequency (max amplitude) was found to be ∼2600Hz which is within the error estimate. The amplitude of the clamped arm was able to be estimated from the number of oscillations of the signal per cycle. Each oscillation was $\frac{\lambda}{2}$ due to the round trip of the interferometer. The estimated amplitude was on the order of 10-20 oscillations, roughly 5 microns.

Horizontal Dual-beam Trap

Laser Diode Tuning

For anti-Stokes cooling, it is important to tune our lasers on and off resonance for the chosen rare-earth dopant. Our laser diodes are tunable around 1030 nm, the correct resonance for cooling the Yb:YAG particles, but we must first characterize the diodes to make sure they tune relatively smoothly around 1030nm.

The laser diodes are used with temperature controlled mounts and are connected to ILX Lightwave laser diode controllers. As the temperature and current are changed, the wavelength of light that is emitted from the diode also changes. We are able to monitor the spectral output of each laser diode with an optical spectrum analyzer

(Ando, now Yokogawa: AQ-6315E). The wavelength/temperature coefficient is ∼0.3 nm/°C Figure 4.10 shows the results of current tuning for one of our 1030 nm laser diodes.

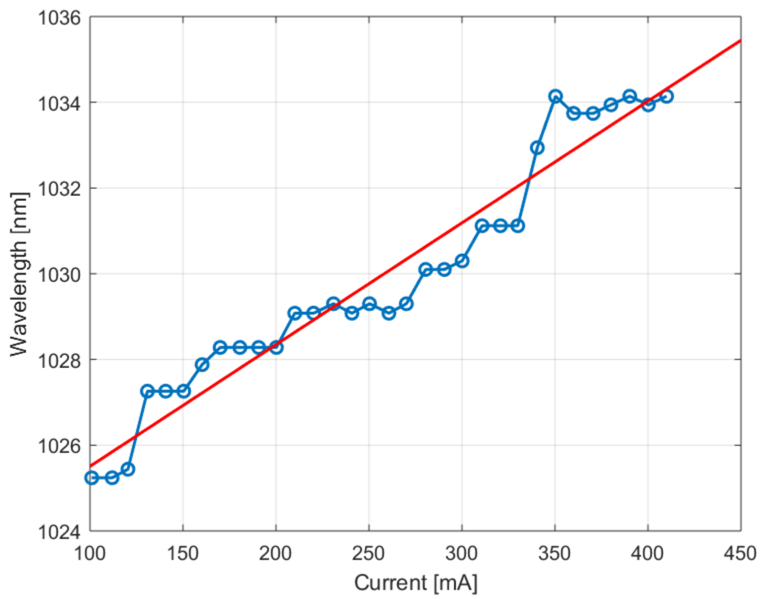

Figure 4.10: Current tuning curve for 1030 nm laser diode (QLD-1030-250S, QPhotonics, LLC) at 25°C with current in mA along the horizontal axis and wavelength in nm along the vertical axis.

Lasers are commonly characterized by their free spectral range (FSR) which can be defined as the spacing between adjacent modes (in frequency or wavelength). We observed both of our laser diodes to have a FSR of $\sim 1nm$ when two modes were present. While jumping occurs, the broadness of the cooling transition is $\sim 3nm$ (measured by Dr. Charles Thiel and Tino Woodburn), which makes this tuning quality acceptable.

Optical Setup Designs

A horizontal dual-beam optical trap uses the gradient and scattering forces of the two laser beams to create a stable three dimensional trap, as described in Chapter

2. If the two beams are not aligned correctly (i.e. focus aligned on same axis or separated by an appropriate distance) the configuration will not form a stable trap, thus position control of the optical beams is critical. Each iteration of our horizontal design (as described below) was designed to improve our control over the optical beams.

Setup 1: Single Laser Diode Figure 4.11 shows a schematic of the first horizontal dual-beam trap in air. The 1030nm laser diode is expanded through a telescope and passed through a Babinet-compensator (BC). The Babinet-compensator was adjusted to be a half wave-plate at 1030nm and was rotated to balance the powers of the two beams (B1 and B2) that are created from the polarizing beam splitter (PBS). Two 8mm aspheric lenses (Thorlabs: A240TM-B) are placed inside the vacuum chamber to focus each laser beam. One lens is placed into a stationary mount and another is placed into a mount attached to an XYZ-translation stage. The two beams are aligned using a 5-micron pinhole attached to an XYZ-translation stage that could be inserted between the lenses for alignment and removed for trapping.

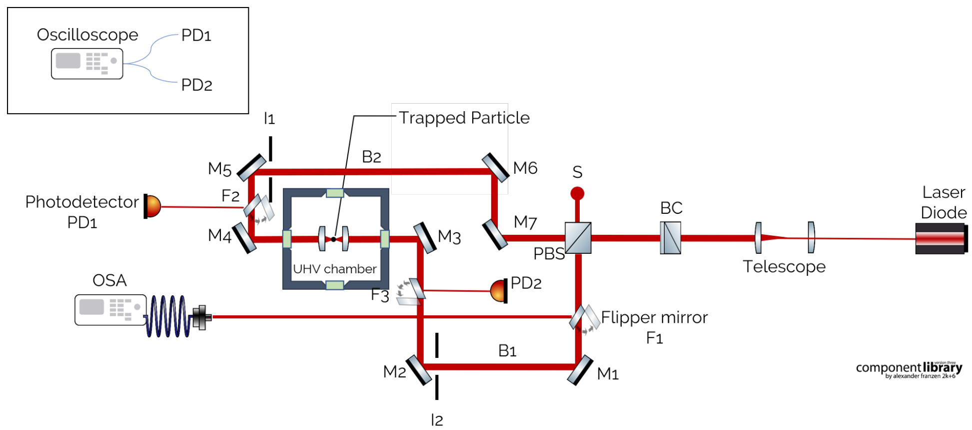

Figure 4.11: A schematic of our first horizontal dual-beam optical trap for trapping particles in air. A single 1030nm laser beam is split into two counter-propagating beams (B1 and B2) with a polarizing beam splitter (PBS) and balanced in power with a Babinet-compensator (BC). The beams enter the vacuum chamber and each pass through an 8mm aspheric lens.

Beam 1 was determined to be our 'standard' beam, which means once this beam is aligned through the entire system (back to spot S) it should no longer be adjusted and it is time to overlap Beam 2 by using the pinhole. The XYZ-translation stage for the pinhole was screwed to a metal plate to be mounted on the top edge of the vacuum chamber when the chamber top is removed. Making sure everything was secured tightly was important so that everything was level for alignment. The pinhole was housed in an aluminum machined mount on an optical post that would allow us to drop the pinhole inside the chamber between the two lenses from above (see Figure 4.12). Flipper mirrors (F2 and F3) were used to direct light from the beams (B1 and B2) to individual photodetectors (PD1 and PD2) that were connected to an oscilloscope for observation.

Each beam had to be aligned independently with the pinhole from the other and there was a constant 'back and forth' between the two beams. If you weren't careful, you'd forget to put the opposite flipper mirror down and wonder why your changes weren't being detected on the oscilloscope! The XYZ-translation stage was used to find the focal point of Beam 1 by a blind search away from the focus until a signal was seen on the oscilloscope (with 1MΩ input). As the pinhole was moved closer and closer to the focus, a 50 ohm resistor was added to the oscilloscope to make sure we were not saturating the detector (maximum voltage $\sim$ 200mV). Once the focus was found, the pinhole was no longer adjusted with its XYZ-stage.

Next, the flipper mirrors were adjusted to observe Beam 2, and the XYZ-translation stage inside the chamber was used for Beam 2 adjustment. This part of the procedure required your hand to be placed inside the chamber to make any changes and you'd hope that the pinhole mount wouldn't get bumped. Otherwise, you'd have to start the entire process over! Once the two beams were sufficiently overlapped, the pinhole was carefully removed from the chamber and the XYZ-stage and metal plate were removed from the top of the vacuum chamber.

The launching mechanism described in the previous sections was very carefully placed between the two lenses inside the chamber and the vacuum chamber was finally ready to try to trap particles. Figure 4.13 shows a soda lime glass particle trapped in Version 1 of the horizontal dual-beam trap setup. A 1030nm laser diode was used as the trapping laser and the particle was 5-25 microns in size. This success gave us confidence we were able to trap particles. However, the trapping yield was very low.

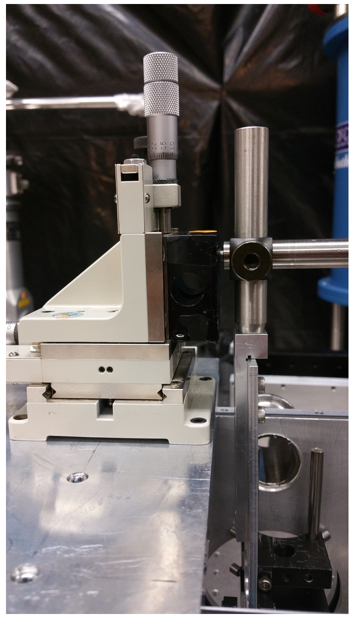

Figure 4.12: A 5μm pinhole in an aluminum mount which is attached to an XYZ-translation stage that sits atop the vacuum chamber for dual-beam alignment.

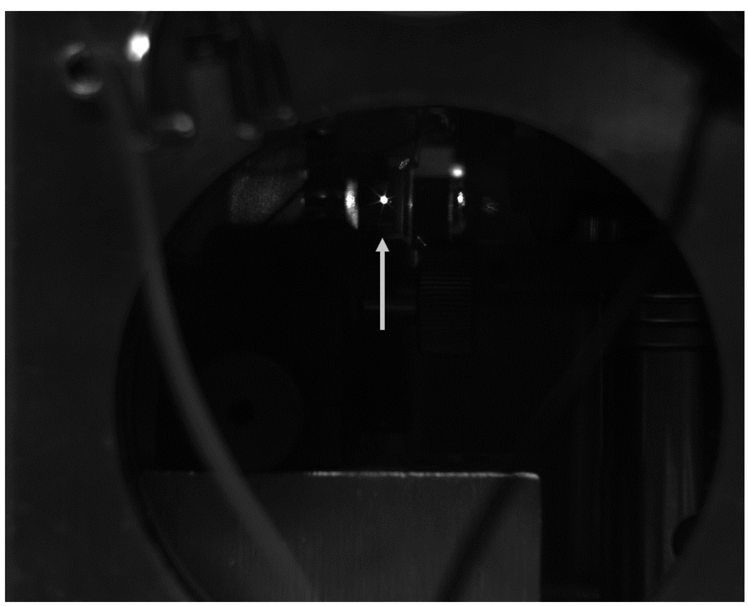

Figure 4.13: Trapped soda lime glass particle (5-25 micron diameter) in horizontal dual-beam optical trap.

Setup 2: Two Laser Diodes In an effort to be more successful with trapping particles, a redesign to double the power in each arm of the dual-beam trap and reduce coherent interference was considered and implemented in Version 2. This second design is nearly identical to Version 1 in concept, but different in implementation as seen in Figure 4.14. A second 1030nm laser diode was added and roughly half the mirrors were removed to simplify the alignment process. Both lasers have an output power of 250mW and Laser 2 still passed through the Babinet-compensator, but it is now just used to rotate the light coming from the diode to have the opposite polarization to that of Laser 1 instead of balancing the powers.

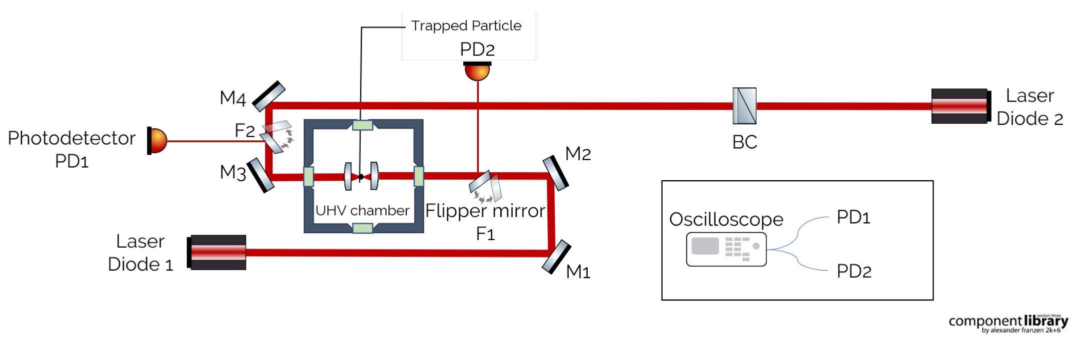

Figure 4.14: A schematic of our second horizontal dual-beam optical trap for trapping particles in air. Two 1030 nm laser beams (Laser 1 and Laser 2) enter the vacuum chamber and each pass through an 8 mm aspheric lens to create the trap. Laser 2 passes through a Babinet-compensator to change the polarization of the beam.

Several trapping attempts with various adjustments of this setup were made, but without successful trapping of a particle. During this phase of experimentation we realized how tedious our alignment procedure had become with the pinhole. The process was time consuming and we did not have high confidence that the alignment was very accurate due to the way the pinhole was mounted. Additionally, the XYZ-stage inside the vacuum chamber was not giving us enough control over our axial separation of the beams without messing up the transverse alignment. Each misalignment required re-installing the entire pinhole assembly and starting the alignment process over. One of our final concerns during this phase was also the quality of our beams since they were each coming from separate lasers, unlike version 1, and visually the beams were not Gaussian modes. Good beam quality is important for achieving good traps [23].

Setup 3: Fiber System Version 3 of our horizontal dual-beam trap addressed the issues found from Version 2. We implemented two polarization maintaining single mode fibers to act as spatial filters for each of our lasers that are Gaussian in nature with $w_x = w_y$. We added a 3:1 anamorphic prism pair after each laser beam, as shown in Figure 4.15, to better match the mode of the laser to the fibers for better efficiency. By switching to a fiber system, we were able to remove the 5-micron pinhole from our alignment procedure completely. For alignment, we now rely on Laser 1 being efficiently coupled into Fiber 2 as for ensuring beam overlap in the trap. We rely heavily on a floating photodetector (not pictured) that is outside the chamber for monitoring coupling efficiencies during this alignment procedure.

The alignment procedure described here begins after the lasers have been directed through the system to the vacuum chamber without the optical fibers or trap lenses in place. The fiber couplers will need to be aligned so that the light entering is collimated when it exits. We generally followed the procedure listed on the Thorlabs website with advice from Dr. Zeb Barber to accomplish this. Laser 1 must be well coupled into Fiber 1 and Laser 2 must be well coupled into Fiber 2. For both sides, the process is the same. A visible laser is attached to the end of the fiber to send light back towards M1 and M2 through the coupler (M7 and M8 for Fiber 2). Using mirrors M1 and M2, the laser light is overlapped with the visible light. Once the beams are overlapped, we remove the visible light from the end of the fiber and reattach to lens L1 (or the bulkhead for Fiber 2) and maximize the amount of light

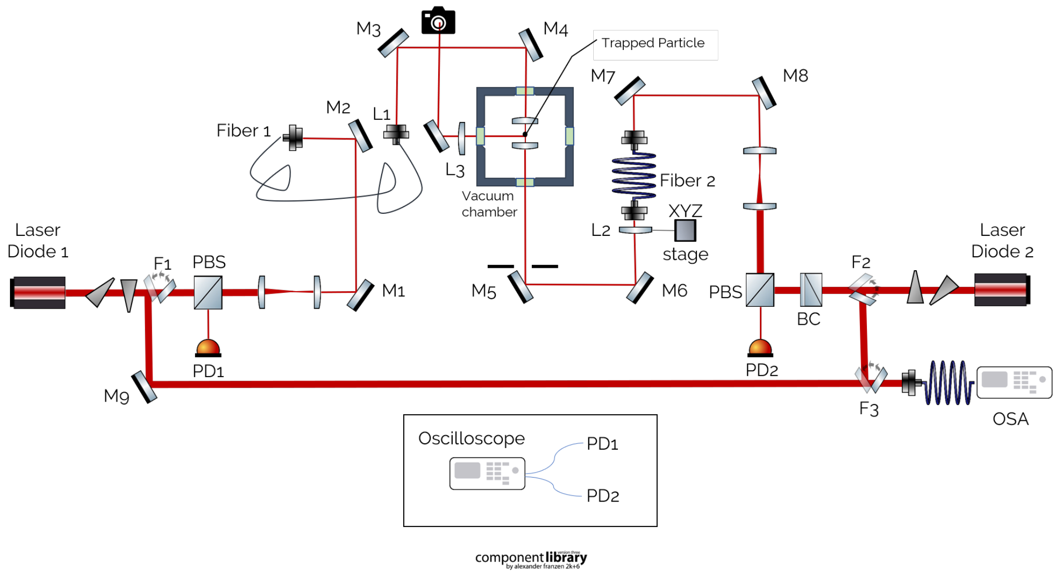

Figure 4.15: A schematic of our third horizontal dual-beam optical trap for trapping particles in air. Two 1030 nm laser beams (Laser 1 and Laser 2) pass through anamorphic prism pairs and polarization maintaing fibers. Beams then enter the vacuum chamber and pass through an 8 mm aspheric lens to create the trap. Laser 2 passes through a Babinet-compensator to change the polarization of the beam. A single plano-convex lens on an XYZ-stage serves as our fine control over separation of the two focal points inside the chamber.

that is exiting. Laser 1 is aligned again through the vacuum chamber and overlapped with Laser 2 by using mirrors M5 and M6. We use the floating photodetector to monitor Laser 1 after it exits Fiber 2 in order to maximize the light. At this point, the laser beams should be well-overlapped.

Next, we add the trap lenses back in the vacuum chamber and make sure the beams stay overlapped and collimated by only adjusting the XYZ-stage that is inside the chamber. The final adjustment is using M5 to maximize the light coming out of Fiber 2 from Laser 1. Now, we are able to adjust any separation of our beams from outside the chamber. This is possible with the single 40mm plano-convex lens mounted to the XYZ-stage right after Fiber 2. We are able to make any necessary adjustments without the risk of completely misaligning our beams since we are working outside of the chamber. The magnification between the movements (longitudinal and transverse) of the XYZ stage that held the 40 mm lens and the focus in the trap region are functions of the focal lengths of the two lenses. For transverse movement, the ratio of the lens movement to the laser spot movement is the ratio of the XYZ lens (40 mm) to the trap lens (8 mm) or 5:1 (actually inverted, but here we are interested only in magnitude of displacement). For longitudinal movement, the ratio is squared, so 25:1. Here we do care about the sign or at least the sense of the relative displacements. If the distance between the 40 mm lens and fiber is increased, the focal spot will move towards the 8mm lens (the one closest to the 40 mm lens), causing a positive z_{sep}, which is what is needed for good trapping. A negative z_{sep} will lead to an unstable trap. These movements were verified using an Excel spreadsheet calculator (developed by Prof. Babbitt) that followed the Gaussian beam propagation and ray tracing of the system from the fiber tip to the trap focus. The 25:1 ratio was valid (linear) up to about 100 micron lens movement. For 500 microns, the displacement of spot was 24 microns (20:1). For 1000 microns, the displacement of spot was 61 microns (16:1). Using the Excel program, the proper lens movement for any desired z_{sep} could be determined. The precision micrometers on the stage allowed for repeatable adjustments and accurate control of z_{sep}. Figure 4.16 shows the inside of the chamber for this design with the final iteration of the aluminum cantilever launcher and the two 8 mm aspheric lenses.

Overall, this final design is simpler to use when it comes to the alignment of the two beams. The precise control over the beam separation has been a nice addition. However, coupling into the fibers does produce a significant amount of power loss coming from each of our lasers at the moment (greater than 50%). We also discovered the confidence from trapping a "soda lime glass particle" amounted to "fake confidence". Although we did not have a successful attempt to trap a particle, we believe this set up will be capable of trapping particles, at least up to 8 microns in diameter. We will have greater ease of alignment and better adjustment of trap parameters with this design.

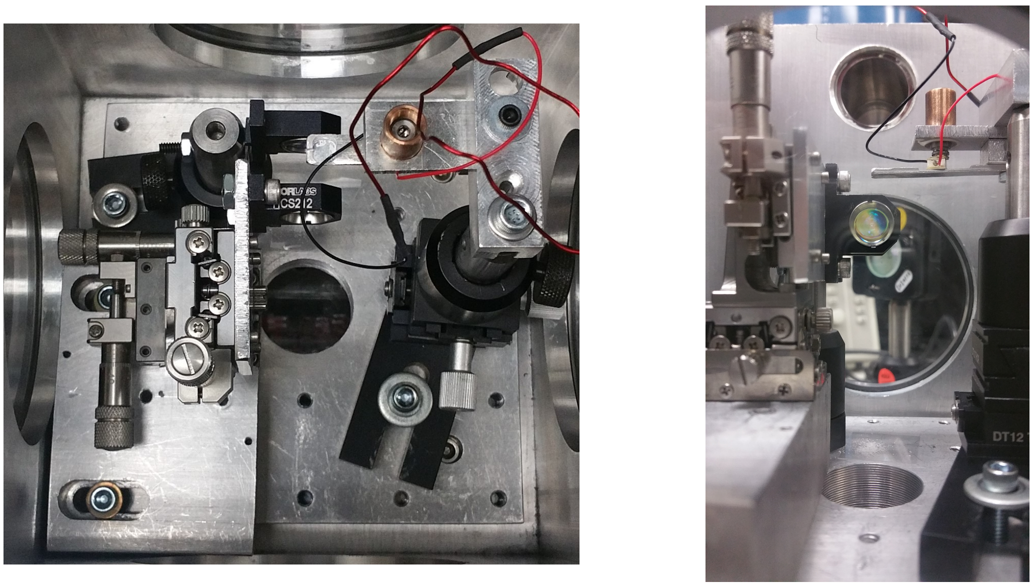

Figure 4.16: A look inside the vacuum chamber with the aluminum cantilever launcher and two 8 mm aspheric lenses in place. Left: Top view. Right: Side view.

Imaging

Imaging of a trapped particle consists of a CCD camera (Thorlabs: DCC1545M) and MATLAB code in collaboration with undergraduate Alec Dinerstein. The camera is placed on the side of the vacuum chamber as shown in the schematic in Figure 4.15 to view both lenses and the trap between them.

The MATLAB code written for image detection is designed to alert the user with a sound when a particle has been successfully trapped and to create an Image Report with details about the trapped particle. Figure 4.17 shows an example Image Report created with a test spot of a HeNe laser beam that was focused with a 125mm lens onto a beam stop. Each report produces a cropped image of the particle as shown in the top left image. Additionally, it provides information regarding the horizontal and vertical intensity of the particle shown by the graphs in the top right and bottom left respectively. The text on the bottom right of the Image Report shows *image energy* which is the total integrated power of all pixels in the vicinity of the spot with a subtracted background, *trap time* which is how long it took to trap the particle (with multiple attempts), and the *horizontal and vertical radius* of the particle, which is calculated from the image centroid. We also are utilizing the ThorCam software provided by Thorlabs to take images and video of trapped particles.

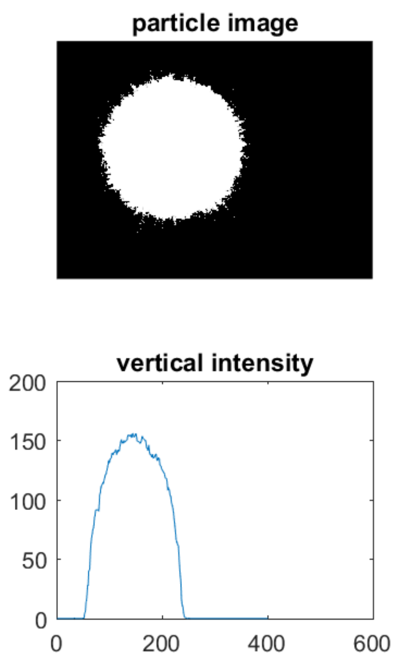

Figure 4.17: Example Image Report created from our 'Main Detection' MATLAB code. This example report was created with the spot of a HeNe laser beam focused by a 125mm lens. Every report includes a photo of the trapped particle (top left), horizontal (top right) and vertical (bottom left) intensity profiles of the trapped particle and text information about the time it took for a particle to become trapped, the horizontal and vertical radius as determined from the image and the image energy.

Time-lapse Imaging

To capture loading and trapping events, a 100mm lens (L3 in Figure 4.15) was added to magnify the trap region. A new MATLAB program was written to capture many frames as the loader was pulsed. Zoomed images in Figures 4.18 and 4.19 show two different time-lapse captures of silica particles falling into the trap region. Each row is one second in time and has six frames, $\frac{1}{6}s$ each (camera frame rate was limited to 6 frames per second). The loader is turned on in frame one (first row, first column) and turned off after a specified time ($\sim 4s$ in these examples). It takes about 2.5 seconds to reach the trap (4mm/s for terminal velocity $\sim 1cm$ above trap region). As particles fall from the loader and pass through the laser beams, they become bright white in the images. In both figures, bright spots appear in multiple frames, many without trapping.

Figure 4.18 is interesting because it shows four consecutive frames at the end of the image capture (row five, columns 2-5) where a particle is in the same position in each frame. The last image in row five is black because the camera had been turned off. Figure 4.19 shows a similar situation in row four, columns 3-6, though much dimmer compared to Figure 4.18. Although these current images are on a short timescale, they show the motion of particles as they interact with the trap and the possibility of capturing images of a particle as it initially becomes trapped and then stays in the trap for a long period of time. With this, we will be able to monitor the particle's motion over time and compare it to our simulations. Eventually, a quadrant photodetector will be used to measure a particle's well dynamics.

Without changing the lens position or focus, we were able to zoom out and take an image of the loader inside the trap and use it as a calibration measurement for the images in the time-lapse runs as the camera settings remained the same. Figure 4.20 shows the loader which is 5mm wide along the longitudinal axis of the laser. From

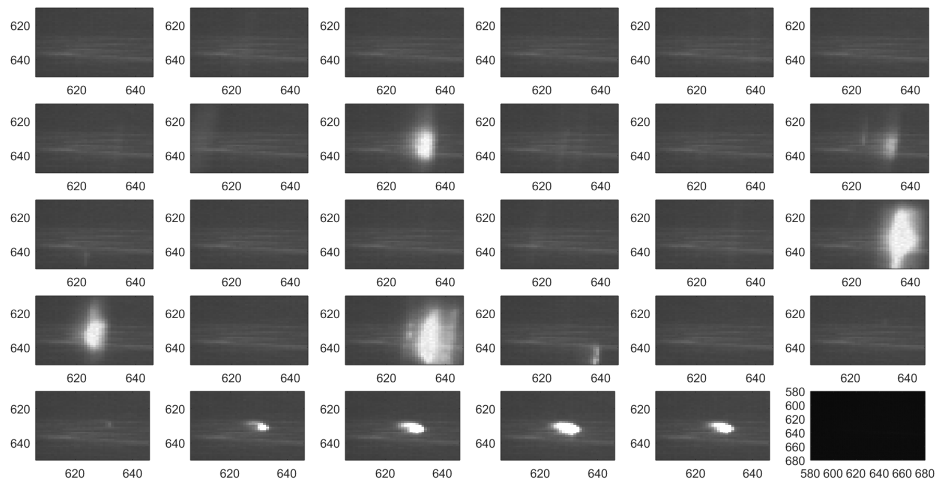

Figure 4.18: Time-lapse images of silica particles falling into the trap region. Z-separation is set to $-75\mu m$ during this capture. Each row is one second in time and each frame is $\frac{1}{6}s$. When particles interact with the laser beam they become bright white in the image.

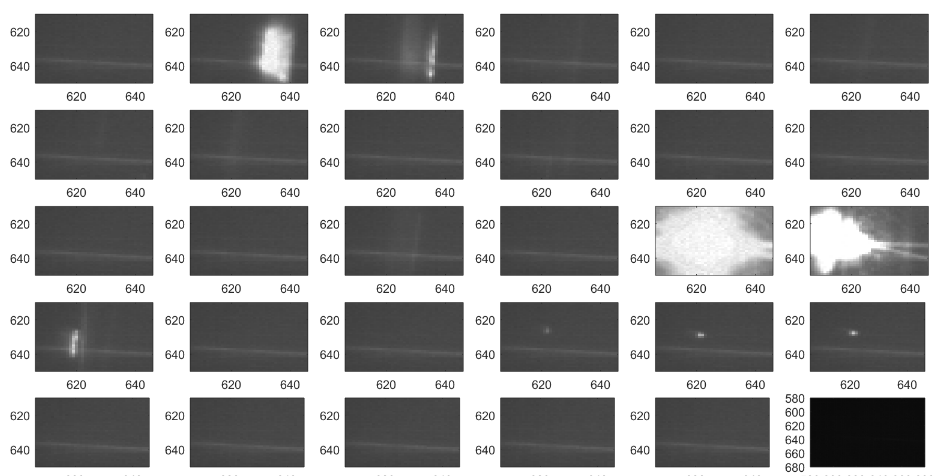

Figure 4.19: Time-lapse images of silica particles falling into the trap region. Z-separation is set to $-50\mu m$ during this capture. Each row is one second in time and each frame is $\frac{1}{6}s$. When particles interact with the laser beam they become bright white in the image.

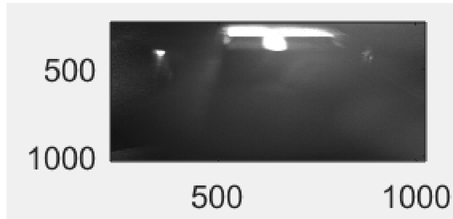

Figure 4.20: Image of loader inside vacuum chamber along the longitudinal axis of laser beams to use as a calibration measurement of μm/pixel with MATLAB tools. This calibration indicated $\sim 19\mu m$/pixel wide.

here we were able to find that the loader is ~265 pixels wide by using MATLAB tools. Therefore, each pixel is $\sim 19\mu m$ wide. Knowing this is important because it tells us that we should see the particle in each consecutive image stay centered the same pixel if it is indeed trapped.

Figures 4.21 and 4.22 show the individual zoomed in frames from Figures 4.18 and 4.19, respectively, where silica particles remain roughly in the same spot in the optical trap over time. Frames are now positioned such that time progresses from the top image to the bottom image ($\sim \frac{1}{6}$s per frame). The camera was shut off for the time-lapse photos in Figure 4.21, so the particle may have been trapped longer. The striations that are seen in the images still need further investigation.

By zooming in further and measuring the center of the spot, we could see tha the particles in Figure 4.21 were centered at $x = 631 \pm 2$ pixels , $y = 632 \pm 2$ pixels and Figure 4.22 were centered at $x = 621 \pm 1$pixel, $y = 627 \pm 2$ pixels, indicating a likely trapping event. Both of these examples, however, had the separation moved in the negative direction, instead of the positive direction. The difference is overlapping the foci past one another instead of pulling them apart.

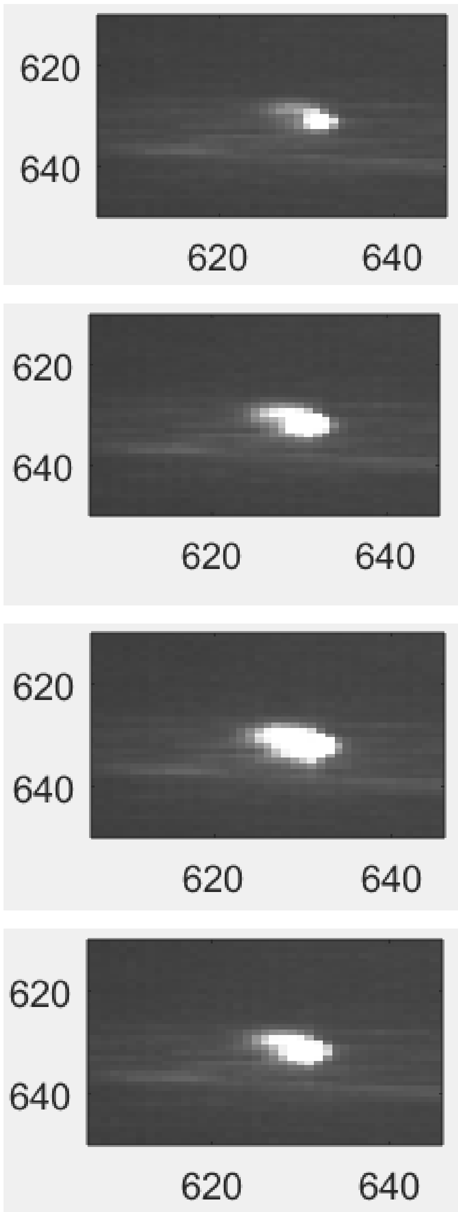

Figure 4.21: Four individual frames from Figure 4.18 of a silica particle remaining in the same position over time in images from top to bottom. The camera was shut off before more frames were captured. Z-separation is $\sim 75\mu m$.

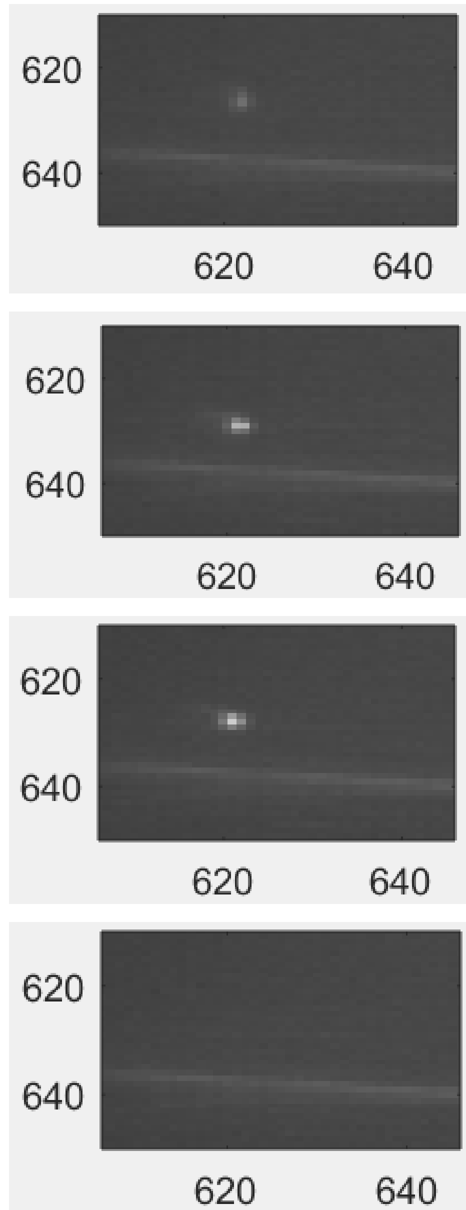

Figure 4.22: Four individual frames from Figure 4.19 of a silica particle traveling through the trap in roughly the same position and then being lost over time in images from top to bottom. Z-separation is $\sim 50\mu m$.

SYSTEM ANALYSIS

Silica Particles

Previous Discussion

Chapter 3 outlined the 'ideal trapping conditions' as defined by perfect alignment with no separations and balanced powers for an $8\mu m$ diameter silica particle. However, this configuration is nearly impossible to practically obtain. In addition, Chapter 3 went through the steps of adding in separations between the foci in both the longitudinal and transverse directions to achieve a practical stable trap and how this configuration would impact the optical trap. We know what conditions we are physically capable of achieving in the lab due to the analysis from Chapter 4. We must combine these two understandings in order to determine our best practical trapping configuration.

X-Tolerance

The x-transverse direction will be harder to trap than the longitudinal direction, as the particle enters this trap with a determined velocity of 4mm/s. In Chapter 4, we determined a 5:1 ratio in the transverse direction in terms of our ability to physically align the beams outside of the vacuum chamber (i.e. a 5 micron movement of external XYZ stage is equal to 1 micron movement inside the chamber). Here, we first focus on the tolerancing behavior in the transverse direction by running our MATLAB programs.

For a trap with balanced powers (30mW), no z-separation, and an $8\mu m$ diameter silica particle, changes in x-separation were explored. Figures 5.1 - 5.5 show plots for x-separation 0 - $10\mu m$ in $2.5\mu m$ increments between figures. Each figure has three plots (from top to bottom): transverse forces, potential well, and particle dynamics as the particle enters the well with terminal velocity. As an x-separation of $5\mu m$ is reached, a double-well begins to form which is defined in the potential well plot (middle plot). In all dynamics plots, the particle is initially dropped from the same point above the trap ($18\mu m$ - blue, $10\mu m$ - red) and would successfully be trapped in the transverse direction with these conditions. A double well would cause instabilities or uncertainties in trapped particle location. Therefore, we conclude that if we are able to keep our x-separation less than $2\mu m$ in practical lab conditions, we will be able to achieve stable and efficient trapping. Given the 5:1 ratio, this requires a $10\mu m$ control on the external XYZ-stage (in X and Y, at least). The XYZ-stage holding the 40mm lens has tick marks with $10\mu m$ precision and physically can be adjusted within $\frac{1}{10}$ of a tick, so sub-micron control is achievable with current setup, which is well within the tolerances needed.

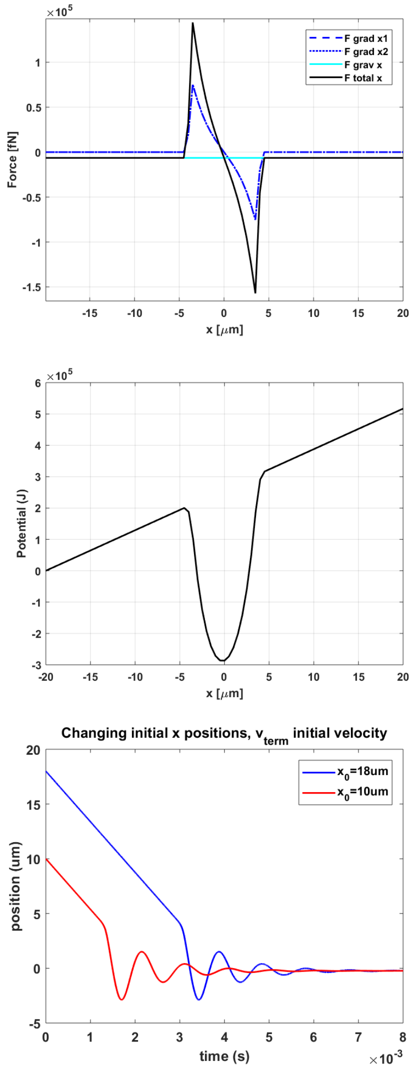

Figure 5.1: An $8\mu m$ diameter silica particle is analyzed in 3 plots for no z-separation and no x-separation. Transverse forces, transverse potential well, and particle dynamics as the particle is dropped above the trap region with terminal velocity are shown.

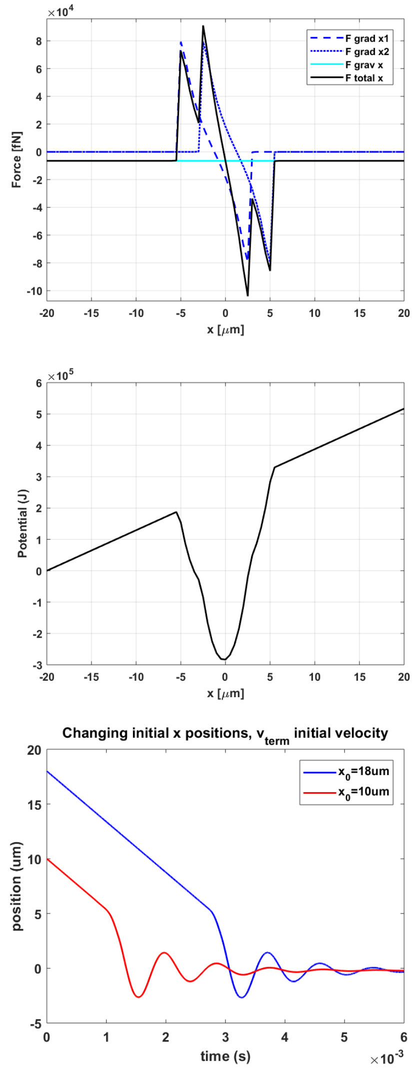

Figure 5.2: An $8\mu m$ diameter silica particle is analyzed in 3 plots for no z-separation and $2.5\mu m$ x-separation. Transverse forces, transverse potential well, and particle dynamics as the particle is dropped above the trap region with terminal velocity are shown.

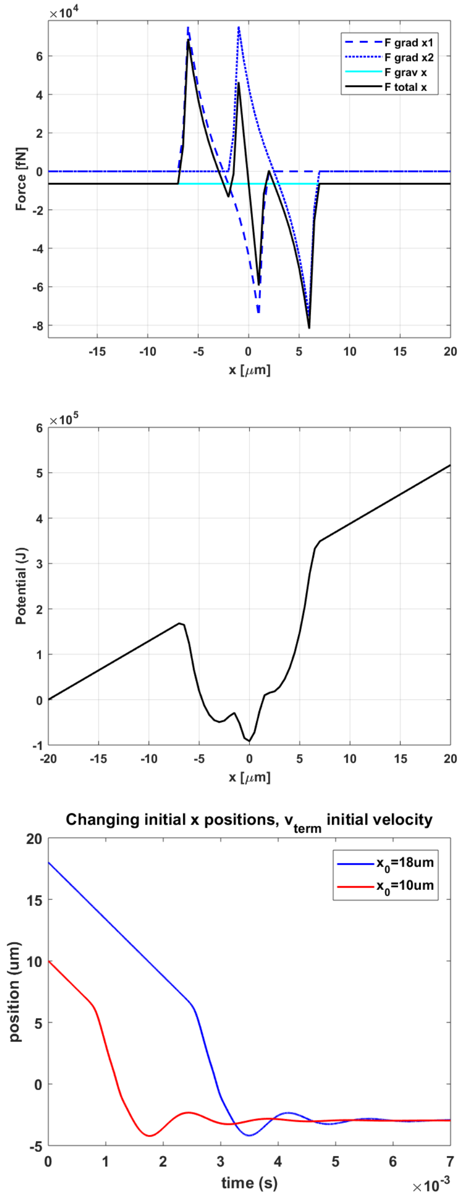

Figure 5.3: An $8\mu m$ diameter silica particle is analyzed in 3 plots for no z-separation and $5\mu m$ x-separation. Transverse forces, transverse potential well, and particle dynamics as the particle is dropped above the trap region with terminal velocity are shown.

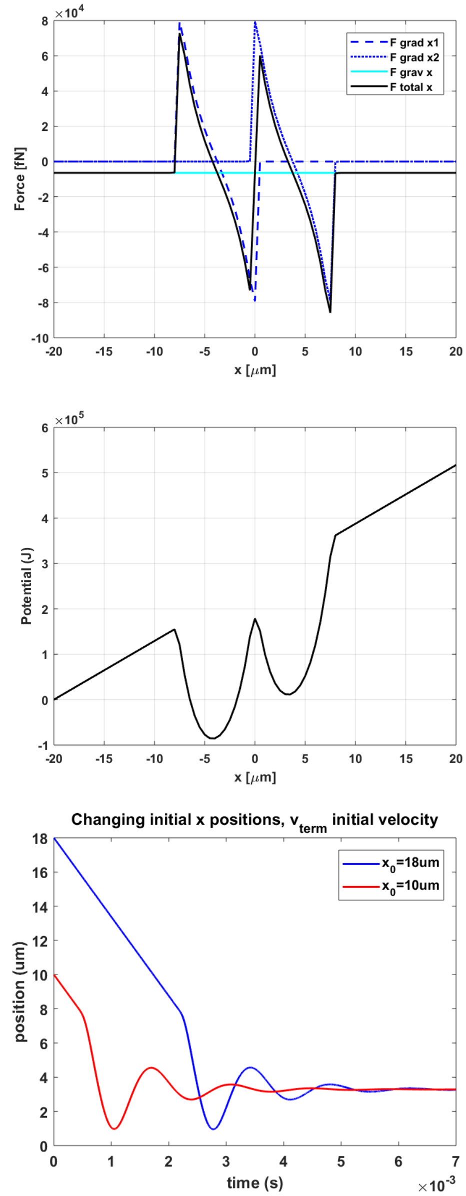

Figure 5.4: An $8\mu m$ diameter silica particle is analyzed in 3 plots for no z-separation and $7.5\mu m$ x-separation. Transverse forces, transverse potential well, and particle dynamics as the particle is dropped above the trap region with terminal velocity are shown.

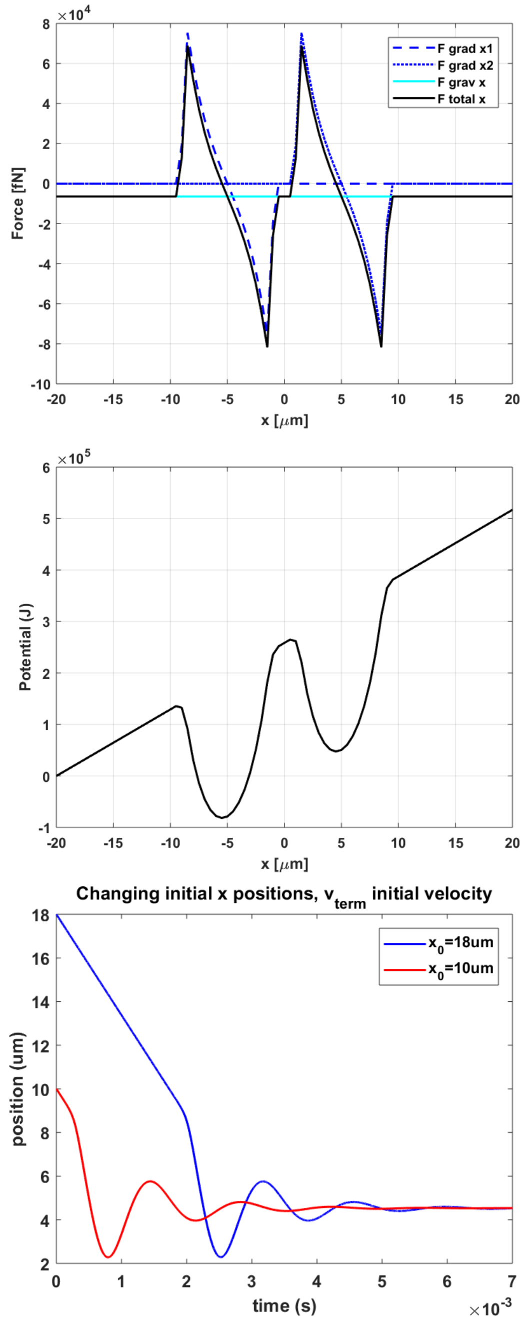

Figure 5.5: An $8\mu m$ diameter silica particle is analyzed in 3 plots for no z-separation and $10\mu m$ x-separation. Transverse forces, transverse potential well, and particle dynamics as the particle is dropped above the trap region with terminal velocity are shown.

Z-tolerance

Also, we want to know the tolerance in the longitudinal direction. In Chapter 4, we determined a 25:1 ratio (z-movement of XYZ-stage to z-movement of the focus of beam 2 in trap region) for being able to physically separate the beams along the longitudinal axis. A z-separation of $30\mu m$ has been chosen as our practical trapping condition because it is a value that produces reliable trapping over a range of x-separation values, 0-$4\mu m$, but is not excessively large and is physically obtainable. Figures 5.6-5.10 show plots for the $8\mu m$ diameter silica particle with our chosen z-separation and with x-separation from 0-$4\mu m$ in $1\mu m$ increments between figures. Traps are formed in each figure for the longitudinal direction. (These longitudinal dynamics plots are critically damped scenarios.) Therefore, using an experimental setup with balanced powers (30mW), $z_{sep} = 30\mu m$, $x_{sep} < 2\mu m$ should result in a stable trap for particles that are launched from above the trap region with terminal velocity.

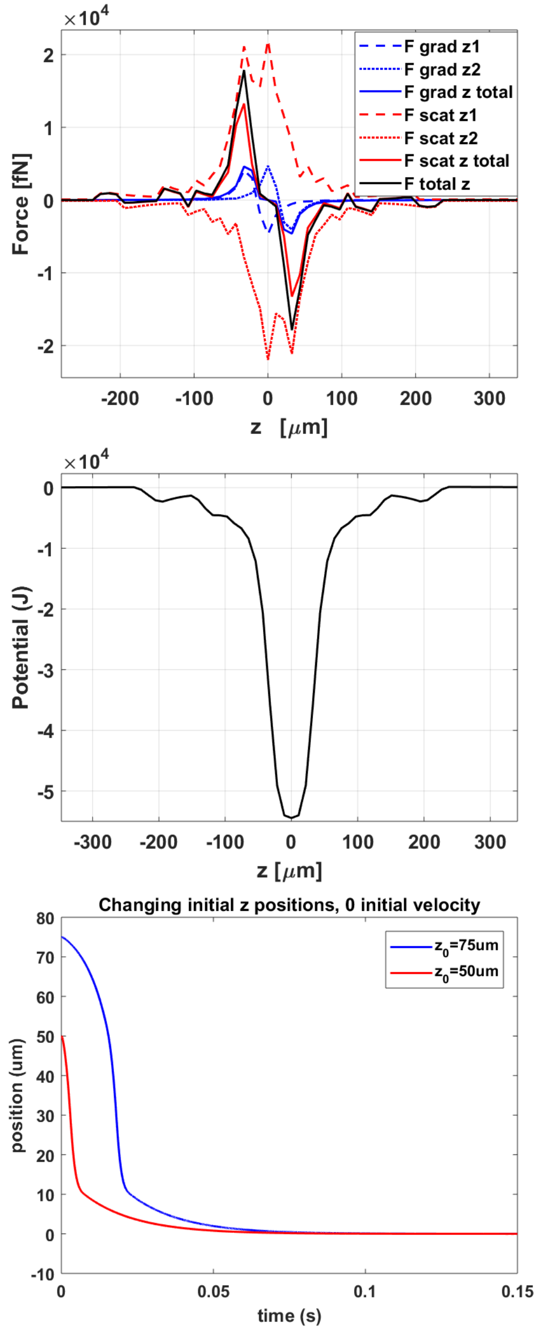

Figure 5.6: An $8\mu m$ diameter silica particle is analyzed in 3 plots for $30\mu m$ z-separation and no x-separation. Transverse forces, transverse potential well, and particle dynamics as the particle is dropped above the trap region with terminal velocity are shown.

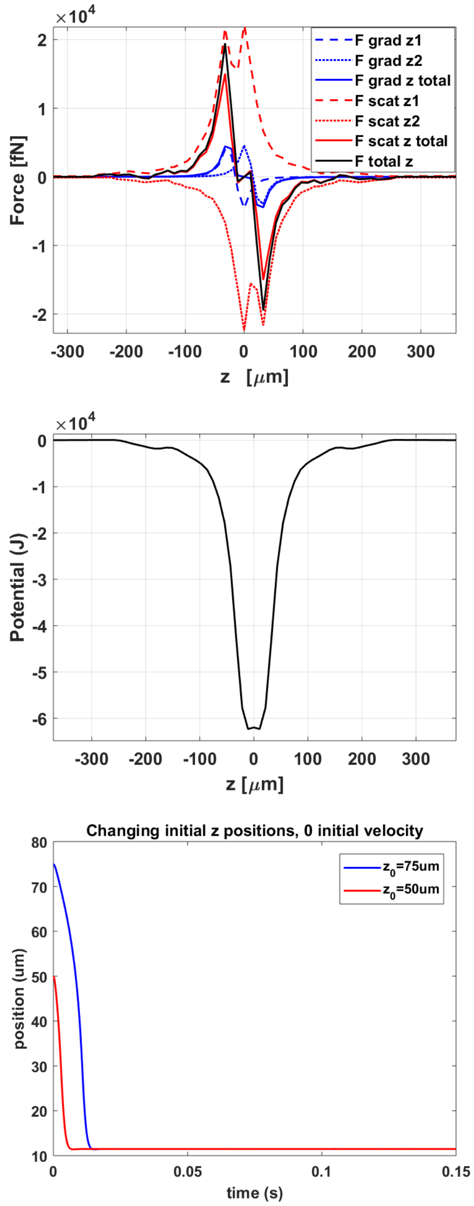

Figure 5.7: An $8\mu m$ diameter silica particle is analyzed in 3 plots for $30\mu m$ z-separation and $1\mu m$ x-separation. Longitudinal forces, longitudinal potential well, and particle dynamics as the particle is dropped above the trap region with 0 initial velocity are shown.

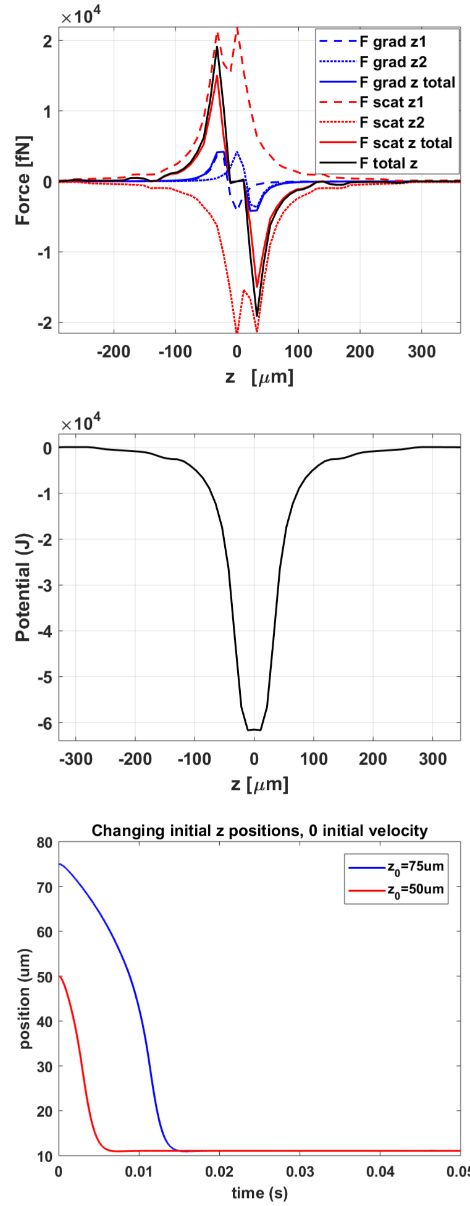

Figure 5.8: An $8\mu m$ diameter silica particle is analyzed in 3 plots for $30\mu m$ z-separation and $2\mu m$ x-separation. Longitudinal forces, longitudinal potential well, and particle dynamics as the particle is dropped above the trap region with 0 initial velocity are shown.

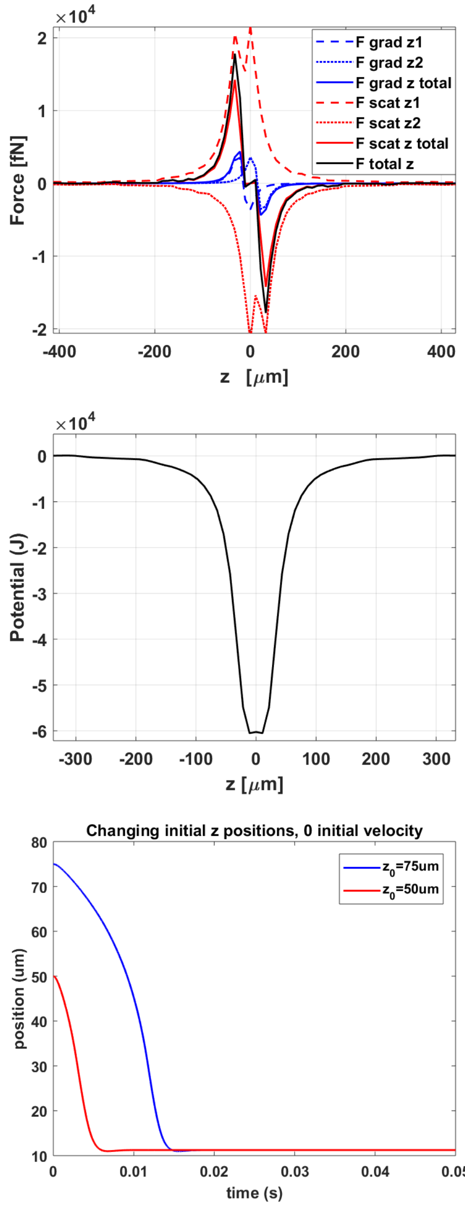

Figure 5.9: An $8\mu m$ diameter silica particle is analyzed in 3 plots for $30\mu m$ z-separation and $3\mu m$ x-separation. Longitudinal forces, longitudinal potential well, and particle dynamics as the particle is dropped above the trap region with 0 initial velocity are shown.

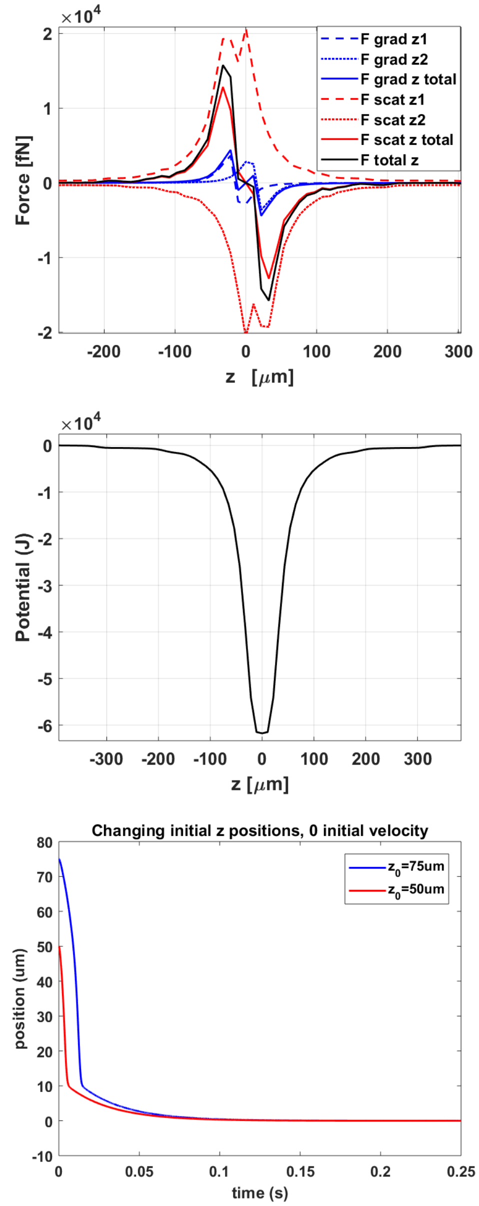

Figure 5.10: An $8\mu m$ diameter silica particle is analyzed in 3 plots for $30\mu m$ z-separation and $4\mu m$ x-separation. Longitudinal forces, longitudinal potential well, and particle dynamics as the particle is dropped above the trap region with 0 initial velocity are shown.

YAG Particles

Practical Lab Conditions

The ultimate goal is to be using rare-earth doped crystals that are fabricated in Dr. Charles Thiel's lab for optical trapping. Here, we use the same practical lab conditions for 8μm silica particles to look at the trapping potential of 8μm YAG particles. The two trapping beams are unbalanced with 40mW of power in Laser1 and 30mW of power in Laser 2. The two beams have z-separation set to 30μm and x-separation set to 0μm. Figures 5.11 and 5.12 show the transverse and longitudinal directions, respectively. In the transverse forces shown in the top plot of Figure 5.11, we can see gravity playing a much larger role than it did for the same size silica particle due to the change in density of the material.

We recognize that although we should be able to trap with these practical lab conditions for 8μm YAG, it is beyond the scope of this thesis to trap large YAG particles. The next section will shown an analysis for a large YAG particle 20μm in diameter.

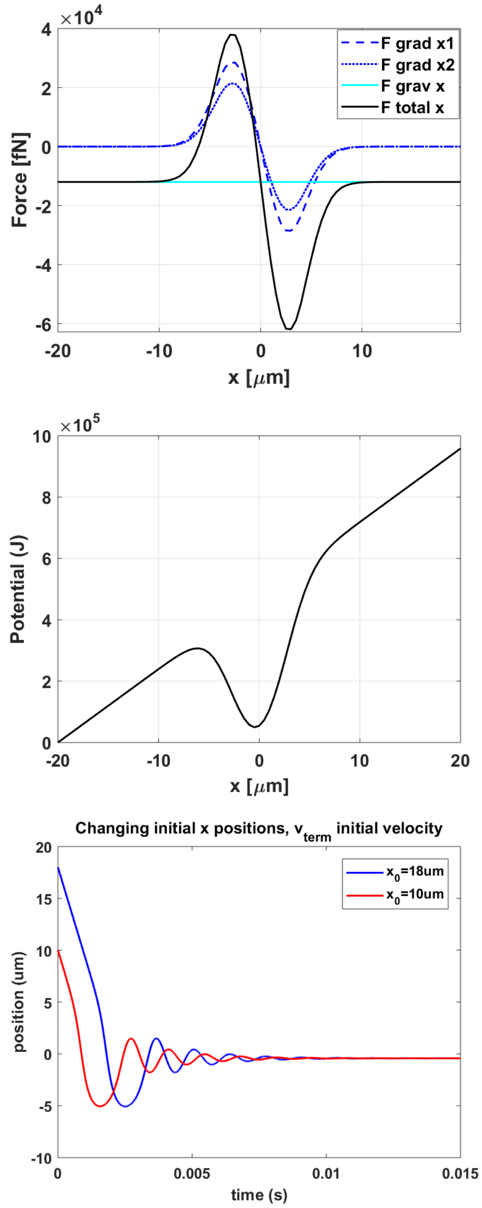

Figure 5.11: An $8\mu m$ diameter YAG particle is analyzed in 3 plots for 30 z-separation and no x-separation. Transverse forces, transverse potential well, and particle dynamics as the particle is dropped above the trap region with terminal velocity are shown.

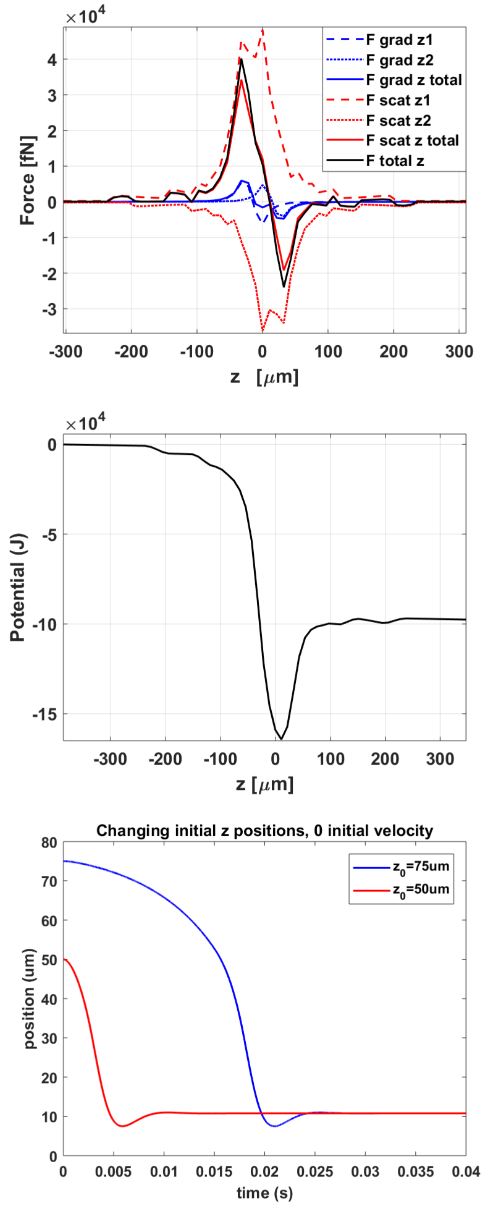

Figure 5.12: An $8\mu m$ diameter YAG particle is analyzed in 3 plots for 30 z-separation and no x-separation. Longitudinal forces, longitudinal potential well, and particle dynamics as the particle is dropped above the trap region with 0 initial velocity are shown.

Large YAG Particles

A larger YAG particle, $20\mu m$ in diameter, would not be trapped with our current experimental setup. Figure 5.13 shows the x-transverse direction for z-separation set to $30\mu m$ and x-separation set to $0\mu m$ with 40mW of power in Laser 1 and 30mW of power in Laser 2. Gravity has overtaken the forces of the trap, as shown in the top plot, and there is no potential well formed.

We then want to know what will it take to trap large YAG particles that would also be practical for future cooling experiments. Figures 5.14 and 5.15 show the transverse and longitudinal directions of new practical lab conditions, respectively. Z-separation is set to $30\mu m$ with x-separation set to $0\mu m$. The powers of the trapping beams are now balanced, but the power has increased to 100mW in each beam. We are not currently capable of 100mW of power for our experimental setup. The other major change is in the location of the particle launcher. It has been moved to below the trap region, whereas before, the particles were being launched from above the trap region.

When a $20\mu m$ particle is modeled with these conditions from above the trap region, it does not trap. In the plots shown here, the $20\mu m$ particle is below the trap region with an initial velocity set to $.1 * v_{term}$. Under these conditions, a $20\mu m$ YAG particle should be trapped in both the transverse and longitudinal directions if the placement of the loader is in an appropriate position. In the transverse dynamics plot of Figure 5.14, it can be seen that an initial x-location of -$18\mu m$ for the particle does not trap, but -$10\mu m$ would. Further analysis on the placement and characterization of the loader would be needed before moving forward.

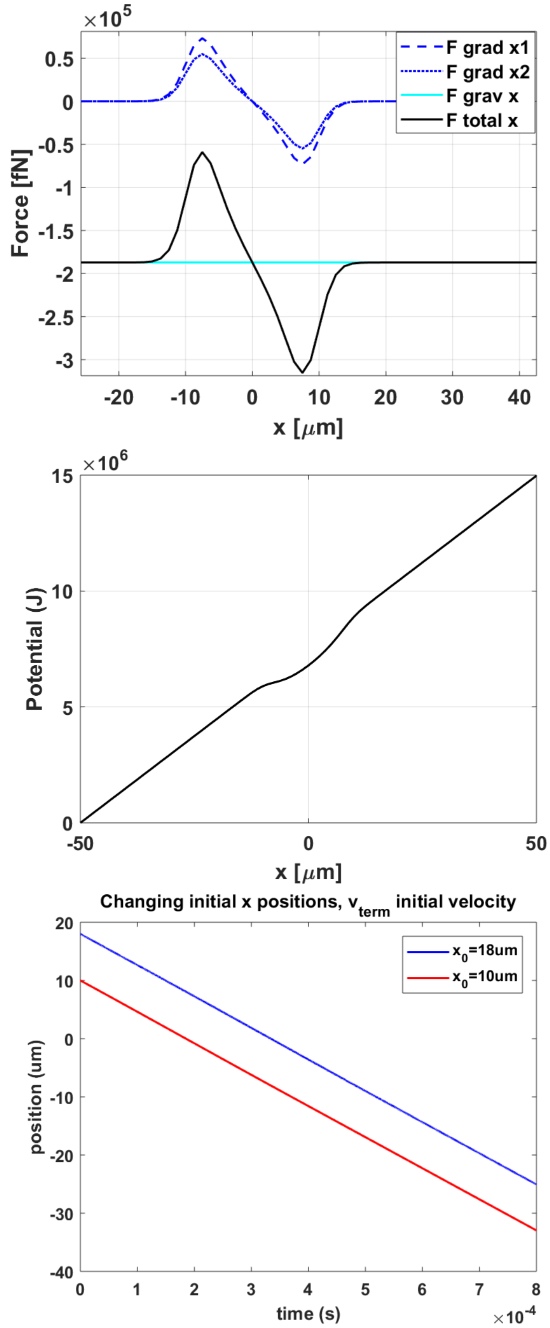

Figure 5.13: A $20\mu m$ diameter YAG particle is analyzed in 3 plots for $30\mu m$ z-separation and no x-separation. Transverse forces, transverse potential well, and particle dynamics as the particle is dropped above the trap region with terminal velocity are shown.

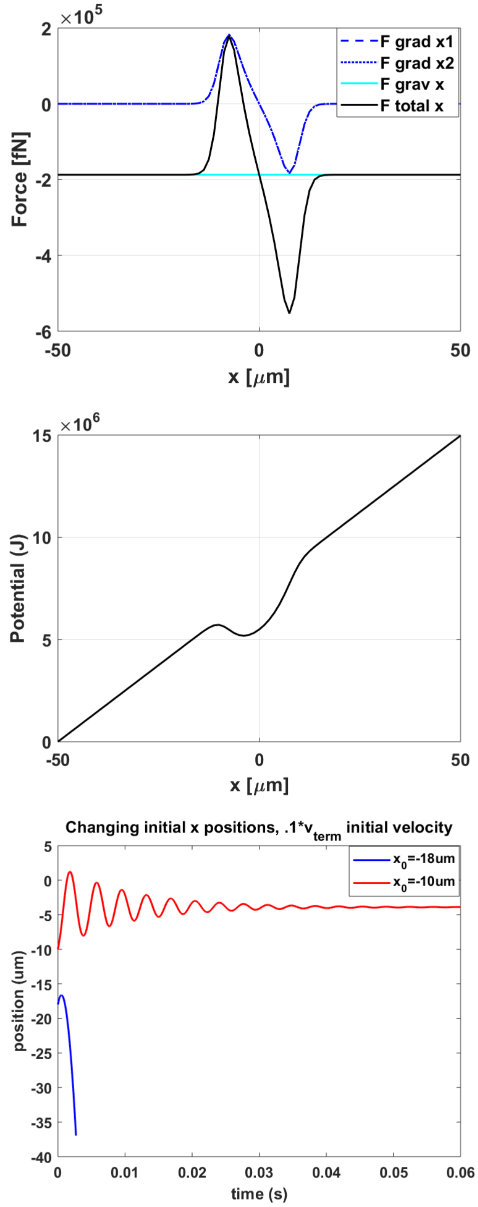

Figure 5.14: An 20μm diameter YAG particle is analyzed in 3 plots for 30μm z-separation and no x-separation. Transverse forces, transverse potential well, and particle dynamics as the particle is dropped above the trap region with 0 initial velocity are shown.

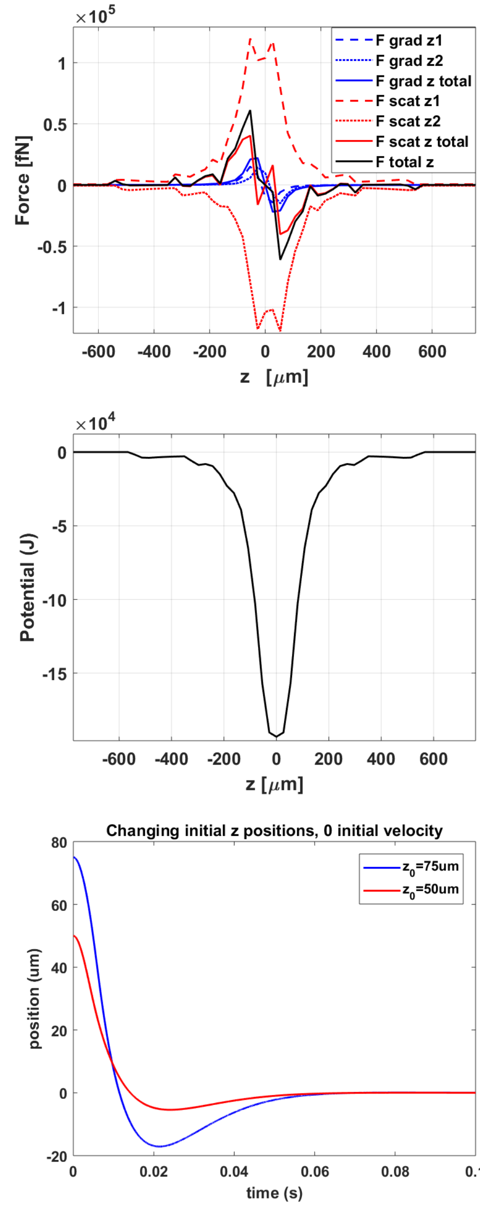

Figure 5.15: An 20μm diameter YAG particle is analyzed in 3 plots for 30μm z-separation and no x-separation. Longitudinal forces, longitudinal potential well, and particle dynamics as the particle is dropped above the trap region with 0 initial velocity are shown.

CONCLUSIONS

As we move to trapping large particles (10-30 microns) for testing the reduction or elimination of loss pressure, improvements are still needed. We believe that with the improved experimental design and a new launching mechanism, we will be able to take loss pressure measurements as the chamber is pumped down to vacuum. Additional imaging will be required to monitor the particle's motion for future studies. Future work on these experiments will continue in Babbitt and Thiel Labs at Montana State University.

Recommendations for Current Experimental Setup

We have been able to show that large particles ($\sim 20\mu m$) will not be trapped given the capabilities of our current design. Increasing the power used to trap particles is the next necessary change to the setup. The beam quality of our free space Qphotonics lasers required us to switch to a fiber system to clean up the mode of our lasers. However, the power of the current Fabry Perot laser is limited and fiber coupling has significant loss. One way to increase power is to use a gain chip. Qphotonics offers a gain chip, QGC-1030-160-200, but it does not provide much power beyond the capabilities of our current laser diodes (QLD-1030-250S). Although a gain chip is fairly cheap, it is not the recommended option.

A better option would be to purchase two single mode fiber coupled laser diodes with output 400mW at 1030nm. Qphotonics offers two models, QFBGLD-1030-400 or QFLD-1030-400S. The first model (QFBGLD-1030-400) is a single mode fiber Bragg grating 400mW laser diode with a tuning range of 18nm, 1017nm to 1035nm, at 9pm/°C. The second model (QFLD-1030-400S) is a 400mW fiber single mode Fabry Perot laser with a tuning range of 80nm, 1010nm to 1090 nm at 0.3nm/°C. Using one of these two models would allow for both increase in power and elimination of losses from fiber coupling. It also reduces some of the optical components, thus reducing the complexity of the overall experimental setup. The Fabry Perot laser is $1,960 and the fiber Bragg grating laser is $2,290. Either of these options (times two) would be a significant investment; however, at twice the power and half the losses, this is a significant increase ($\sim 4x$) in power, allowing either slightly larger particles, or quick and efficient trapping of 8-10μm particles.

Future Work

Launching Improvements

Although our current launching methods are proving to be reliable in their functionality, we have another design in mind when moving forward for this project. We will still utilize our same Arduino and MATLAB codes for driving a lever arm and automatic loading. The modification would be a 'cup' at the end of the lever arm (reservoir only) that is placed underneath the trapping region, which shoots particles upwards.

One of the disadvantages of our current launching method is that once particles fall out of the milled reservoir they just fall to the bottom of the chamber if they are not trapped. We currently keep a microscope slide on the bottom of the chamber to collect these particles with the intention of reusing them, which may lead to contamination issues. This also leads to frequent manual reloading of our launcher and we would like to keep the entire system as automated as possible. The idea is that if particles shoot up from the loader, then they are at the top of their trajectory and would be more easily trapped. This cup would allow for non-trapped particles to be recaptured as they fall under the force of gravity and relaunched into the system. This design will still require some damping of particle motion to facilitate trap loading. This damping could come from buffer gas or air. However, it could be accomplished by modulating the trap power or adding a pulsed vertical laser from the top, synchronized with loader oscillations, which may enable this to work in vacuum. This would eliminate the need to pump down chamber on each loading. Design, fabrication, and testing of this launcher are still needed.

Imaging Improvements

An addition to our imaging techniques will be a quadrant photo detector (QPD) that will image trapped particles vertically above the trap focus and/or from the side. This QPD will be used for measuring particle location and movement, enabling trap frequencies to be measured along with center-of-mass excitation. The detector has a "head," which is a circuit containing the quadrant photodiode and current-to-voltage amplifiers for transporting the measured signal to a "body" circuit through a multi-connector cable. The body circuit contains the necessary addition and multiplication amplifiers for converting the raw photodiode voltages to a meaningful position signal. The design and printed circuit boards are depicted in Figure 5.4 The population of these boards and testing are still needed.

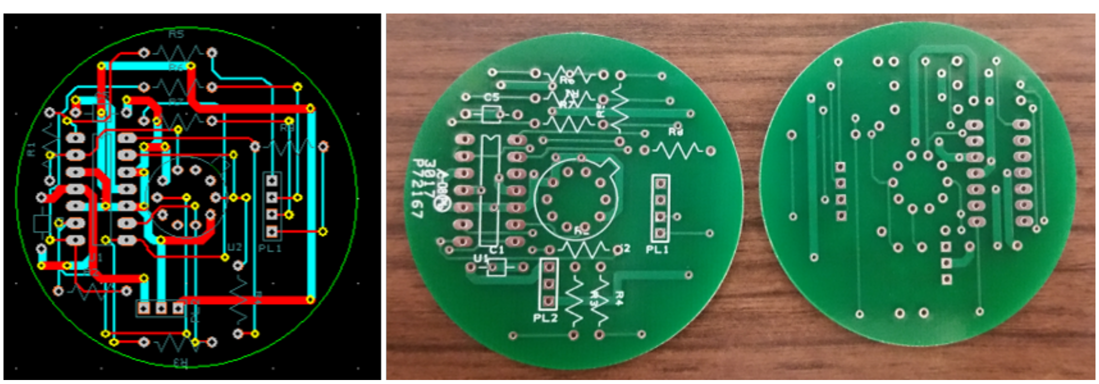

Figure 6.1: Left: Quadrant photodetector design. Right: Printed circuit boards for quadrant photodetector.

Code

Improvements to the already written MATLAB code are also in the process of being implemented. We have three individual codes for the pulsed loading/particle detection that should be combined into one program that additionally allows for the ThorCam software to be open and run while the MATLAB detection code is also running. This would allow the monitoring of the system as particles are being launched and not yet trapped, enabling any necessary adjustments to the placement of our launcher inside the vacuum chamber to be made.

The MATLAB program that created the time lapse images shown at the end of Chapter 4 can also be improved. We want to make sure we are 'watching' long enough to image a trapped particle after it initially falls in the trap region. This will vary among particle types and sizes due to terminal velocity so there will need to be an efficient way to update the code.

Cooling and Loss Pressure

The next phase of experiments is to trap rare-earth doped particles fabricated by Charles Thiel's group. Once these particles are trapped, we will apply the techniques developed from laser tuning to tune our lasers on and off resonance for the chosen rare-earth dopant. Right now our focus is on Yb:YAG as described in Chapter 2. The main addition that will be required is two bandpass filters to observe cooling. Observing this cooling effect is an important step to testing our main motivation. The main motivation of the next phase of experiments is to reduce or eliminate loss pressure when pumping down the vacuum chamber once a particle is trapped in air, specifically for large particles.

With our ability to model the particle loading dynamics and the proposed improvements, mentioned above, we now understand the changes that will need to be implemented and have highlighted areas that will need further study. We learned throughout this work that our goal of trapping large particles should be achievable in order to take the desired loss pressure measurements.

REFERENCES CITED

[1] A. Ashkin. Acceleration and trapping of particles by radiation pressure. *Phys. Rev. Lett.*, 24:156–159, Jan 1970.

[2] A. Ashkin and J. M. Dziedzic. Optical levitation by radiation pressure. *Applied Physics Letters*, 19(8):283–285, 1971.

[3] A. Ashkin and J. M. Dziedzic. Optical levitation in high vacuum. *Applied Physics Letters*, 28(6):333–335, 1976.

[4] Asimina Arvanitaki and Andrew A. Geraci. Detecting high-frequency gravitational waves with optically levitated sensors. *Phys. Rev. Lett.*, 110:071105, Feb 2013.

[5] Alexander G. Krause, Martin Winger, Tim D. Blasius, Qiang Lin, and Oskar Painter. A high-resolution microchip optomechanical accelerometer. *Nat Photon*, 6:768–772, 11 2012.

[6] ATMA Rahman, AC Frangeskou, MS Kim, S Bose, GW Morley, and PF Barker. Burning and graphitization of optically levitated nanodiamonds in vacuum. *Scientific reports*, 6:21633, 2016.

[7] Gambhir Ranjit, David P Atherton, Jordan H Stutz, Mark Cunningham, and Andrew A Geraci. Attonewton force detection using microspheres in a dual-beam optical trap in high vacuum. *Physical Review A*, 91(5):051805, 2015.

[8] Nikolai Kiesel, Florian Blaser, Uro Deli, David Grass, Rainer Kaltenbaek, and Markus Aspelmeyer. Cavity cooling of an optically levitated submicron particle. *Proceedings of the National Academy of Sciences*, 110(35):14180–14185, 2013.

[9] J Millen, T. Deesuwan, P. Barker, and J. Anders. Nanoscale temperature measurements using non-equilibrium Brownian dynamics of a levitated nanosphere. *Nature Nanotechnology*, 9:425, 2014.

[10] David P Atherton. *Sensitive Force Measurements With Optically Trapped Micro-Spheres in High Vacuum.* University of Nevada, Reno, 2015.

[11] A.T.M.A. Rahman and P F Barker. Laser refrigeration, alignment and rotation of levitated Yb^{3+}:YLF nanocrystals. *Nature Photonics*, 11(10):634–638, 2017.

[12] Arthur Ashkin, James M Dziedzic, JE Bjorkholm, and Steven Chu. Observation of a single-beam gradient force optical trap for dielectric particles. *Optics letters*, 11(5):288–290, 1986.

[13] Arthur Ashkin. Forces of a single-beam gradient laser trap on a dielectric sphere in the ray optics regime. *Biophysical journal*, 61(2):569–582, 1992.

[14] Agnese Callegari, Mite Mijalkov, A Burak Gököz, and Giovanni Volpe. Computational toolbox for optical tweezers in geometrical optics. *JOSA B*, 32(5):B11–B19, 2015.

[15] Yasuhiro Harada and Toshimitsu Asakura. Radiation forces on a dielectric sphere in the rayleigh scattering regime. *Optics communications*, 124(5-6):529–541, 1996.

[16] Christian Mätzler. Matlab functions for mie scattering and absorption, version 2. *IAP Res. Rep*, 8:1–24, 2002.

[17] Denis V Seletskiy, Richard Epstein, and Mansoor Sheik-Bahae. Laser cooling in solids: advances and prospects. *Reports on Progress in Physics*, 79(9):096401, 2016.

[18] Denis V Seletskiy, Markus P Hehlen, Richard I Epstein, and Mansoor Sheik-Bahae. Cryogenic optical refrigeration. *Advances in Optics and Photonics*, 4(1):78–107, 2012.

[19] Demi St John, Philip JT Woodburn, David Atherton, Charles Thiel, Zeb Barber, and Wm Randall Babbitt. Solid-state laser cooling of optically levitated particles. In *Optical Trapping and Optical Micromanipulation XV*, volume 10723, page 1072311. International Society for Optics and Photonics, 2018.

[20] Charles Thiel. private communication.

[21] Onofrio M. Marag Philip H. Jones and Giovanni Volpe. Optical tweezers: Principles and applications. [Online; accessed 6-November-2018].

[22] Hyperphysics R. Nave. Bar vibrational modes. [Online; accessed 6-November-2018].

[23] Andrew Geraci. private communication.

APPENDICES

APPENDIX A

RAYLEIGH DUAL-BEAM THEORY

The following MATLAB code is *Rayleigh_Dual_Beam_Horz_DRS_012218.m*. This file models the forces of a horizontal dual-beam trap in the Rayleigh regime for spherical particles. Case 2 was used for the analysis presented in this thesis. This code was written and modified by Demi St. John and Dr. Randy Babbitt.

```
%Rayleigh_Dual_Beam_Horz_DRS_012218.m
clear
figure(11);clf;
format compact
c=3e8; %speed of light (m/s)
k_boltzman=1.38e-23;%(J/K)
kT4K=4.0*k_boltzman;
g=9.9; %m/s^2
rho_Si=2.46*1e-3*1e6;%kg/m^3
rho_YAG=4.56*1e-3*1e6;%kg/m^3
rho_Diamond=3.5*1e-3*1e6;%kg/m^3
rho_AlO=3.97*1e-3*1e6;%kg/m^3


%Superfluid Parameters
n_He=sqrt(1.0576);
kappa=9.97e-4*1e-4; %m^2/s  quantum = h/(2*m_He)
Rho_s=[0.134 0.099 0.06]*1e-3*1e6; %kg/m^3  superfluid density
rho_s=Rho_s(1);

a_vari_case=0
switch a_vari_case
    case 0
        A_Vary = [1];
    case 1
        A_Vary=[1.03]*1e-6;
    case 2
        A_Vary=[.35 .375 .4 .425 .45 .475 .5]
    case 3
        A_Vary=(.01:.01:.2)*1e-6
    case 4
        A_Vary=[1.33 1.45 1.5 1.8 2.0]
       case 5
           A_Vary=1;
end

for a_Vary=A_Vary
    expt_case=2;
    switch expt_case
        case 1  %NSF proposal higher frefuency
           ******************************************
```

```
        n_1=1.5;    %index of particle
        n_2=sqrt(1.0576); %index of medium
        P1=0.01; % power of laser beam (W)
        P2=1.0*P1; % power of laser beam (W)
        z_sep=0*1e-6;
        lambda=1.500e-6; %wavelength
        a_p=3e-6; %particle radius (m)
        na=.68;   %NA of lens
        rho_p=rho_Si;%rho_Si;  %density of particle (kg/m^3)
  case 2   %Demi's project
n_1=1.5;    %index of particle
        n_2=sqrt(1); %index of medium
        P1=2.2; % power of laser beam (W)
        P2=1.0*P1; % power of laser beam (W)
        z_sep=-10*1e-6;
        lambda=1.06400e-6; %wavelength
        a_p=1e-6; %particle radius (m)
        na=.6;   %NA of lens
        rho_p=rho_Si;%rho_Si;  %density of particle (kg/m^3)

  case 3   %NSF proposal
      ******************************************
        n_1=1.8;    %index of particle
        n_2=sqrt(1.0576); %index of medium
        P1=0.2; % power of laser beam (W)
        P2=1.0*P1; % power of laser beam (W)
        z_sep=8*1e-6;
        lambda=0.800e-6; %wavelength
        a_p=0.1e-6; %particle radius (m)
        na=.23;   %NA of lens
        rho_p=rho_YAG;%rho_Si;  %density of particle (kg/m^3)
case 4   %AlO Sapphire
     ******************************************
        n_1=1.77;    %index of particle
        n_2=sqrt(1.0576); %index of medium
        P=1; % power of laser beam (W)
        lambda=0.800e-6; %wavelength
        a_p=0.04e-6; %particle radius (m)
        na=.46;   %NA of lens
        rho_p=rho_AlO;%rho_Si;  %density of particle (kg/m^3)
  case 5   %into Mie regime
        n_1=1.46;
        n_2=sqrt(1.0576);
        P=0.01; % power of laser beam (W)
        lambda=0.800e-6; %wavelength
```

```
        a_p=0.3e-6; %particle radius (m)
        na=.2;
        %_0=10e-6;
        rho_p=rho_Si;
end
switch a_vari_case
    case 0
        a_Vary=[];
    case 1
        lambda=a_Vary;
    case 2
        na=a_Vary;
    case 3
        a_p=a_Vary
    case 4
        n_1=a_Vary;
    case 5
end

w_0=n_2*lambda/(pi*na); %waist (m)

m=n_1/n_2;
k=2*pi*n_2/lambda;
rayleighrange=(k*w_0^2);

% z is along horizontal beam path, y is up, and x is
    transverse in
% horizontal plan.  The focus of the beams is seperate by
    z_sep
% z is measure from focus of beam 1 which comes from negative
     z
% Beam2 comes from positive z and focuses at z=z_sep
%positive z_sep means the beams cross after both come to
    focus
%The beam are assume to have the same waists, but different
    powers
xz_minmax=50e-6
x=0;
y=0;
xx=x/w_0;
yy=y/w_0;
Nz=201;
Z=linspace(-xz_minmax-z_sep,xz_minmax+z_sep,Nz);%*k*w_0^2;
ZZ=Z/(k*w_0^2);
ZZ_sep=z_sep/(k*w_0^2);
```

```
I1=2*P1/(pi*w_0^2); %Same as Mie code
I2=2*P2/(pi*w_0^2); %Same as Mie code

a_F_scat1=(8/3)*((n_2/c)*pi*(k^4))*(((m^2-1)/(m^2+2))^2)*I1;
F_scat_z1=a_F_scat1*(a_p^6)./(1+(2*ZZ).^2).*exp(-2*(xx^2+yy
    ^2)./(1+(2*ZZ).^2));
a_F_scat2=(8/3)*((n_2/c)*pi*(k^4))*(((m^2-1)/(m^2+2))^2)*I2;
F_scat_z2=-a_F_scat2*(a_p^6)./(1+(2*(ZZ-ZZ_sep)).^2).*exp
    (-2*(xx^2+yy^2)./(1+(2*(ZZ-ZZ_sep)).^2));

a_F_grad_z1=2*pi*n_2*8/(c*k*w_0^2)*(((m^2-1)/(m^2+2)))*I1;
F_grad_z1=-a_F_grad_z1*(a_p^3).*ZZ./((1+(2*ZZ).^2).^2)
    .*(1-2*(xx^2+yy^2)./(1+(2*ZZ).^2)).*exp(-2*(xx^2+yy^2)
    ./(1+(2*ZZ).^2));
a_F_grad_z2=2*pi*n_2*8/(c*k*w_0^2)*(((m^2-1)/(m^2+2)))*I2;
F_grad_z2=-a_F_grad_z2*(a_p^3).*(ZZ-ZZ_sep)./((1+(2*(ZZ-
    ZZ_sep)).^2).^2).*(1-2*(xx^2+yy^2)./(1+(2*(ZZ-ZZ_sep)).^2)
    ).*exp(-2*(xx^2+yy^2)./(1+(2*(ZZ-ZZ_sep)).^2));

%z=1*k*w_0^2/(2*sqrt(3));
z=z_sep/2;
zz1=z/(k*w_0^2);
zz2=(z-z_sep)/(k*w_0^2);
Nx=201;
X=linspace(-xz_minmax,xz_minmax,Nx);%*w_0;
XX=X/w_0;

a_F_grad_x1=2*pi*n_2*4/(c*w_0)*(((m^2-1)/(m^2+2)))*(I1);   %in
     paper, Harada has I0/2, but it doesn't make sense
F_grad_x1=-a_F_grad_x1*(a_p^3).*XX/((1+(2*zz1)^2)^2).*exp
    (-2*(XX.^2+yy^2)/(1+(2*zz1)^2));
a_F_grad_x2=2*pi*n_2*4/(c*w_0)*(((m^2-1)/(m^2+2)))*(I2);   %in
     paper, Harada has I0/2, but it doesn't make sense
F_grad_x2=-a_F_grad_x2*(a_p^3).*XX/((1+(2*zz2)^2)^2).*exp
    (-2*(XX.^2+yy^2)/(1+(2*zz2)^2));

mass_p=rho_p*(4*pi/3)*a_p^3;
F_grav_x=-mass_p*g;
F_total_z=F_grad_z1+F_grad_z2+F_scat_z1+F_scat_z2;
F_total_x=F_grad_x1+F_grad_x2+F_grav_x;
figure(11);clf;
plot((Z-z_sep/2)*1e6,F_grad_z1*1e15,'g--','linewidth',2)
hold on
plot((Z-z_sep/2)*1e6,F_grad_z2*1e15,'g:','linewidth',2)
```

```
plot((Z-z_sep/2)*1e6,F_scat_z1*1e15,'m--','linewidth',2)
plot((Z-z_sep/2)*1e6,F_scat_z2*1e15,'m:','linewidth',2)
plot((Z-z_sep/2)*1e6,F_total_z*1e15,'r-','linewidth',2)
plot(X*1e6,F_grav_x*1e15*ones(1,length(ZZ)),'c:','linewidth'
    ,2)
plot(X*1e6,F_grad_x1*1e15,'b:','linewidth',2)
plot(X*1e6,F_grad_x2*1e15,'b--','linewidth',2)
plot(X*1e6,F_total_x*1e15,'k-','linewidth',2)
grid on
legend('F grad z1','F grad z2','F scat z1','F scat z2','F 
   total z','F grav x','F grad x1','F grad x1','F total x');
ylabel('Force (fN)','FontWeight','bold')
xlabel('z - zsep/2 for Fz (um)  and  x for Fx (um) ','
   FontWeight','bold')
title1=['Rayleigh: Dual Beam Horizontal Trapping Forces'];
title2=['Beam: Wavelength1=' num2str(lambda*1e6) 'um, N.A.='
   num2str(na)];
title3=['Waist=' num2str(w_0*1e6) 'um, Power1=' num2str(P1*1
   e3) 'mW, Power2=' num2str(P2*1e3) 'mW, z sep=' num2str(
   z_sep*1e6) 'um'];
title4=['Particle: Radius=' num2str(a_p*1e6) 'um; Density='
   num2str(rho_p*1e-3) 'g/cm^3, Index=' num2str(n_1) ];
ylimmax=max(max(abs(F_total_x)),max(abs(F_scat_z1)));
ylim([-1.1*ylimmax 1.1*ylimmax]*1e15);
%ylim([-1.5*abs(F_scat_z1)) max(1.5*abs(F_scat_z1))]*1e15);
%ylim([-1500 1500]);
%ylim([-max(1.5*abs(F_scat_z1)) max(1.5*abs(F_scat_z1))]*1e15
   );

%ylim([-max(1.5*abs(F_total_x)) max(1.5*abs(F_total_x))]*1e15
   );
%ylim([-1500 1500]);
xlim([-(xz_minmax) (xz_minmax)]*1e6);
%title({title1;title2;title3;title4})
ax = gca;
ax.FontWeight='bold';


%analysis
if(1)  %trap
    %analysis Z trap
    i_Fz_max=find(F_total_z==max(F_total_z));
    i_Fz_min=find(F_total_z==min(F_total_z));
    F_trap_max_z=min(max(F_total_z),-min(F_total_z));
    [dum i_zero]=min(abs(F_total_z(i_Fz_max:i_Fz_min)));
```

```
i_zero=i_zero+i_Fz_max-1;
trap_well_depth_z=-sum(F_total_z(i_zero:i_Fz_min))*(Z(2)-
    Z(1));
U_grad_z=2*pi*n_2*(a_p^3)/c*(((m^2-1)/(m^2+2)))*I1;

amp_z=min(Z(i_zero)-Z(i_Fz_max),Z(i_Fz_min)-Z(i_zero));
k_osc_z=-(F_total_z(i_zero+1)-F_total_z(i_zero-1))/(Z(
    i_zero+1)-Z(i_zero-1));
f_osc_z=sqrt(k_osc_z/mass_p)/(2*pi);
%analysis X trap
i_Fx_max=find(F_total_x==max(F_total_x));
i_Fx_min=find(F_total_x==min(F_total_x));
trap_well_depth_x=-sum(F_total_x(round((Nx+1)/2):i_Fx_min
    ))*(X(2)-X(1));

F_trap_max_x=min(max(F_total_x),-min(F_total_x));

[dum i_zero]=min(abs(F_total_x(i_Fx_max:i_Fx_min)));
i_zero=i_zero+i_Fx_max-1;
amp_x=min(X(i_zero)-X(i_Fx_max),X(i_Fx_min)-X(i_zero));
k_osc_x=-(F_total_x(i_zero+1)-F_total_x(i_zero-1))/(X(
    i_zero+1)-X(i_zero-1));
f_osc_x=sqrt(k_osc_x/mass_p)/(2*pi);
%Analyze superfluid expt
a=a_p; %radius of particle (m)
s=a_p; %Peak trap force is less than F_trap at s=a_p
F_V_trap_max=(a/s)^3*rho_s*kappa^2/(3*pi);   %peak force
    of vortex  (N)
amp_z_critical=2.6*sqrt(kappa/(2*pi*f_osc_z));
amp_x_critical=2.6*sqrt(kappa/(2*pi*f_osc_x));
V_peak_z=2*pi*f_osc_z*amp_z;
V_peak_x=2*pi*f_osc_x*amp_x;

disp('********')
if(1)
    fprintf('F_Trap_max_z=%2.2f fN;    amp_z=%2.2f um;   
       f_osc_z=%2.2f kHz; z_min=%2.2f um;   \n',
       F_trap_max_z*1e15,amp_z*1e6,f_osc_z*1e-3,Z(i_zero)
       *1e6);
    fprintf('F_Trap_max_x=%3.2f fN;    amp_x=%3.2f um;   
       f_osc_x=%3.2f kHz \n',F_trap_max_x*1e15,amp_x*1e6
       ,f_osc_x*1e-3);
    fprintf('kT4K=%2.2e fJ;    U_grad_z=%2.2e fJ;       
       Trap_depth_z=%2.2e fJ;    Trap_depth_x=%2.2e fJ;  
          \n',kT4K*1e15,U_grad_z*1e15,trap_well_depth_z*1
```

```
            e15,trap_well_depth_x*1e15);
          fprintf('rayleigh␣range=%2.2f␣um;␣beam␣waist=%2.2f␣um
            ␣\n',rayleighrange*1e6, w_0*1e6);
          fprintf('Max␣Vortex␣Trap␣Force=%3.2f␣fN␣\n',
            F_V_trap_max*1e15);
          fprintf('V_peak_z=%2.2f␣m/s␣␣␣␣V_peak_x=%2.2f␣m/s␣\n'
            ,V_peak_z,V_peak_x);
          fprintf('Amp_z_trap=%2.2f␣um␣␣␣␣Amp_x_trap=%2.2f␣um␣\
            n',amp_z*1e6,amp_x*1e6);
          fprintf('Amp_z_crit=%2.2f␣um␣␣␣␣Amp_x_trap=%2.2f␣um␣\
            n',amp_z_critical*1e6,amp_x_critical*1e6);
        end
        disp(a_Vary)
        fprintf('z_ampRatio=%2.2d␣␣␣␣␣␣␣␣x_ampRatio=%2.2f␣␣␣
          Trap_Ratio=%2.2f␣\n',amp_z/amp_z_critical,amp_x/
          amp_x_critical,F_trap_max_z/F_V_trap_max);

    else
        disp('No␣trap')
    end

end
```

APPENDIX B

OTGO DUAL-BEAM THEORY

The following MATLAB code is *OTGO_RAY_dual_beam_horz_DRS_101518.m*. This is a modified file from reference [8]. The original MATLAB file was *efficiencies_beam.m* from the author's example code. It has been modified to represent a horizontal dual-beam trap for spherical particles by plotting the forces and potential wells. This program also feeds the force values as global variables to the Particle Loading Dynamics code in Appendix D. This code has been edited and modified by Demi St. John, Dr. Randy Babbitt, and Norhan Abbas.

```
%OTGO_RAY_dual_beam_horz_DRS_101518.m
% EFFICIENCIES_BEAM Scattering of a beam on a spherical particle
%
% Calculation of the trapping efficiencies corresponding to the
    scattering
% of a focused beam on a spherical particle as a function of the
    position
% of the particle with respect to the focal point.
%
% See also Ray, BeamGauss, ParticleSpherical.
%
% This example is part of the OTGO - Optical Tweezers in
    Geometrical Optics
% software package, which complements the article by
% Agnese Callegari, Mite Mijalkov, Burak Gokoz & Giovanni Volpe
% 'Computational toolbox for optical tweezers in geometrical
    optics'
% (2014).

% Author: Agnese Callegari
% Date: 2014/01/01
% Version: 1.0.0

% Workspace initialization

%Changes to this code have been made by: Demi St. John, Wm.
    Randall Babbitt
%& Norhan Abbas from Montana State University

%Last changes made: 10/15/2018

%z is along horizontal beam path, x is up, and y is transverse in
     horizontal plane.
%I've made beam 2 'negative' in regards to scattering force to
    represent
%beam 2 coming from the opposite direction of beam 1
clear;
```

```
clc;
tic
global FX_total FZ_total x z k_spring_x
% Figure Parameters
N_fig=50;
figure(N_fig+1);clf;
figure(N_fig+2);clf;
figure(N_fig+3);clf;
figure(N_fig+4);clf;

% Medium
nm = 1.0; % Medium refractive index

%Constants
c=3e8; %speed of light (m/s)
k_boltzman=1.38e-23;%(J/K)
kT4K=4.0*k_boltzman;
g=9.8; %m/s^2 - gravity

%Density of Particles
rho_Si=2.46*1e-3*1e6;%kg/m^3
rho_YAG=4.56*1e-3*1e6;%kg/m^3
rho_Diamond=3.5*1e-3*1e6;%kg/m^3
rho_AlO=3.97*1e-3*1e6;%kg/m^3
n_YAG=1.8;
n_Si=1.5;

% Spherical particle
R = 10e-6; % Particle radius [m]
np = n_YAG; % Particle refractive index
rho_p=rho_YAG;
mass = 4.0/3.0*pi*R^3*rho_p;%4560 % Particle mass (kg) = volume*
    density(kg/m^3)
z_sep=30e-6; %Longitudinal Separation of waists (by moving beam
    1 -z_sep/2 and beam 2 +z_sep/2
x_sep=0e-6; %Transverse Separation of waists (by moving beam 1 -
    x_sep/2 and beam 2 +x_sep/2

% Force of Gravity on Spherical Particle
gravity_x = -mass*9.8;

% Focusing Beam 1
lambda=1030e-9; %meters
f = .008;%50000e-6; % Focal length [m]
D=2*0.004;%20000e-6; diameter of rays at lens
```

```
%NA = 0.4; % numerical aperture
NA=nm*D/(2*f);
L = f*NA/nm; % Iris aperture [m]
waist1=nm*lambda/(pi*NA); %waist at z=0

% Focusing Beam 2
lambda2=1030e-9;%meters
f2 = .008;%50000e-6; % Focal length [m]
D2=2*0.004;%20000e-6;
%NA = 0.4; % numerical aperture
NA2=nm*D2/(2*f2);
L2 = f2*NA2/nm; % Iris aperture [m]
waist2=nm*lambda2/(pi*NA2); %waist at z=0

% Trapping beam 1
Ex0 = 1; % x electric field [V/m]
Ey0 = 1i*0; % y electric field [V/m]
w0 = D/2/2; % Beam waist at lens [m]
Nphi = 40; % Azimuthal divisions
Nr = 40; % Radial divisions
power = .1; % Power [W]

% Trapping beam 2
Ex2 = 1; % x electric field [V/m]
Ey2 = 1i*0; % y electric field [V/m]
w02 = D2/2/2; % Beam waist at lens[m]
Nphi2 = Nphi; % Azimuthal divisions
Nr2 = Nr; % Radial divisions
power2 = .1; % Power [W]

% Positions where to calculate the trapping forces
Nxz=40;%This number dictates how long it will take to run your
    plots and the quality (curvy vs sharp)
z_max_factor=108;
x_max_factor=5;
dx=x_max_factor/Nxz;
dz=z_max_factor/Nxz;
z = [-z_max_factor:dz:z_max_factor]*R; % Longitudinal (z)
    direction [m]
x = [-x_max_factor:dx:x_max_factor]*R; % Transversal (x)
    direction [m] **Defined x the same as z to remove the plotting
     of 0 twice**
% z = 10*[-1.6:0.02:1.6]*R; % Longitudinal (z) direction [m]
% x = [0:0.02:1.6]*R; % Transversal (x) direction [m]
```

```
% Initialization

% Trapping beam 1
bg = BeamGauss(Ex0,Ey0,w0,L,Nphi,Nr);
bg = bg.normalize(power); % Set the power

% Trapping beam 2
bg2 = BeamGauss(Ex2,Ey2,w02,L2,Nphi2,Nr2);
bg2 = bg2.normalize(power2); % Set the power

% Calculates set of rays corresponding to optical beams
r = Ray.beam2focused(bg,f);
r2 = Ray.beam2focused(bg2,f2);

% New focal points pertaining to transverse separation of waists
    (by moving
% beam 1 -x_sep/2 and beam 2 +x_sep/2)
o_x1 = -x_sep/2; %% x coordinate of the focal point of the first
     beam
o_x2 = x_sep/2;  %% x coordinate of the focal point of the second
     beam
o_z1 = -z_sep/2; %% z coordinate of the focal point of the first
     beam
o_z2 = z_sep/2;  %% z coordinate of the focal point of the second
     beam

% translation along the x axis
r.v.X = r.v.X + o_x1;
r2.v.X = r2.v.X + o_x2;

% translation along the z axis
r.v.Z = r.v.Z + o_z1;
r2.v.Z = r2.v.Z + o_z2;

% Simulation - Longitudinal

% Preallocation variables

% Force components
fz_z1 = zeros(1,numel(z));
fz_x1 = zeros(1,numel(z));

fz_z2 = zeros(1,numel(z));
fz_x2 = zeros(1,numel(z));
```

```
% Trapping efficiencies
%qz_x1 = zeros(1,numel(z));
%qz_z1 = zeros(1,numel(z));

%qz_x2 = zeros(1,numel(z));
%qz_z2 = zeros(1,numel(z));

% Scattering and gradient forces
fz_s1 = zeros(3,numel(z)); % Total Scattering force beam 1
fz_g1 = zeros(3,numel(z)); % Total Gradient force beam 1

fz_s2 = zeros(3,numel(z)); % Total Scattering force beam 2
fz_g2 = zeros(3,numel(z)); % Total Gradient force beam 2

% Scattering and gradient trapping efficiencies
%qz_s1 = zeros(3,numel(z)); % Scattering trapping efficiency beam
    1
%qz_g1 = zeros(3,numel(z)); % Gradient trapping efficiency beam 1

%qz_s2 = zeros(3,numel(z)); % Scattering trapping efficiency beam
    2
%qz_g2 = zeros(3,numel(z)); % Gradient trapping efficiency beam 2

for i = 1:1:length(z)

    % Display update message
    disp(['Longitudinal force calculation ' int2str(i) '/'
       int2str(length(z))])

    % Spherical particle
    bead = ParticleSpherical(Point(0,0,z(i)),R,nm,np);

    % Calculate force
    forces1 = bead.force(r);
    forces2 = bead.force(r2);


    force1 = Vector(0,0,z(i), ...
        sum(forces1.Vx(isfinite(forces1.Vx))), ...
        sum(forces1.Vy(isfinite(forces1.Vy))), ...
        sum(forces1.Vz(isfinite(forces1.Vz))) ...
        );

    force2 = Vector(0,0,z(i), ...
        sum(forces2.Vx(isfinite(forces2.Vx))), ...
```

```
    sum(forces2.Vy(isfinite(forces2.Vy))), ...
    sum(forces2.Vz(isfinite(forces2.Vz))) ...
    );

fz_z1(i) = force1.Vz; %Longitudinal beam 1
fz_x1(i) = force1.Vx; %Transverse beam 1

fz_z2(i) = force2.Vz; %Longitudinal beam 2
fz_x2(i) = force2.Vx; %Transverse beam 2


%qz_z1(i) = fz_z1(i)/power*(PhysConst.c0/nm);
%qz_x1(i) = fz_x1(i)/power*(PhysConst.c0/nm);

%qz_z2(i) = fz_z2(i)/power*(PhysConst.c0/nm);
%qz_x2(i) = fz_x2(i)/power*(PhysConst.c0/nm);

% Scattering force
fs1 = r.v .* (forces1.*r.v); %Total scattering force beam 1

fz_s1(1,i) = sum(fs1.Vx(isfinite(fs1.Vx)));
fz_s1(2,i) = sum(fs1.Vy(isfinite(fs1.Vy)));
fz_s1(3,i) = sum(fs1.Vz(isfinite(fs1.Vz)));

fs2 = -(r2.v .* (forces2.*r2.v)); %Total scattering force
   beam 2

fz_s2(1,i) = sum(fs2.Vx(isfinite(fs2.Vx)));
fz_s2(2,i) = sum(fs2.Vy(isfinite(fs2.Vy)));
fz_s2(3,i) = sum(fs2.Vz(isfinite(fs2.Vz)));

% Scattering trapping efficiencies - not using this parameter
%qz_s1(1,i) = fz_s1(1,i)/power*PhysConst.c0/nm;
%qz_s1(2,i) = fz_s1(2,i)/power*PhysConst.c0/nm;
%qz_s1(3,i) = fz_s1(3,i)/power*PhysConst.c0/nm;

% qz_s2(1,i) = fz_s2(1,i)/power*PhysConst.c0/nm;
% qz_s2(2,i) = fz_s2(2,i)/power*PhysConst.c0/nm;
% qz_s2(3,i) = fz_s2(3,i)/power*PhysConst.c0/nm;

% Gradient force
fg1 = (forces1 - fs1); %Total gradient force beam 1

fz_g1(1,i) = sum(fg1.Vx(isfinite(fg1.Vx)));
fz_g1(2,i) = sum(fg1.Vy(isfinite(fg1.Vy)));
```

```
    fz_g1(3,i) = sum(fg1.Vz(isfinite(fg1.Vz)));

    fg2 = (forces2 + fs2); %Total gradient force beam 2 -- needs
       to be a + because I've defined fs2 to be negative..

    fz_g2(1,i) = sum(fg2.Vx(isfinite(fg2.Vx)));
    fz_g2(2,i) = sum(fg2.Vy(isfinite(fg2.Vy)));
    fz_g2(3,i) = sum(fg2.Vz(isfinite(fg2.Vz)));




  % Gradient trapping efficiencies - not using this parameter
  %  qz_g1(1,i) = fz_g1(1,i)/power*PhysConst.c0/nm;
  %  qz_g1(2,i) = fz_g1(2,i)/power*PhysConst.c0/nm;
  %  qz_g1(3,i) = fz_g1(3,i)/power*PhysConst.c0/nm;

   % qz_g2(1,i) = fz_g2(1,i)/power*PhysConst.c0/nm;
   % qz_g2(2,i) = fz_g2(2,i)/power*PhysConst.c0/nm;
   % qz_g2(3,i) = fz_g2(3,i)/power*PhysConst.c0/nm;

end

FG = fz_g1(3,:) + fz_g2(3,:); %Total Gradient force of both beams
   : z-direction
FS = fz_s1(3,:) + fz_s2(3,:); %Total Scattering force of both
   beams: z-direction
FZ_total = (fz_g1(3,:)+fz_g2(3,:)+fz_s1(3,:)+fz_s2(3,:));

% Figure - Longitudinal

figure(N_fig+1);

p2 = plot(z*1e+6,fz_g1(3,:)*1e+15,'b--','LineWidth',1.5); %
   gradient forces beam 1
hold on
p3 = plot(z*1e+6,fz_g2(3,:)*1e+15,'b:','LineWidth',1.5); %
   gradient forces beam 2
p4 = plot(z*1e+6,FG*1e+15,'b','LineWidth',1.5); %Total gradient
   force of both beams
p5 = plot(z*1e+6,fz_s1(3,:)*1e+15,'r--','LineWidth',1.5); %
   scattering forces beam 1
p6 = plot(z*1e+6,fz_s2(3,:)*1e+15,'r:','LineWidth',1.5); %
   scattering forces beam 2
```

```
p7 = plot(z*1e+6,FS*1e+15,'r','LineWidth',1.5); %Total scattering
     force of both beams
p1 = plot(z*1e+6,FZ_total*1e+15,'k','LineWidth',1.5); %Total
    longitudinal forces both beams
grid on
hold off
legend('F grad z1', 'F grad z2', 'F grad z total', 'F scat z1', '
    F scat z2','F scat z total','F total z')
xlabel('z   [\mum]')
ylabel('Force [fN]')
% line1 = 'Ray Optics Regime:';
% line2 = 'Dual-beam Trapping Forces - Longitudinal (z)';
% line3 = ['Zsep = ' num2str(z_sep*1e6), 'um Xsep =' num2str(
    x_sep*1e6) 'um'];
%line2 = ['Beam: Wavelength1 = ' num2str(lambda)  'm, Wavelength
    2 = ' num2str(lambda2) 'm, NA1 = ' num2str(NA) ', NA2 = '
    num2str(NA2)];
%line3 = ['waist1 = ' num2str(waist1) 'm, waist 2 = ' num2str(
    waist2) 'm, Power1 = ' num2str(power) 'W, Power2 = ' num2str(
    power2) 'W'];
%line4 = ['Particle: Radius = ' num2str(R*1e6) 'um, Density = '
    num2str(rho_p*1e-3) 'g/cm^3, Index = ' num2str(np) 'Xsep ='
    num2str(x_sep*1e6) 'um Zsep =' num2str(z_sep*1e6) 'um'];

xlim([z(1) z(end)]*1e+6)
% title({line1,line2,line3})%{line1,line2,line3,line4}
box on
     ax = gca;
     ax.FontWeight='bold';
     set(ax,'FontSize',14)
drawnow()

%Potential - Longitudinal
figure(N_fig+2)
force_long = FZ_total;
integral_long = [];
for i = 1:(length(force_long))
     integral_long = [integral_long -trapz(force_long(3:i))];%
         trapezoid rule
end
plot(z*1e+6, integral_long*1e+15,'k', 'Linewidth',1.5)
% title({line1,line2,line3})
xlabel('z [\mum]')
ylabel('Potential (J)')
     ax = gca;
```

```
    ax.FontWeight='bold';
    set(ax,'FontSize',14)
box on
grid on
drawnow()
% Simulation - Transversal

% Preallocation variables

% Force components
fx_z1 = zeros(1,numel(x));
fx_x1 = zeros(1,numel(x));

fx_z2 = zeros(1,numel(x));
fx_x2 = zeros(1,numel(x));

% Trapping efficiencies
%qx_z = zeros(1,numel(x));
%qx_x = zeros(1,numel(x));

% Scattering and gradient force
fx_s1 = zeros(3,numel(x)); % Scattering force beam 1
fx_g1 = zeros(3,numel(x)); % Gradient force beam 1

fx_s2 = zeros(3,numel(x)); % Scattering force beam 2
fx_g2 = zeros(3,numel(x)); % Gradient force beam 2

% Scattering and gradient trapping efficiencies
%qx_s = zeros(3,numel(x)); % Scattering trapping efficiency
%qx_g = zeros(3,numel(x)); % Gradient trapping efficiency

for i = 1:1:length(x)

    % Display update message
    disp(['Transversal force calculation ' int2str(i) '/' int2str
       (length(x))])

    % Spherical particle
    bead = ParticleSpherical(Point(x(i),0,0),R,nm,np);

    % Calculate force
    forces1 = bead.force(r); % Forces from beam 1
    force1 = Vector(x(i),0,0, ...
        sum(forces1.Vx(isfinite(forces1.Vx))), ...
        sum(forces1.Vy(isfinite(forces1.Vy))), ...
```

```
        sum(forces1.Vz(isfinite(forces1.Vz))) ...
        );

    fx_z1(i) = force1.Vz;
    fx_x1(i) = force1.Vx;

    forces2 = bead.force(r2); %Forces from beam 2
    force2 = Vector(x(i),0,0, ...
        sum(forces2.Vx(isfinite(forces2.Vx))), ...
        sum(forces2.Vy(isfinite(forces2.Vy))), ...
        sum(forces2.Vz(isfinite(forces2.Vz))) ...
        );

    fx_z2(i) = force2.Vz;
    fx_x2(i) = force2.Vx;

%   qx_x(i) = fx_x(i)/power*PhysConst.c0/nm;
%   qx_z(i) = fx_z(i)/power*PhysConst.c0/nm;

    % Scattering force
        %Beam 1
    fs1 = r.v .* (forces1.*r.v);
    fx_s1(1,i) = sum(fs1.Vx(isfinite(fs1.Vx)));
    fx_s1(2,i) = sum(fs1.Vy(isfinite(fs1.Vy)));
    fx_s1(3,i) = sum(fs1.Vz(isfinite(fs1.Vz)));

        %Beam 2
    fs2 = r2.v .* (forces2.*r2.v);
    fx_s2(1,i) = sum(fs2.Vx(isfinite(fs2.Vx)));
    fx_s2(2,i) = sum(fs2.Vy(isfinite(fs2.Vy)));
    fx_s2(3,i) = sum(fs2.Vz(isfinite(fs2.Vz)));
    % Scattering trapping efficiencies
%   qx_s(1,i) = fx_s(1,i)/power*PhysConst.c0/nm;
%   qx_s(2,i) = fx_s(2,i)/power*PhysConst.c0/nm;
%   qx_s(3,i) = fx_s(3,i)/power*PhysConst.c0/nm;

    % Gradient force
        %Beam 1
    fg1 = forces1 - fs1;
    fx_g1(1,i) = sum(fg1.Vx(isfinite(fg1.Vx)));
    fx_g1(2,i) = sum(fg1.Vy(isfinite(fg1.Vy)));
    fx_g1(3,i) = sum(fg1.Vz(isfinite(fg1.Vz)));

        %Beam 2
    fg2 = forces2 - fs2;
```

```
    fx_g2(1,i) = sum(fg2.Vx(isfinite(fg2.Vx)));
    fx_g2(2,i) = sum(fg2.Vy(isfinite(fg2.Vy)));
    fx_g2(3,i) = sum(fg2.Vz(isfinite(fg2.Vz)));



    % Gradient trapping efficiencies
  %   qx_g(1,i) = fx_g(1,i)/power*PhysConst.c0/nm;
  %   qx_g(2,i) = fx_g(2,i)/power*PhysConst.c0/nm;
  %   qx_g(3,i) = fx_g(3,i)/power*PhysConst.c0/nm;


end
% p2 = plot(z*1e+6,fz_g1(3,:)*1e+15,'b--','LineWidth',1.5); %
    gradient forces beam 1
% Figure - Transversal
FG_x = fx_g1(1,:) + fx_g2(1,:);
FX_total = (fx_g1(1,:)+fx_g2(1,:)+gravity_x*ones(size(x)));

figure(N_fig+3)
plot(x*1e+6,fx_g1(1,:)*1e+15,'b--','LineWidth',1.5)
hold on
plot(x*1e+6,fx_g2(1,:)*1e+15,'b:','LineWidth',1.5)
plot(x*1e+6,gravity_x*ones(size(x))*1e+15,'c-','LineWidth',1.5)
plot(x*1e+6,FX_total*1e+15,'k','LineWidth',1.5)

% line5 = 'Ray Optics Regime:';
% line6 = 'Dual-beam Trapping Forces - Transversal (x)';
% line7 = ['Zsep = ' num2str(z_sep*1e6), 'um Xsep =' num2str(
    x_sep*1e6) 'um'];
%line6 = ['Beam: Wavelength1 = ' num2str(lambda) 'm, Wavelength
    2 = ' num2str(lambda2) 'm, NA1 = ' num2str(NA) ', NA2 = '
    num2str(NA2)];
%line7 = ['waist1 = ' num2str(waist1) 'm, waist 2 = ' num2str(
    waist2) 'm, Power1 = ' num2str(power) 'W, Power2 = ' num2str(
    power2) 'W'];
%line8 = ['Particle: Radius = ' num2str(R*1e6) 'um, Density = '
    num2str(rho_p*1e-3) 'g/cm^3, Index = ' num2str(np)];
%line9 = ['Trap Stiffness = ' num2str(trap_stiffness) '(fN/um)
    Xsep =' num2str(x_sep*1e6) 'um Zsep =' num2str(z_sep*1e6) 'um
    '];
% title({line5, line6,line7})%line7,line8,line9
xlabel('x [\mum]')
ylabel('Force [fN]')
legend('F grad x1', 'F grad x2','F grav x','F total x')
```

```
    ax = gca;
    ax.FontWeight='bold';
    set(ax,'FontSize',14)
%plot([-x(end:-1:1) x]*1e+6,[abs(qx_x(end:-1:1)) abs(qx_x)],'k','
   LineWidth',1.5)
%plot([-x(end:-1:1) x]*1e+6,[-qx_g(1,end:-1:1) qx_g(1,:)],'b','
   LineWidth',1.5)
%plot([-x(end:-1:1) x]*1e+6,[qx_s(3,end:-1:1) qx_s(3,:)],'m','
   LineWidth',1.5)

%title('Trapping efficiencies - Transversal')
%xlabel('x [\mum]')
%ylabel('Q, Q_g, Q_s [adimensional]')
%legend('Q','Q_g','Q_s','Location','SouthWest')
box on
grid on
xlim([-x(end) x(end)]*1e+6)
drawnow()
%   Slope Calculations
[y_max, x_max_index] = max(FX_total)
[y_min, x_min_index] = min(FX_total)
x_actual = [-x(end:-1:1) x]
x_max_actual = x(x_max_index)
x_min_actual = x(x_min_index)
k_spring = (1e-15*(y_min - y_max))/(x_min_actual - x_max_actual)
   %fN/um
k_spring_x = abs(k_spring)
%
figure(N_fig+4)
force = FX_total;
integral = [];
for i = 1:(length(force))
    integral = [integral -trapz(force(1:i))];%trapezoid rule
end
plot(x*1e+6, integral*1e+15,'k', 'Linewidth',1.5)
set(ax,'FontSize',15)
%set(gca,'XTick',-x(end:-1:1):10:x);
% title({line5, line6,line7})%line7,line8,line9
xlabel('x [\mum]')
ylabel('Potential (J)')
    ax = gca;
    ax.FontWeight='bold';
    set(ax,'FontSize',14)
box on
grid on
```

```
xlim([-x(end) x(end)]*1e+6)

toc
```

APPENDIX C

AUTOMATIC LOADING AND IMAGE DETECTION

This appendix is four individual MATLAB codes that allow us to image particles in the trap region inside the vacuum chamber. All programs must be used to create our Image Report. The *Pulsed Loading Program* automates our particle launcher, *Crop Calibration for Main Detection* sets our initial values for the camera, *Threshold Calibration for Main Detection* sets the background values for the main detection program, and *Main Detection Imaging Program* is the program that will produce our Image Report of a trapped particle. These codes were written and modified by Demi St. John, Dr. Randy Babbitt and Alec Dinerstein.

```
%PULSED LOADING PROGRAM

s = daq.createSession('ni');  %create session assosciated with a
    vendor, assign it to variable 's'

addAnalogOutputChannel(s,'Dev1', 'ao0', 'Voltage'); % add analog
    output channel to device

%outputSingleValue = 3 ; % outputs 4V (range +/- 2) on each
    channel
%outputSingleScan(s, outputSingleValue); % outputSingleValue] ) ;
     % generates a single scan on each channel
dummy=[];

while isempty(dummy)
outputSingleValue = 2.5  ; % outputs 2.5V on each channel
outputSingleScan(s, outputSingleValue); % outputSingleValue] ) ;
   % generates a single scan on each channel

pause(.001);

outputSingleValue = 0  ; % outputs 0V (range +/- 2) on each
    channel
outputSingleScan(s, outputSingleValue); % outputSingleValue] ) ;
   % generates a single scan on each channel

pause(0.2);
disp('running')
commandwindow
% dummy=input('hit return to reload, type any number and return
    to stop');

end

%plot(outputSignal1);

%hold on;
```

```
%xlabel('Time');
%ylabel('Voltage');
%queueOutputData(s,outputSignal1);

%s.startForeground;


%CROP CALIBRATION FOR MAIN DETECTION PROGRAM
%TODO: INCLUDE MATLAB.M FILE NAME
%Written by Alec Dinerstein
%Last edits: 5/10/18

% Add NET assembly
% May need to change specific location of library
NET.addAssembly('C:\Program Files\Thorlabs\Scientific Imaging\DCx
    Camera Support\Develop\DotNet\uc480DotNet.dll');
% Create camera object handle
cam = uc480.Camera;
% Open the 1st available camera
cam.Init(0);
% Set display mode to bitmap (DiB)
cam.Display.Mode.Set(uc480.Defines.DisplayMode.DiB);
% Set color mode to 8-bit RGB
cam.PixelFormat.Set(uc480.Defines.ColorMode.RGBA8Packed);
% Set trigger mode to software (single image acquisition)
cam.Trigger.Set(uc480.Defines.TriggerMode.Software);
% Allocate image memory
[~, MemId] = cam.Memory.Allocate(true);
% Obtain image information
[~, Width, Height, Bits, ~] = cam.Memory.Inquire(MemId);
 % Acquire image
cam.Acquisition.Freeze(uc480.Defines.DeviceParameter.Wait);
% Copy image from memory
[~, tmp] = cam.Memory.CopyToArray(MemId);
% Reshape image
Data = reshape(uint8(tmp), [Bits/8, Width, Height]);
Data = Data(1:3, 1:Width, 1:Height);
Data = permute(Data, [3,2,1]);


% turn image from RGB to Grayscale and Crop
rect =[700 500 860 825];
I = rgb2gray(Data);

%grayscale image with cropzone
```

```
subplot (2,2,1);
imshow(I);
hold on
plot([rect(1) rect(3)],[rect(2) rect(4)],'r-');

%cropped image
I2 = imcrop(I,[rect(1) rect(2) (rect(3)-rect(1)) (rect(4)-rect(2)
    )]);
subplot(2,2,2);
imshow(I2);

%background energy of crop

cam.Exit;

%THRESHOLD CALIBRATION PROGRAM FOR MAIN DETECTION PROGRAM
%TODO: INCLUDE MATLAB.M FILE NAME
%Written by Alec Dinerstein
%Last edits: 5/10/18

% Add NET assembly
% May need to change specific location of library
NET.addAssembly('C:\Program Files\Thorlabs\Scientific Imaging\DCx
    Camera Support\Develop\DotNet\uc480DotNet.dll');
% Create camera object handle
cam = uc480.Camera;
% Open the 1st available camera
cam.Init(0);
% Set display mode to bitmap (DiB)
cam.Display.Mode.Set(uc480.Defines.DisplayMode.DiB);
% Set color mode to 8-bit RGB
cam.PixelFormat.Set(uc480.Defines.ColorMode.RGBA8Packed);
% Set trigger mode to software (single image acquisition)
cam.Trigger.Set(uc480.Defines.TriggerMode.Software);
% Allocate image memory
[~, MemId] = cam.Memory.Allocate(true);
% Obtain image information
[~, Width, Height, Bits, ~] = cam.Memory.Inquire(MemId);
% Acquire image
cam.Acquisition.Freeze(uc480.Defines.DeviceParameter.Wait);
% Copy image from memory
[~, tmp] = cam.Memory.CopyToArray(MemId);
% Reshape image
Data = reshape(uint8(tmp), [Bits/8, Width, Height]);
Data = Data(1:3, 1:Width, 1:Height);
```

```
Data = permute(Data, [3,2,1]);

% define crop metrics
% a = 400; % top left corner x coord
% b = 300;% top left corner y coord
% c = 800; % bottom right corner x coord
% d = 600; % bottom right corner y coord
rect =[650 300 750 400]; % region that image will be cropped down
    to using a,b,c,d
I = rgb2gray(Data); % turns Data from rgb to grayscale
I2 = imcrop(I,[rect(1) rect(2) (rect(3)-rect(1)) (rect(4)-rect(2)
   )]); % crops  I


% thresholding// max of the background perimeter
max1 = max(I2(1,:));
max2 = max(I2(:,1));
max3 = max(I2(end,:));
max4 = max(I2(:,end));
thr = 4;
thrshld = thr*max([max1, max2, max3, max4]);
I_0 = find(I2 < thrshld);
I2(I_0) = 0;

% Horizontal intensity
xx = 1:size(I2,1); % pixel values for x coord
I2xx = mean(I2,2)'; %
I2xx = I2xx - min(I2xx); % removes background intensity


%vertical intensity
yy = 1:size(I2,2); % pixel values for y coord
I2yy = mean(I2,1);
I2yy = I2yy - min(I2yy); % removes backgound intensity

%find image centroid
Cxx = sum(xx.*I2xx)/ sum(I2xx); % x coord
Cyy = sum(yy.*I2yy)/ sum(I2yy); % y coord

%find radius
Wxx = sqrt(sum(((xx-Cxx).^2).* I2xx)/ sum(I2xx)); % vertical
   radius
Wyy = sqrt(sum(((yy-Cyy).^2).* I2yy)/ sum(I2yy)); % horizontal
   radius
```

```
%calculates intensity accounting for background light
Energy =(sum(sum(I2)))
cam.Exit;

%MAIN DETECTION IMAGING PROGRAM
%TODO: INCLUDE MATLAB.M FILE NAME
%Last Edits made on 5/16 by A. Dinerstein

% Add NET assembly
% May need to change specific location of library
NET.addAssembly('C:\Program Files\Thorlabs\Scientific Imaging\DCx
    Camera Support\Develop\DotNet\uc480DotNet.dll');
% Create camera object handle
cam = uc480.Camera;
% Open the 1st available camera
cam.Init(0);
disp('camera opened')
% Set display mode to bitmap (DiB)
cam.Display.Mode.Set(uc480.Defines.DisplayMode.DiB);
% Set color mode to 8-bit RGB
cam.PixelFormat.Set(uc480.Defines.ColorMode.RGBA8Packed);
% Set trigger mode to software (single image acquisition)
cam.Trigger.Set(uc480.Defines.TriggerMode.Software);
% Allocate image memory
[~, MemId] = cam.Memory.Allocate(true);
% Obtain image information
[~, Width, Height, Bits, ~] = cam.Memory.Inquire(MemId);

% While loop will run until a particle is detected
particle = 0;
tic % start timer
while particle < 2
    % Acquire image
    cam.Acquisition.Freeze(uc480.Defines.DeviceParameter.Wait);
    % Copy image from memory
    [~, tmp] = cam.Memory.CopyToArray(MemId);
    % Reshape image
    Data = reshape(uint8(tmp), [Bits/8, Width, Height]);
    Data = Data(1:3, 1:Width, 1:Height);
    Data = permute(Data, [3,2,1]);
    %figure(1);clf;
    %imshow(Data);

% turn image from RGB to Grayscale and Crop
% define crop metrics
```

```
%       a = 400; % top left corner x coord
%       b = 300;% top left corner y coord
%       c = 800; % bottom right corner x coord
%       d = 600; % bottom right corner y coord
     rect =[700 630 780 800]; % region that image will be cropped
        down to using a,b,c,d
     I = rgb2gray(Data); % turns Data from rgb to grayscale
     I2 = imcrop(I,[rect(1) rect(2) (rect(3)-rect(1)) (rect(4)-
        rect(2))]); % crops  I


% thresholding// max of the background perimeter
     max1 = max(I2(1,:));
     max2 = max(I2(:,1));
     max3 = max(I2(end,:));
     max4 = max(I2(:,end));
     thr = 4;
     thrshld = thr*max([max1, max2, max3, max4]);
     I_0 = find(I2 < thrshld);
     I2(I_0) = 0;
% Horizontal intensity
     xx = 1:size(I2,1); % pixel values for x coord
     I2xx = mean(I2,2)'; %
     I2xx = I2xx - min(I2xx); % removes background intensity


%vertical intensity
     yy = 1:size(I2,2); % pixel values for y coord
     I2yy = mean(I2,1);
     I2yy = I2yy - min(I2yy); % removes backgound intensity

%find image centroid
     Cxx = sum(xx.*I2xx)/ sum(I2xx); % x coord
     Cyy = sum(yy.*I2yy)/ sum(I2yy); % y coord

%find radius
     Wxx = sqrt(sum(((xx-Cxx).^2).* I2xx)/ sum(I2xx)); % vertical
        radius
     Wyy = sqrt(sum(((yy-Cyy).^2).* I2yy)/ sum(I2yy)); %
        horizontal radius

%calculates intensity accounting for background light
     Energy =(sum(sum(I2)));

%set threshhold energy
```

```
    ThrEnergy = 50000;

%determine if energy of picture exceeds the threshold
    if Energy > ThrEnergy
        if particle > 0
            particle = particle + 1 ;
        else
            particle = particle + 1 ;
     % introduce 1 sec time delay to space out images
            pause(1)
        end
    else
        particle = 0;
    end

end
tt = toc;% stop timer, elapsed time ~ approx detection period
tt = num2str(tt);
% tt = strcat('Trap time: ',tt,'s');

%alert that particle is trapped
disp('particle in trap');
load train.mat;
sound(y,Fs);

%create trapped particle report
%picture of particle
t = datestr(now,'mm-dd-yyyy HH-MM-SS');
s = 'trapped particle report- ';
st = strcat(s,t);
figure('Name',st,'NumberTitle','off');
clf;
subplot(2,2,1);
imshow(I2);
title('particle image');

%horizontal intensity plot
subplot(2,2,2);
plot(xx, I2xx);
title('horizontal intensity');

%vertical intensity plot
subplot(2,2,3);
plot(yy, I2yy);
title('vertical intensity');
```

```
%horizontal and vertical radii, Energy
ax = subplot(2, 2, 4);
centerx = ['Horizontal center : ',num2str(Cxx)];
centery = ['Vertical center: ',num2str(Cyy)];
text(.1,.25, {centerx, centery});
h = ['Horizontal radius: ',num2str(Wxx)];
v = ['Vertical radius: ',num2str(Wyy)];
e = ['Image energy: ',num2str(Energy)];
text(.1,.5, {h, v});
% text(.1,.75,{e,tt});
set ( ax, 'visible', 'off')

%do you want to save the particle report y/n
answer = questdlg('Would you like to save report?', ...
        'trapped particle report', ...
        'yes','no','no');
% Handle response
switch answer
    case 'yes';
        report = 1;
    case 'no';
        report = 0;
end
%save trapped particle report
    name = fullfile('C:\Users\Babbit Lab\Desktop\Trapped Particle
       Reports', st);
    saveas(gcf, name, 'png');
if report>1
    disp('saved')
else
    disp('not saved')
end

%do you want to save particle data in a text file (Wxx, Wyy,
   Energy, Trap
%time) y/n

answer = questdlg('Would you like to save data to a text file?',
   ...
    'particle data', ...
    'yes', 'no', 'no');
% handle response
switch answer
    case 'yes';
```

```
        datalog = 1;
    case 'no';
        datalog = 0;
end

if datalog>1
    disp('saved');
else
    disp('not saved');
end
% Close camera
cam.Exit;
disp('camera stopped')
```

APPENDIX D

PARTICLE LOADING DYNAMICS

This MATLAB code is *DRS_attempt_damped_well.m* and simulates a particle entering the trap region from both the longitudinal and transverse directions. Forces are imported as global variables from the code in Appendix B. This code was written and modified by Demi St. John and Dr. Randy Babbitt.

```
%Particle Loading Dynamics
%DRS_attempt_damped_well.m

function main()
global k_spring mass gamma p_Fx F_x X x z FX_total FZ_total Z
    p_Fz FX FZ
k_spring=1;
mass=1;
omega=sqrt(k_spring/mass);

beta=.2;
t_0=0;
t_f=0.06;

%Approximate the polynominal for F(x)
%produce fake Force data
X=x;%m
FX_total; %N
%F_x=-k_spring*X.*exp(-beta*X.^2);
%fit poly to Force data
n_fit=20;
p_Fx=polyfit(X,FX_total,n_fit);
F_x_poly=polyval(p_Fx,X);

% %compare Force data with poly fit
% %figure(1);clf
% %plot(X*1e+6,FX_total*1e+15,'b','LineWidth',1.5);
% hold on
% %plot(X*1e+6,F_x_poly*1e+15,'r','LineWidth',1.5);
% XV_test=X;
% xlabel('Position (um)'),ylabel('Force (fN)');
% legend('F_x', 'F_x_p_o_l_y')
% title('Compare Force_X data with poly fit')

%fit poly to Force data
Z=z;%m
FZ_total; %N
n_fit=36;
p_Fz=polyfit(Z,FZ_total,n_fit);
F_z_poly=polyval(p_Fz,Z);
```

```
% %figure(3);clf
% Z=z;
% %plot(Z*1e+6,FZ_total*1e+15,'b','LineWidth',1.5);
% hold on
% %plot(Z*1e+6,F_z_poly*1e+15,'r','LineWidth',1.5);
% XV1_test=Z;
% xlabel('Position (um)'),ylabel('Force (fN)');
% legend('F_z', 'F_z_p_o_l_y')
% title('Compare Force_Z data with poly fit')
% tic

c=3e8; %speed of light (m/s)
k_boltzman=1.38e-23;%(J/K)
Temp=295; %temperature (K)
g=9.8; %m/s^2 - gravity

%Density of Particles
rho_Si=2.46*1e-3*1e6%kg/m^3
rho_YAG=4.56*1e-3*1e6;%kg/m^3
rho_Diamond=3.5*1e-3*1e6;%kg/m^3
rho_AlO=3.97*1e-3*1e6;%kg/m^3

% Spherical particle in trap in air
r_p = 10e-6; % Particle radius [m]
rho_p=rho_YAG;
mass = 4.0/3.0*pi*r_p^3*rho_p;%4560 % Particle mass (kg) = volume
    *density(kg/m^3)
k_spring=(4e5*1e-15)/15e-6;  %force/meter  (slope from OTGO)
omega=sqrt(k_spring/mass);
f_osc=omega/(2*pi);

mu=18.54e-6;%Pa-sec  =  kg/ (m*sec)
gamma=6*pi*r_p*mu;


%Terminal Velocity

%v_term=2/9*rho_p*g*r_p^2/mu;  %m/s
v_term=mass*g/(6*pi*r_p*mu) %(m/s)

%captured
  X1 = -.000018;
  X2 = -.00001;
% X1 = .000075;
% X2 = .00005;
```

```
XV_0=[X1;   .1*v_term]; %[m; m/s]
%[t,XV] = ode45(@OPG,[t_0  t_f],XV_0);   %variable steps
[t,XV] = ode45(@OPG,[t_0:(t_f-t_0)/12000:t_f],XV_0); %fixed steps
figure(2);clf;
plot(t,XV(:,1)*1e+6,'b','LineWidth',1.5)%
% %Changing initial position
XV_01=[X2;   .1*v_term]; %[m; m/s]
%[t,XV] = ode45(@OPG,[t_0  t_f],XV_0);   %variable steps
[t,XV] = ode45(@OPG,[t_0:(t_f-t_0)/2000:t_f],XV_01); %fixed steps
figure(2);
hold on
plot(t,XV(:,1)*1e+6,'r','LineWidth',1.5)
title('Changing initial x positions, .1*v_{term} initial velocity
   ')
%title('Changing initial z positions, 0 initial velocity')
legend(strcat('x_0= ', num2str(X1*1e+6), 'um'), strcat('x_0= ',
   num2str(X2*1e+6),'um'));
%legend(strcat('z_0= ', num2str(X1*1e+6), 'um'), strcat('z_0= ',
   num2str(X2*1e+6),'um'));
%legend('x_0' num2str(), 'x_0' num2str(X2*1e+6));
xlabel('time (s)');ylabel('position (um)')
    ax = gca;
    ax.FontWeight='bold';
    set(ax,'FontSize',12)
toc
hold off
end
%
function dXVdt = OPG(t,XV)
global k_spring mass gamma p_Fx F_x X x z FX_total FZ_total tlast
    FZ FX
dXVdt = zeros(2,1);
dXVdt(1) =XV(2);%dx/dt=v (m/s)
%dXVdt(2) =-(k_spring/mass)*XV(1)-gamma/mass*XV(2); %by Exact
   formula dv/dt=-(k/m)x-g*v
%dXVdt(2) =polyval(p_Fx,XV(1))/mass-gamma/mass*XV(2);%by polyfit
dXVdt(2) =interp1(x,FX_total,XV(1))/mass-gamma/mass*XV(2);%by
   interpulation [m, N,] acceleration
end
```